Dissertation zur Erlangung des Doktorgrades der
Fakultät für Chemie und Pharmazie
der Ludwig-Maximilians-Universität München

Strand-specific ChIP-sequencing reveals nucleosome dynamics at DNA double-strand breaks

---

Martina Peritore

aus

Borgomanero, Italy

2022

Erklärung

Diese Dissertation wurde im Sinne von § 7 der Promotionsordnung vom 28. November 2011 von Frau Prof. Dr. Elena Conti betreut.

Eidesstattliche Versicherung

Diese Dissertation wurde eigenständig und ohne unerlaubte Hilfe erarbeitet.

München, 13.04.2022

_____

Martina Peritore

Dissertation eingereicht am	13.04.2022
1. Gutachterin:	Frau Prof. Dr. Elena Conti
2. Gutachter:	Herr Prof. Dr. Boris Pfander
Mündliche Prüfung am	30.06.2022

The work presented in this thesis was published in the journal Molecular Cell with the title “Strand-specific ChIP-seq at DNA breaks distinguishes ssDNA versus dsDNA binding and refutes single-stranded nucleosomes” (Peritore et al., 2021).
ChIP-sequencing data were deposited in GEO and can be found under the accession number: GSE149807.

Contributions

The AsiSI double-strand break induction system (Figures 20 – 30) was established by Dr. Susanne C. S. Bantele (*Boris Pfander laboratory, Max Planck Institute of Biochemistry, Martinsried – present address: Jiri Lukas laboratory, Novo Nordisk Foundation Center for Protein Research, Copenhagen, Denmark)* using the pCL096 plasmid kindly provided by Dr. Claudio Lademann (*Department of Molecular Cell Biology, Max Planck Institute of Biochemistry, Martinsried*). All experiments were carried out by myself.

The auxin-inducible degron strains (Figure 30) were generated and tested by Dr. Karl-Uwe Reusswig (*Boris Pfander laboratory, Max Planck Institute of Biochemistry, Martinsried – present address: David Pellman laboratory, Dana-Farber Cancer Institute, Harvard Medical School, Boston, USA).*

Bioinformatic analysis of ChIP-seq data was either carried out by Dr. Tobias Straub (*BMC, Core Facility Bioinformatics, LMU, Munich)* or carried out by myself and supervised by Dr. Tobias Straub.

Next-Generation Sequencing was carried out by Dr. Stefan Krebs at LAFUGA (*Gene center, LMU, Munich*) and by Dr. Marja Driessen and Dr. Rin Ho Kim at the NGS core facility in the Max Planck Institute of Biochemistry.

Table of content

TABLE OF CONTENT 7

SUMMARY 1

1. INTRODUCTION 2

1.1 SOURCES OF DNA DOUBLE-STRAND BREAKS 2
1.1.1 Exogenous sources of DNA double-strand breaks 3
1.1.2 Endogenous sources of DNA double-strand breaks 4
1.1.3 Programmed DNA double-strand breaks 6
1.2 REPAIR OF DNA DOUBLE-STRAND BREAKS 9
1.2.1 DSB repair by end-joining 9
1.2.2 DSB repair by Homologous Recombination 13
1.2.3 Molecular mechanism of homologous recombination 15
1.3 THE ROLE OF CHROMATIN IN DOUBLE-STRAND BREAK REPAIR 19
1.3.1 Histones PTMs in response to DNA double-strand breaks 20
1.3.2 Effects of chromatin remodelers on nucleosome organization 22
1.3.3 Nucleosome eviction and resection of double-strand breaks 24
1.3.4 Nucleosome positioning at double-strand breaks 26
1.3.5 Nucleosome editing at double-strand breaks 27
1.3.6 Alternative roles of chromatin remodelers at double-strand breaks: the antagonism between Fun30 and Rad9 29

2. AIM OF THE STUDY 31

3. RESULTS 32

3.1 STRAND-SPECIFIC CHIP-SEQUENCING 32
3.2 STRAND-SPECIFIC CHIP-SEQUENCING RECAPITULATES RPA BINDING TO SSDNA AT RESECTED DSBS 34
3.3 DPB11 AND THE 9-1-1 COMPLEX LOCALIZE ON DOUBLE-STRANDED DNA 35
3.4 STRAND-SPECIFIC CHIP-SEQ DETECTS RAD51 FILAMENTS AND HOMOLOGY SEARCH INTERMEDIATES 38
3.5 NUCLEOSOME EVICTION AT A RESECTED DSB IN THE *MAT* LOCUS 40
3.5.1 γH2A is lost at a resected DSB 41
3.5.2 Nucleosomes are lost at a DSB upon resection 44
3.5.3 Nucleosomes are fully evicted upon resection 48
3.6 NUCLEOSOME EVICTION DOES NOT DEPEND ON GENOMIC LOCATION 50
3.6.1 Characterization of the pGAL-AsiSI system in budding yeast 51
3.6.2 Nucleosome eviction upon resection occurs throughout the yeast genome 54
3.7 RESECTION AND NUCLEOSOME EVICTION ARE COUPLED 59

3.7.1 Fun30 is dispensable for nucleosome eviction 59
3.7.2 The INO80 complex is not required for nucleosome eviction 61
3.7.3 RSC and SWI/SNF are crucial for nucleosome eviction and resection 63

4. DISCUSSION 65

4.1 STRAND-SPECIFIC CHIP-SEQUENCING IS ABLE TO DISCRIMINATE BETWEEN SSDNA AND DSDNA BINDING 65
4.1.1 Strand-specific ChIP-seq is a powerful method to address any DNA transaction that generates strand asymmetry 66
4.2 THE 9-1-1 COMPLEX AND ITS INTERACTOR DPB11 ASSOCIATE TO DSDNA AT THE LEADING EDGE OF RESECTION 68
4.3 THE ROLE OF GENOME ARCHITECTURE IN DNA REPAIR 70
4.3.1 Homology search is guided by the chromosomal architecture 70
4.3.2 γH2A spreading recapitulates the chromosomal architecture 72
4.4 STRAND-SPECIFIC CHIP-SEQ REVEALS NUCLEOSOME DYNAMICS AT DOUBLE-STRANDED BREAKS 73
4.4.1 DNA end resection and nucleosome eviction are intrinsically coupled 73
4.4.2 RSC and SWI/SNF act redundantly to promote nucleosome eviction and DNA end resection 75

5. MATERIALS AND METHODS 80

5.1 MICROBIOLOGY METHODS 80
5.1.1 E. coli techniques 80
5.1.2 S. cerevisiae techniques 81
5.2 MOLECULAR BIOLOGY METHODS 85
5.2.1 Standard molecular biology techniques 85
5.2.2 Strand-specific ChIP-sequencing 87
5.3 BIOCHEMISTRY METHODS 92

APPENDIX 95

REFERENCES 97

ACKNOWLEDGEMENTS 123

Summary

DNA double-strand breaks (DSBs) are highly toxic lesions that, if not correctly repaired, can have detrimental consequences on genome integrity and cell survival. During the course of evolution, different mechanisms developed to repair DSBs including non-homologous end-joining (NHEJ) and homologous recombination (HR). A pivotal step of the cellular repair pathway decision is the processing of DSB ends during DNA end resection, which, through the degradation of 5'-terminated strands, generates a long stretch of single-stranded DNA (ssDNA) that prevents re-ligation by NHEJ factors and guides repair towards HR. At the same time, resection divides the chromatin surrounding a DSB in distinct ssDNA and dsDNA domains. Establishment of these domains is crucial for HR repair as well as for DNA damage signaling and checkpoint activation, but the protein composition and the interactions between these compartments were not fully understood. Specifically, it was unclear whether nucleosomes, the fundamental unit of chromatin, could be found in the ssDNA domain as well. This would have considerable implications for the recruitment of repair factors to DSBs and for the maintenance of the epigenetic information during repair. However, previously used techniques were inadequate to address this question.

Here, we combined site-specific induction of DSBs with chromatin immunoprecipitation, followed by strand-specific library preparation and next-generation sequencing to analyze the *in vivo* DNA binding mode of key DSB repair proteins as well as nucleosomes. In proof-of-principle experiments, strand-specific ChIP-sequencing recapitulated the characteristic binding pattern of RPA and Rad51 to ssDNA at resected DSBs. Using this technique, we were also able to detect Rad51 binding to dsDNA during homology search. The 9-1-1 signaling platform was suggested to bind at the ss-dsDNA junction at resected DSBs. We showed that, *in vivo*, 9-1-1 associates with the dsDNA compartment and locates at the leading edge of resection. Furthermore, we did not find evidence of the presence of nucleosomes on ssDNA and, therefore, they do not represent a major species at resected DSBs. In contrast, we found that nucleosomes become fully evicted in concomitance with resection and that the chromatin remodelers RSC and SWI/SNF act redundantly to promote such nucleosome eviction. Taken together, our study revealed that nucleosome eviction is intrinsically coupled with resection and that the ssDNA and dsDNA domains generated by resection are characterized by distinct properties.

1. Introduction

DNA, together with its epigenetic signature, constitutes the molecular blueprint of cells and organisms. Faithful transmission of this information to the next generation is crucial for survival and function. However, both environmental factors and the internal cellular metabolism pose a constant threat to the integrity of the genetic information, because of their potential to induce DNA lesions (Ciccia and Elledge, 2010). In humans, the occurrence of DNA damaging events was estimated to be about 10^5 per cell per day (Hoeijmakers, 2009). Accordingly, maintaining this blueprint intact is a highly demanding tasks for a cell. Numerous pathways have evolved to recognize and precisely eliminate the different types of lesions that can affect DNA.

A highly detrimental form of DNA damage are DNA double-strand breaks (DSBs), which form when both strands of the DNA double helix are cleaved. DSB threaten cellular survival by disrupting chromosomal integrity. Moreover, illegitimate repair of DSBs has the potential to cause genomic rearrangements, like deletions or chromosomal translocations. This genome instability is recognized as a major driver of senescence and cancer formation (Schumacher et al., 2021; Tubbs and Nussenzweig, 2017). DSB repair occurs in the context of chromatin. Despite the extensive knowledge we currently have on DNA repair pathways, we still lack a comprehensive understanding of their interplay with chromatin. The focus of this thesis is to investigate how repair of DSBs via homologous recombination affects chromatin.

1.1 Sources of DNA double-strand breaks

DNA double-strand breaks (DSBs) consist in the simultaneous cleavage of phosphodiester bonds in the two complementary DNA strands backbones. DSBs can arise from a variety of different sources, which we can divide in two main categories: exogenous and endogenous (Mehta and Haber, 2014). Ionizing radiation or some chemotherapeutic drugs belong to the first category, while problems during DNA replication can be a potential endogenous source of DSBs. In addition, formation of enzyme-induced DSBs is required for several natural processes like segregation of homologous chromosomes during meiosis, mating type switching in yeast and immunoglobulin class switching in

humans. The different origins of DSBs will be discussed in more details in the next paragraphs.

1.1.1 Exogenous sources of DNA double-strand breaks

As mentioned above, one type of environmental source of DSBs is ionizing radiation. Examples of ionizing radiations are gamma rays and X-rays, which are used in medicine as therapeutic or diagnostic tools, cosmic rays or the radiation emitted by the naturally occurring radioactive gas radon. Ionizing radiations (IR) consist in electromagnetic waves or subatomic particles carrying enough energy to remove electrons from atoms, thereby producing ions (Cannan and Pederson, 2016). Chemical bonds in molecules affected by IR can break and generate highly reactive free radicals. In particular, the aqueous environment inside cells favors the formation of reactive oxygen species (ROS), which, in turn, can damage biological molecules (Barnard et al., 2013; Ward, 1988). Therefore, IR can affect DNA in two ways, either directly or indirectly through production of radicals. Direct collision of photons or high energy particles with DNA can lead to cleavage of the phosphodiester backbone of one DNA strand, producing single-strand breaks (SSBs) (Cannan and Pederson, 2016). Importantly, IR produces clustered DNA damage, where multiple lesions occur in close proximity to one another (Ward, 1994). As a result, DSBs are generated when two adjacent SSBs affect opposite DNA strands (Eccles et al., 2011). In addition, breaks generated by IR often produce DNA ends that cannot be directly re-ligated, as they do not present "clean" 3'-hydroxyl and 5'-phosphate termini, but, for example, terminal nucleotides or phosphoglycolates, which require specialized enzymatic activities to be repaired (Mehta and Haber, 2014).

Besides IR, several chemical compounds are well-known DNA damaging agents, some of which are widely used as chemotherapeutic drugs. These compounds can be divided in classes depending on their mechanism of action: DNA alkylating agents, cross-linking agents, radiomimetic compounds and topoisomerase inhibitors (Mehta and Haber, 2014). DNA alkylating agents, such as methyl methanesulfonate (MMS) and temozolomide, and cross-linking agents like cisplatin do not induce DSBs directly, but cause base modifications (Fu et al., 2012) and inter- and intra-strand cross-linking (Schärer, 2005), respectively. These lesions represent obstacles for the DNA replication machinery and can result in the formation of DSBs from processing of stalled replication structures (Branzei and Foiani, 2010). In addition to these, other chemicals like hydroxyurea or

aphidicolin, are known to hinder DNA replication progression by depleting cells of dNTPs, the building blocks of DNA, or by inhibiting DNA polymerase; thereby promoting DNA damage and genome instability (Mehta and Haber, 2014; Mirkin and Mirkin, 2007). Replication as a source of DSBs will be discussed later in further details (1.1.2). Radiomimetic compounds, such as bleomycin, phleomycin and neocarzinostatin, as their name suggests, have a mechanism of action similar to ionizing radiations, i.e. they can directly induce SSBs or DSBs when interacting with DNA (Chen and Stubbe, 2005). Lastly, topoisomerases are essential enzymes that relieve topological stress in DNA molecules by introducing breaks in a controlled fashion. Topoisomerase inhibitors, such as camptothecin and etoposide, are able to stabilize topoisomerases catalytic intermediates and thereby lead to the induction of SSBs or DSBs. Topoisomerases will be described in more details in paragraph 1.1.3.

1.1.2 Endogenous sources of DNA double-strand breaks

DNA transactions such as DNA replication and transcription can be potential sources of DSBs (Mehta and Haber, 2014). DNA replication is timed and regulated to occur precisely once during the S phase of the cell cycle. Perturbations in this timing or other factors halting replication progression can cause replication stress, which is characterized by stalling of replication forks and has been associated with DNA damage and genome instability, particularly with DSB formation (Bouwman and Crosetto, 2018; Hills and Diffley, 2014). Oncogene activation is a prominent inducer of DNA replication stress. Indeed, oncogenes can interfere with replication timing, stimulating replication initiation outside the S phase of the cell cycle (Hills and Diffley, 2014). This can lead to a condition in which fundamental replication factors, such as nucleotides (dNTPs) pools, histones and RPA, become limiting and, thus, generate replication fork stalling or slowing (Halazonetis et al., 2008). Oncogenes can also promote re-replication, which can cause, besides depletion of replication factors, also collisions with other active replication forks and generate DSBs (Hills and Diffley, 2014).

Stalling of the replication machinery can occur at repetitive sequences as well, since they are inherently more difficult to replicate and they can assume a secondary structure that block fork progression, like G-quadruplexes forming at telomeric repeats (Técher et al., 2017). Generally, any obstacle or damage present on DNA has the potential to cause fork stalling or slower fork progression and, consequently, DSB formation (Figure 1). Notably,

SSBs are highly detrimental during replication, since the replication machinery can potentially pass through and generate a single-end DSB (seDSB) (Figure 1). In addition, pre-existent damage on the DNA template such as inter-strand cross-links, DNA-protein cross-links and base lesions constitute impediments for the DNA replication machinery (Zeman and Cimprich, 2014). Importantly, when unresolved, stalled replication forks can collapse, lead to DSB formation and induce genome instability (Zeman and Cimprich, 2014) (Figure 1). Another form of remodeling of the replication fork structure that leads to a DSB is fork reversal, which involves the annealing of the two newly synthesized strands generating a single-ended DSB (Figure 1). In addition, this four-strand junction is also structurally identical to a Holliday junction and, thus, can be recognized and cleaved by endogenous structure-specific nucleases (Heller and Marians, 2006; Seigneur et al., 1998; Sogo et al., 2002) (Figure 1). In both cases, the resulting seDSB can be later processed by the DNA repair machinery to promote fork restart (Berti et al., 2020; Neelsen and Lopes, 2015).

Transcription can also represent a natural obstacle for DNA replication and induce replication stress when the replication and transcription machineries act on the same DNA molecule and at the same time. Specifically, these machineries can collide in a co-directional or a head-on configuration. Head-on transcription-replication conflicts (TRCs) have been shown to be particularly detrimental, since they promote R-loop formation, resulting in replication fork stalling (Hamperl et al., 2017). R-loops consist in a three-strand structure comprising a RNA:DNA hybrid, arising from the annealing of the nascent RNA with the template DNA, and the displaced non-template DNA strand (Aguilera and García-Muse, 2012). Despite the accumulating evidence that R-loops play an important role in a large number of physiological processes (Niehrs and Luke, 2020), they are also a well-known source of genome instability (Costantino and Koshland, 2018; Rinaldi et al., 2021). Importantly, cells possess mechanisms that keep transcription and replication spatially and temporally distinct, preventing the occurrence of TRCs during S phase (Hamperl and Cimprich, 2016). However, deregulation of the replication program, as it occurs for example in cancer cells, can increase the frequency of TRCs and lead to genome instability. Interestingly, it has been proposed that common fragile sites (CFSs) may be hot-spots of TRCs (García-Muse and Aguilera, 2016). Common fragile sites are large chromosomal regions prone to breakage in metaphase chromosomes upon replication stress and are frequently found associated with chromosomal translocations in cancer

cells (Le Tallec et al., 2013; Wilson et al., 2015). Some features of CFSs are the co-localization with large genes or actively transcribed regions and enrichment in sequences that can stall the replication machinery (García-Muse and Aguilera, 2016). Therefore, a higher persistency of the replication and transcription machineries at these sites may increase the frequency of TRCs and result in DSB formation.

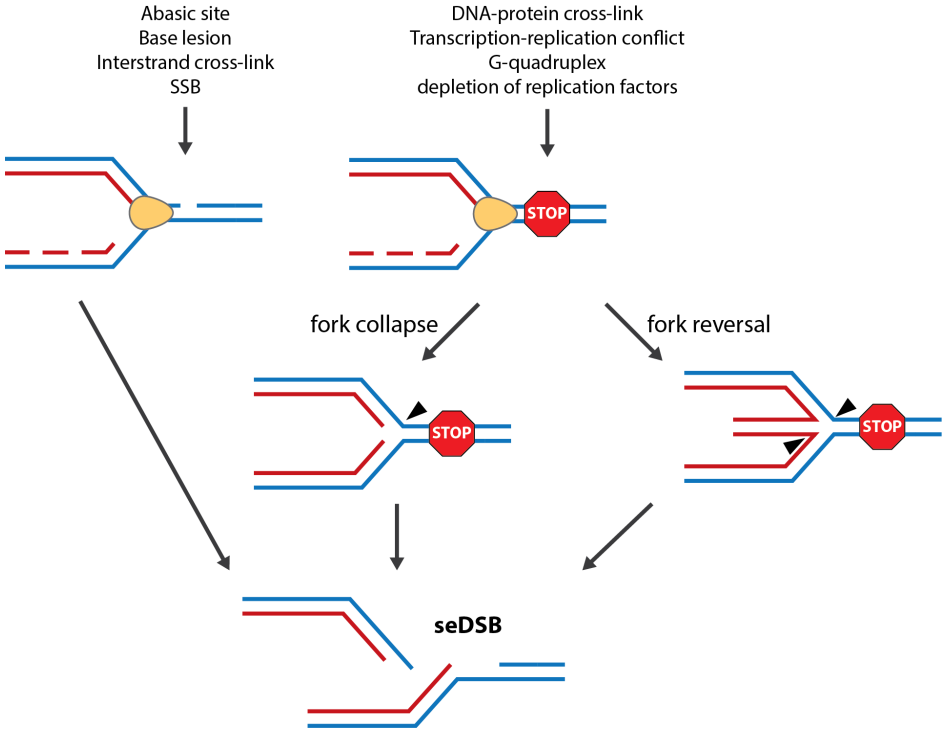

Figure 1. DSB formation at replication forks.
A single-end DSBs can be generated directly by the encounter of the replication machinery (yellow) with a SSB on the template strand (blue). SSB can be produced by exogenous genotoxic agents or result from the cellular processing of different types of DNA damage, such as base lesions, abasic sites and inter-strand cross-links. Fork stalling can arise from several circumstances, like depletion of replication factors and transcription-replication conflicts (TRCs), or can be caused by DNA secondary structures (e.g. G-quadruplexes) or by the presence of bulky DNA lesions (e.g. DNA-protein cross-links). When the replication machinery is blocked, forks can collapse, i.e. replication cannot proceed. Then, the resulting three-strand fork structure can be cleaved to allow repair and continuation of DNA replication. Alternatively, fork stalling leads to fork reversal, when the two newly synthesized strands (red) anneal with each other. Reversed forks, assuming a structure similar to Holliday junctions, are cleaved by specific endonucleases to produce a single-end DSB that is used for fork restart.

1.1.3 Programmed DNA double-strand breaks

DSBs emerged, so far, as very dangerous lesion that pose a threat to genome stability. However, it is important to consider that controlled formation of DSBs play a relevant role in several physiological processes (Mehta and Haber, 2014). Programmed DSB induction

is exploited by cells to carry out three major functions: modification of DNA topology, physical linkage of sister chromosomes and genetic recombination.

Any DNA transaction that requires the opening of the double helix, such as replication and transcription, inevitably produces DNA supercoiling and, consequently, topological stress (Wang, 2002). To relieve topological stress, cells express several essential enzymes dedicated to this function, topoisomerases (Vos et al., 2011). We can distinguish two classes of topoisomerases depending on their mechanism, class I and class II. Generally, topoisomerases introduce a break in DNA, forming a covalent intermediate while a segment of DNA is passed through the gap and, ultimately, they reseal the broken molecule (Wang, 2002). Specifically, class I topoisomerases produce transient SSBs, through which the intact DNA strand is passed to counteract under- or over- winding of the double helix (Wang, 2002). In contrast, class II topoisomerases can cut both DNA strands generating transient DSBs that allow the passage of an intact double-helix segment, thus resolving tangled molecules (Wang, 2002). However, because of their mechanism, class II topoisomerases have the potential to affect genome integrity and, ultimately, have catastrophic effects on cell proliferation (Deweese and Osheroff, 2009). For example, type-II topoisomerases are used as a drug target in cancer therapy (see discussion in 1.1.1).

Meiosis, the specialized cell division through which haploid cells – spores or gametes – are formed, also requires the introduction of DSBs (Lam and Keeney, 2015). DSBs are generated by Spo11, a highly conserved protein evolved from archeal type-II topoisomerases (Keeney et al., 1997). Consistently, Spo11 catalyzes DSB formation via a mechanism similar to class II topoisomerases, leaving Spo11-bound DNA ends (Nichols et al., 1999). DSBs formation is restricted to meiosis I, when it is required to hold together homologous chromosomes for their correct segregation (Lam and Keeney, 2015). Indeed, pairing of homologous chromosomes is achieved through repair of meiosis-specific DSBs via homologous recombination (HR, explained in details in 1.2.3). During HR, Spo11-bound ends are processed to form long ssDNA filaments that associate with a recombinase of the RecA family, which catalyzes the search and strand invasion of a homologous template (Lam and Keeney, 2015). In meiosis, homologous chromosomes, rather than sister chromatids, are preferentially used as template for repair (Lam and Keeney, 2015). Importantly, HR can result in crossover products, which consist in the

exchange of genetic material between homologs and, therefore, promote genetic diversity in the germline.

DSBs are also well-known for their crucial role in lymphocyte development. Diversification of B and T cell antigen-receptors and immunoglobulins (Ig) is fundamental for the recognition of different pathogens. The two processes that ensure their diversity are V(D)J recombination and class-switch recombination (CSR), respectively (Soulas-Sprauel et al., 2007). V(D)J recombination combines different exons to produce a variety of antigen-receptors, whereas CSR exchanges the constant region of immunoglobulin genes to diversify antibody functionality. Both processes begin with the introduction of a DSB, which is mediated by specialized proteins: recombination-activating gene (RAG) endonucleases and the activation-induced cytidine deaminase (AID), respectively (Soulas-Sprauel et al., 2007). These mechanisms are tightly regulated during lymphocyte maturation as incorrect repair can promote chromosomal translocations (Jankovic et al., 2007). Indeed, translocations involving antigen-receptor or immunoglobulin genes were found in several types of lymphoma (Jankovic et al., 2007).

Lastly, mating-type switching in budding yeast is the process by which haploid yeast cells can change their mating type, allowing the formation of diploids starting from a single haploid mother cell (Haber, 2012). Haploid yeast mating type is defined by the expression of either one of two nonhomologous alleles, *MATa* and *MATα* (Haber, 2012). Cells of opposite mating types can conjugate and form a diploid cell; a state in which yeast can proliferate even under environmentally adverse conditions, by undergoing meiosis and sporulation to generate daughter haploid cells (Hanson and Wolfe, 2017). Mating-type switching begins with the introduction of a DSB by the homothallic (HO) endonuclease, which recognizes and cleaves a 24-bp sequence located in the *MAT* locus on chromosome III (Kostriken et al., 1983; Strathern et al., 1982). The DSB generated by HO is subsequently repaired using one of the silenced *MAT* alleles, located in heterochromatic loci at opposite ends of the same chromosome (Haber, 2012). The study of the yeast mating-type switching has been essential to our understanding of the molecular mechanism of homologous recombination as well as of other fundamental processes like gene regulation, heterochromatin formation and chromosomal architecture.

1.2 Repair of DNA double-strand breaks

Eukaryotic cells evolved two principal strategies to repair DNA double-strand breaks: end-joining and homologous recombination (HR). Among the end-joining mechanisms, we can discriminate canonical non-homologous end-joining (NHEJ) and microhomology-mediated end-joining (MMEJ), both of which involve the direct re-ligation of the two broken ends with only little or no sequence homology (Pannunzio et al., 2018). Since these pathways have no template requirement, they can occur independently of the cell cycle phase or chromosomal context. End-joining pathways are rather fast repair strategies, but also potentially mutagenic. Indeed, while canonical NHEJ can be error-free or produce small alterations at the break site, MMEJ will always introduce deletions. Moreover, if end-joining is carried out in the presence of multiple DSBs, incorrect ends can be used as a substrate for ligation, potentially leading to large deletions or chromosomal translocations (Chang et al., 2017). A key limitation of end-joining pathways is that they can only process two-ended DSBs that present a canonical end structure and no bulky adducts, such as covalently attached proteins, which might be inhibitory for end-joining (Ranjha et al., 2018).

On the contrary, homologous recombination requires a homologous template for repair. In cells undergoing mitotic divisions, HR repair will mostly occur during S, G2 and M phases of the cell cycle, when the respective sister chromatid is present and can serve as repair template. For this reason, HR is tightly controlled by cell cycle dependent mechanisms (Orthwein et al., 2015). Notably, HR allows the repair of both single-ended and double-ended DSBs, as well as the repair of protein-bound DSBs (Ranjha et al., 2018). The choice between these different DSB repair mechanisms is determined at the level of DNA end resection (Symington and Gautier, 2011). Resection is a crucial step for HR and consists in extensive nucleolytic degradation of one DNA strand to produce long 3' single-stranded DNA (ssDNA) ends. Therefore, resection disrupts the substrate for re-ligation, thereby preventing NHEJ and committing cells to repair via HR or MMEJ (Symington and Gautier, 2011).

1.2.1 DSB repair by end-joining

End-joining repair can be divided in two sub-pathways: non-homologous end-joining (NHEJ) and microhomology-mediated end-joining (MMEJ) (Figure 2). NHEJ requires little (<4 nt) or no sequence homology between the broken ends, in contrast, MMEJ involves

the annealing of short homologous regions (2-20 nt) that are internal to the broken ends. Therefore, while canonical NHEJ can potentially occur without introducing mutations, MMEJ is always associated with deletions flanking the DSB (Sfeir and Symington, 2015).

Briefly, the mechanism of canonical NHEJ consists in the following steps: DNA end protection, end tethering and alignment, end processing when DNA ends are incompatible for direct ligation and, finally, end ligation. In the first step of NHEJ, the broken ends are protected by the binding of a highly conserved heterodimer, the yeast Yku70-80 (Ku70-80 in human)(Doherty et al., 2001). Yku70-80 inhibits end degradation by resection nucleases (Clerici et al., 2008; Mimitou and Symington, 2010) and is required for recruitment of subsequent NHEJ factors (Chen and Tomkinson, 2011; Gottlieb and Jackson, 1993; Palmbos et al., 2008; Ramsden and Gellert, 1998; Wu et al., 2008; Zhang et al., 2007). In yeast, end tethering, as well as ligation, appears to be dependent on the MRX complex (Mre11-Rad50-Xrs2) (Chen et al., 2001; Moore and Haber, 1996; Zhang et al., 2007), which, in contrast to other NHEJ proteins, is also involved in HR (see 1.2.3 for more details). The role of MRN (MRE11-RAD50-NBS1), the mammalian homologue of MRX, in NHEJ is, thus far, less understood. Nonetheless, similar to yeast, it was reported to have an analogous structural function (Huang and Dynan, 2002; Rass et al., 2009; Xie et al., 2009). In mammalian cells, Ku-bound ends recruit DNA-dependent protein kinase (DNA-PK), which keeps them in close proximity and also stimulates the recruitment and activation of end-processing factors (Chang et al., 2017; Goodarzi et al., 2006; Gu et al., 2010; Löbrich and Jeggo, 2017; Ma et al., 2002). Frequently, DSB ends present overhangs, gaps, chemical modifications or hairpin structures that are not directly ligatable. Therefore, end-processing by nucleases and polymerases is necessary. Several nucleases and polymerases involved in NHEJ have been identified in both yeast and mammals. However, end processing in yeast is much less understood than in mammalian cells. To date, the most studied factors that have been involved in yeast NHEJ are Pol4, responsible for gap filling (Bebenek et al., 2005; Daley and Wilson, 2008; Daley et al., 2005; Tseng and Tomkinson, 2002; Wilson and Lieber, 1999), and Rad27, a flap endonuclease homologue of mammalian FEN1 (Daley and Wilson, 2008; Tseng and Tomkinson, 2004; Wu et al., 1999; Yang et al., 2015). In contrast, a well-known NHEJ nuclease in mammals is Artemis, which is able to cleave a variety of substrates at the boundary between single-stranded and double-stranded DNA (Chang et al., 2017; Goodarzi et al., 2006; Löbrich and Jeggo, 2017; Ma et al., 2002). Similar to yeast, gaps are filled by polymerases related to Pol4, in

particular μ and λ (Bebenek et al., 2014; Moon et al., 2014). Lastly, the final step of NHEJ consists in the ligation of compatible DNA ends by the DNA ligase 4 (Dnl4)-Lif1 complex in yeast and the DNA ligase 4 (LIG4)-XRCC4 complex in mammals (Deshpande and Wilson, 2007; Herrmann et al., 1998; Sibanda et al., 2001; Teo and Jackson, 2000; Wilson et al., 1997).

MMEJ is often considered to contain elements of NHEJ and HR. First, the principle of repair is based on ligation, similar as in NHEJ, but MMEJ requires limited amounts of DNA end resection to expose short homologous sequences and it involves annealing of these homologous sequences prior to ligation (Ranjha et al., 2018; Seol et al., 2018). In addition, several DNA end resection factors, such as the MRX/ MRN complex and DNA2 in human cells, have been involved in MMEJ (Howard et al., 2015; Ranjha et al., 2018). Moreover, canonical NHEJ proteins are not necessary for MMEJ, instead, some of these are even inhibitory, like YKu70-80 (Mimitou and Symington, 2010; Ranjha et al., 2018). The mechanism of microhomology annealing during MMEJ has not been clarified yet, however, it has been shown that RPA interferes with this process probably through its association with ssDNA (Ahrabi et al., 2016; Deng et al., 2014; Mateos-Gomez et al., 2017). Thus, extensive resection producing long ssDNA tracts covered by RPA will inhibit repair via MMEJ and rather promote HR. After annealing of the homologous sequences, non-homologous tails are cleaved by the structure-specific nuclease complexes Rad1-Rad10 and XPF-ERCC1, in yeast and in mammals, respectively. The resulting gap is then filled by Polδ and Pol4 in yeast or Polθ, in mammals (Seol et al., 2018). Interestingly, Polθ was also found to remove RPA from ssDNA, thereby counteracting RPA-dependent inhibition (Mateos-Gomez et al., 2017). Moreover, Polθ is able to prevent Rad51 filament and D-loop formation *in vitro* (Ceccaldi et al., 2015). Together, these observations point towards a key role of Polθ in the regulation of MMEJ, which sometimes is referred to as θ-mediated end-joining (Sfeir and Symington, 2015). Completion of MMEJ is achieved by ligation of ssDNA nicks by LIG3 or LIG1, which act redundantly in mammalian cells, while in yeast, lacking LIG3 or LIG1 homologs, ligation relies on Dnl4 (Seol et al., 2018). In mammals, also XRCC1 and PARP1 have been implicated in MMEJ, specifically in ligation and end tethering, respectively (Seol et al., 2018). Generally, factors involved in MMEJ appear to be divergent between species, suggesting the existence of different MMEJ/alternative-NHEJ pathways. Overall, end-joining mechanisms are a major DSB repair strategy utilized by mammalian cells, in contrast yeast cells mainly employ HR (Sfeir and Symington, 2015). This

difference could reflect cell cycle distribution, as human cells spend most of their time in a G1 cell cycle state, even during proliferation, while yeast cells spend most of their time in G2 and M phases.

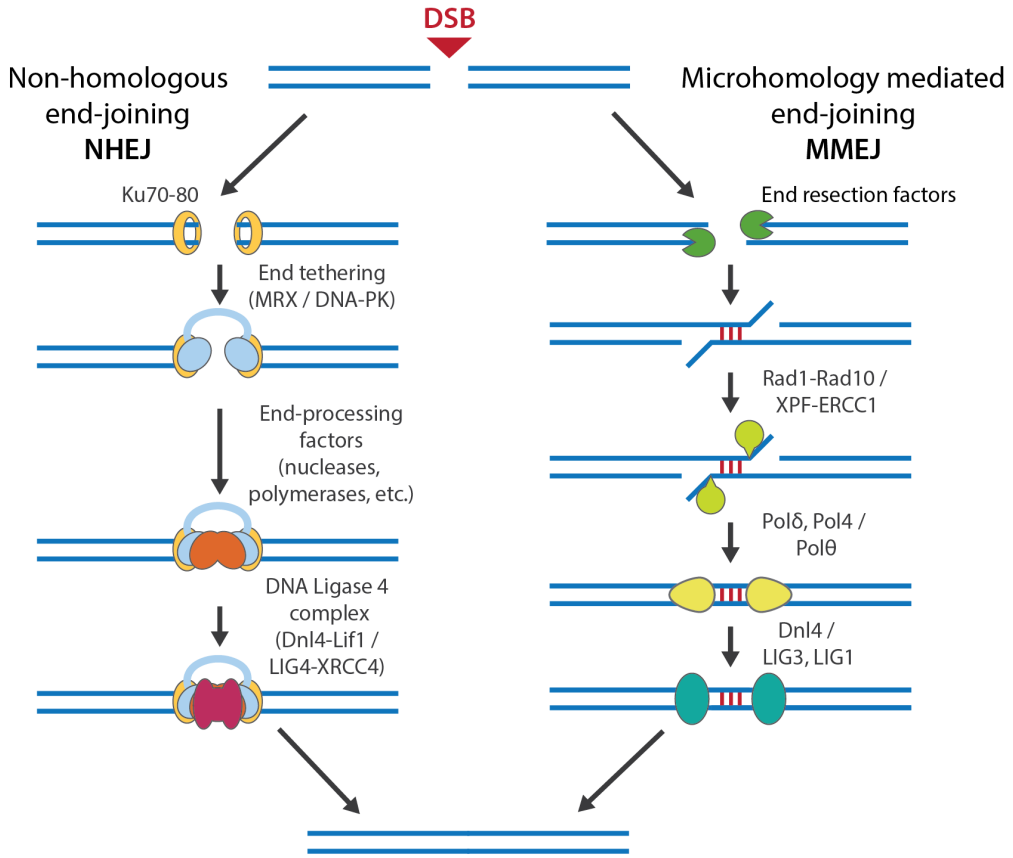

Figure 2. Overview of end-joining repair mechanisms
Schematic representation of the main steps of non-homologous end-joining (NHEJ – left) and microhomology-mediated end-joining (MMEJ – right). Where possible, the names of the yeast / mammalian proteins involved in a specific step are indicated in the figure. NHEJ may involve little or no homology between the broken ends, here, for simplicity, a DSB with blunt ends is represented. NHEJ begins with the protection of broken DNA ends by the binding of Ku70-80. Then, DSB ends are kept in close proximity by MRX/DNA-PK. Subsequently, when the DSB ends are incompatible for ligation, various end-processing factors, such as nucleases and polymerases, are recruited. These include the nuclease Artemis, the flap endonuclease Rad27/FEN1, Pol4/Polμ, Polλ. Repair is completed by ligation of the broken ends catalyzed by a DNA ligase 4 complex. MMEJ, despite being an end-joining mechanism, substantially differs from canonical NHEJ. At the beginning of MMEJ, DSB ends are processed by DNA end resection factors. Resection of the broken ends exposes micro-homologous sequences, which anneal via an unknow mechanism. Then, the Rad1-Rad10/XPF-ERCC1 nuclease complex cleaves non-homologous flanking regions and gaps are filled by Polδ, Pol4/Polθ. Lastly, ligation is performed redundantly by LIG3 and LIG1 in mammals and Dnl4 in yeast.

1.2.2 DSB repair by Homologous Recombination

Recombination comprises several sub-pathways: canonical homologous recombination (HR), synthesis-dependent strand annealing (SDSA), break-induced replication (BIR) and single-strand annealing (SSA) (Kowalczykowski, 2015; Ranjha et al., 2018). The general features and outcomes of these pathways will be discussed in this paragraph (Figure 3). Generally, recombination can produce crossover or non-crossover products, depending on whether one of the regions flaking the DSB is swapped with the template molecule or not, respectively (Figure 3). Crossovers can be genetically silent when they occur reciprocally between sister chromatids. Nonetheless, crossovers can also lead to gross chromosomal rearrangements when they involve unequal exchange of genetic material, for example when recombination takes place between non-homologous chromosomes or between non-homologous loci on sister chromatids.

All recombination pathways involve the process of DNA end resection, which consist in the degradation of one DNA strand resulting in a long ssDNA tract at the break. In HR, SDSA and BIR, this ssDNA filament invades the duplex DNA template displacing one strand (Kowalczykowski, 2015; Ranjha et al., 2018). The resulting three-stranded structure consists of a joint molecule called D-loop (Figure 3). After D-loop formation, the invading strand is extended via DNA synthesis to restore the information lost at the DSB (Wright et al., 2018).

In canonical HR, D-loop formation is followed by the so-called second end capture, which consists in the annealing of the second broken end to the displaced strand of a D-loop, resulting in a double Holliday junction. Double Holliday junctions can be later processed to result in crossover or non-crossover products (Figure 3). Details about the molecular mechanism of recombination will be covered in the next paragraph.

In contrast to HR, during SDSA, the D-loop is disrupted and the newly synthesized DNA anneals to the second end of the broken molecule. This mechanism leads to non-crossover products and, thus, SDSA is one of the most conservative repair processes (Figure 3).

During BIR, extension of the invading strand in the D-loop proceeds until the end of the template chromosome, replicating a whole chromosome arm and resulting in a crossover product (Sakofsky and Malkova, 2017) (Figure 3). Notably, BIR allows the repair of single-ended DSB that are generated, for example, by the collapse of DNA replication forks (Sakofsky and Malkova, 2017).

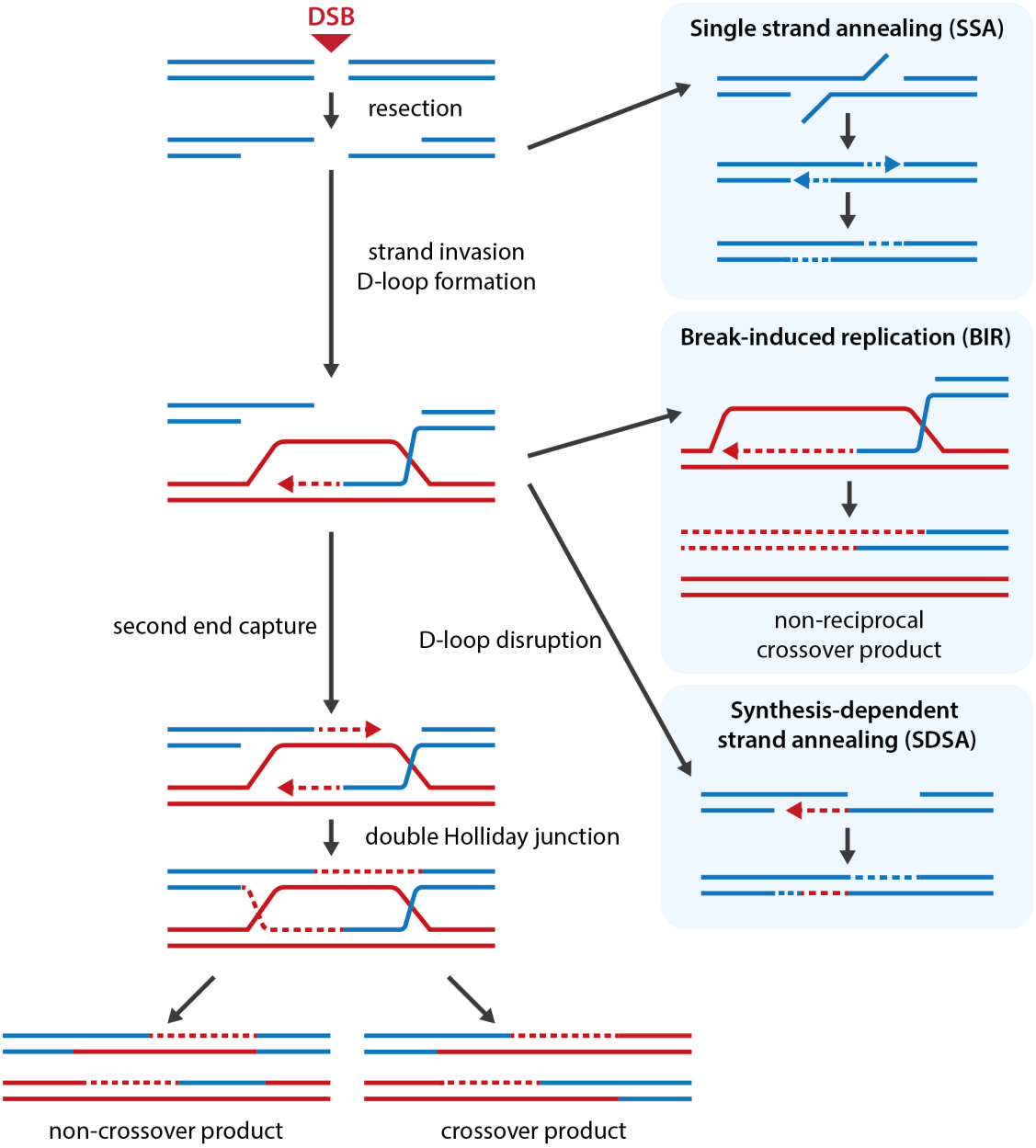

Figure 3. Overview of recombinatorial repair mechanisms
Schematic representation of the main steps of homologous recombination (HR) and the different subpathways: single-strand annealing (SSA), break-induced replication (BIR), synthesis-dependent strand annealing (SDSA) (blue panels). The broken molecule is depicted in blue, the template molecule in red and newly synthesized DNA is represented by dashed lines. The products resulting from different repair pathways involving a template molecule can lead to crossovers or not as indicated, SSA and SDSA never produce crossovers. Refer to paragraph 1.2.2 for more details.

Similar to MMEJ, also SSA involves the exposure of homologous sequences through resection and their subsequent annealing. Non-annealing sequences are removed and the broken ends ligated. However, in contrast to MMEJ, SSA occurs between regions of significant homology (> 200 bp) (Sugawara et al., 2000) and requires extensive DNA end resection. Moreover, the enzymatic machinery taking part in SSA is partially shared with

other recombination sub-pathways and, thus, substantially different from the one involved in MMEJ (Bhargava et al., 2016). SSA is considered a highly mutagenic process, since it occurs between DSB-flanking repeats with the consequent deletion of the region in between (Figure 3).

1.2.3 Molecular mechanism of homologous recombination

Regardless of the sub-pathway of HR, the first step of recombination consists in DNA end resection: the extensive nucleolytic degradation of the 5'-terminated strand at a DSB that produces a long ssDNA tract (Figure 4) (Kowalczykowski, 2015; Ranjha et al., 2018). Resection can be divided in two steps: initiation and elongation, which are also referred to as short-range resection and long-range resection, respectively (Mimitou and Symington, 2008; Zhu et al., 2008). Short-range resection is performed by the evolutionarily conserved MRX/MRN complex together with Sae2/CtIP in budding yeast and human, respectively (Johzuka and Ogawa, 1995; Keeney and Kleckner, 1995; Paull and Gellert, 1998; Sartori et al., 2007; Symington and Gautier, 2011). The MRX/N complex comprises the nuclease Mre11/MRE11, possessing single-strand endonuclease and 3'-5' exonuclease activities; Rad50/RAD50, a member of the structural maintenance of chromosomes (SMC) family that regulates Mre11/MRE11 nuclease activity and is involved in DNA end tethering; Xrs2/NBS1, the least conserved member that has a regulatory function and is involved in the activation of the DNA damage response (DDR) (Desai-Mehta et al., 2001; Deshpande et al., 2016; Furuse et al., 1998; Hopfner et al., 2000, 2002; Jager et al., 2001; Paull and Gellert, 1998; Tsukamoto et al., 2005; Wiltzius et al., 2005). Importantly, after cell cycle-dependent phosphorylation, Sae2 and its orthologue CtIP stimulate Mre11/MRE11 nuclease, thereby constituting the crucial control mechanism that allows resection to occur only during S, G2 and M phases of the cell cycle (Anand et al., 2016; Cannavo and Cejka, 2014; Huertas and Jackson, 2009; Huertas et al., 2008). Resection initiates with the endonucleolytic cutting of the 5'-terminated strand by MRX/N. One the one hand, this creates an entry point for long-range resection nucleases. On the other hand, Mre11/MRE11 catalyzes the degradation the 5'-terminated strand with 3'-5' directionality, resecting towards the DSB, which results in a first 3' ssDNA overhang. Resection by the MRX/N complex occurs only in proximity to the DSB ends and up to approximately 300 nt (Symington and Gautier, 2011). Notably, MRX/N activity is necessary to process chemically modified or protein-bound ends (such as the ones

produced, for example, by IR and Spo11, respectively), while, at least in yeast, it may be dispensable when ends present "clean" 3' hydroxyl and 5' phosphate group (Ranjha et al., 2018; Symington and Gautier, 2011).

In a second step, long-range resection nucleases catalyze further degradation of the 5'-terminated strand with 5'-3' directionality, away from the DSB, to produce up to several kilobases of ssDNA (Figure 4). Long-range resection nucleases are highly conserved between eukaryotes and comprise Exo1/EXO1 and Dna2/DNA2 (Mimitou and Symington, 2008; Zhu et al., 2008). Exo1/EXO1 is an exonuclease that specifically degrades the 5'-terminated strand within dsDNA in 5'-3' direction (Tran et al., 2002), while Dna2/DNA2 can only process ssDNA and, therefore, requires an additional helicase activity (Bae et al., 1998; Zhu et al., 2008). Indeed, Dna2/DNA2 associates with a RecQ family helicase, Sgs1 in yeast and BLM or WRN, in human, to simultaneously open duplex DNA and degrade the 5'-terminated strand (Levikova et al., 2017; Pinto et al., 2016; Sturzenegger et al., 2014).

The 3' ssDNA overhang produced by resection is instantly coated by the ssDNA-binding protein RPA, which prevents its degradation and inhibits secondary structure formation (Figure 4) (Wold, 1997). In the subsequent step of homologous recombination, RPA is exchanged with the recombination protein Rad51/RAD51 to form a nucleoprotein filament (or presynaptic filament), which is key for the recombination mechanism (Figure 4). Indeed, the presynaptic filament catalyzes the fundamental processes of homology search, pairing with template dsDNA to form a so-called synaptic complex, and, ultimately, strand invasion of donor dsDNA generating a D-loop structure (Figure 4) (Heyer et al., 2010; San Filippo et al., 2008; Sung and Robberson, 1995). Rad51/RAD51 loading is mediated by additional recombination factors, so-called mediators, the most important of which are Rad52 in yeast and BRCA2 in higher eukaryotes. Generally, these factors promote RPA displacement and stabilize Rad51/RAD51 binding to ssDNA (Kowalczykowski, 2015). Formation of the presynaptic filament is followed by homology search. The precise mechanism of homology search is still unclear; however, the current model suggests it occurs through proximity-based probing of sequences. While intrinsic chromosome dynamics may be sufficient to find homologies within the damaged chromosome, larger chromatin movements in the nucleus may be required to find more distal homologies (Dion and Gasser, 2013; Miné-Hattab and Rothstein, 2013; Renkawitz et al., 2014).

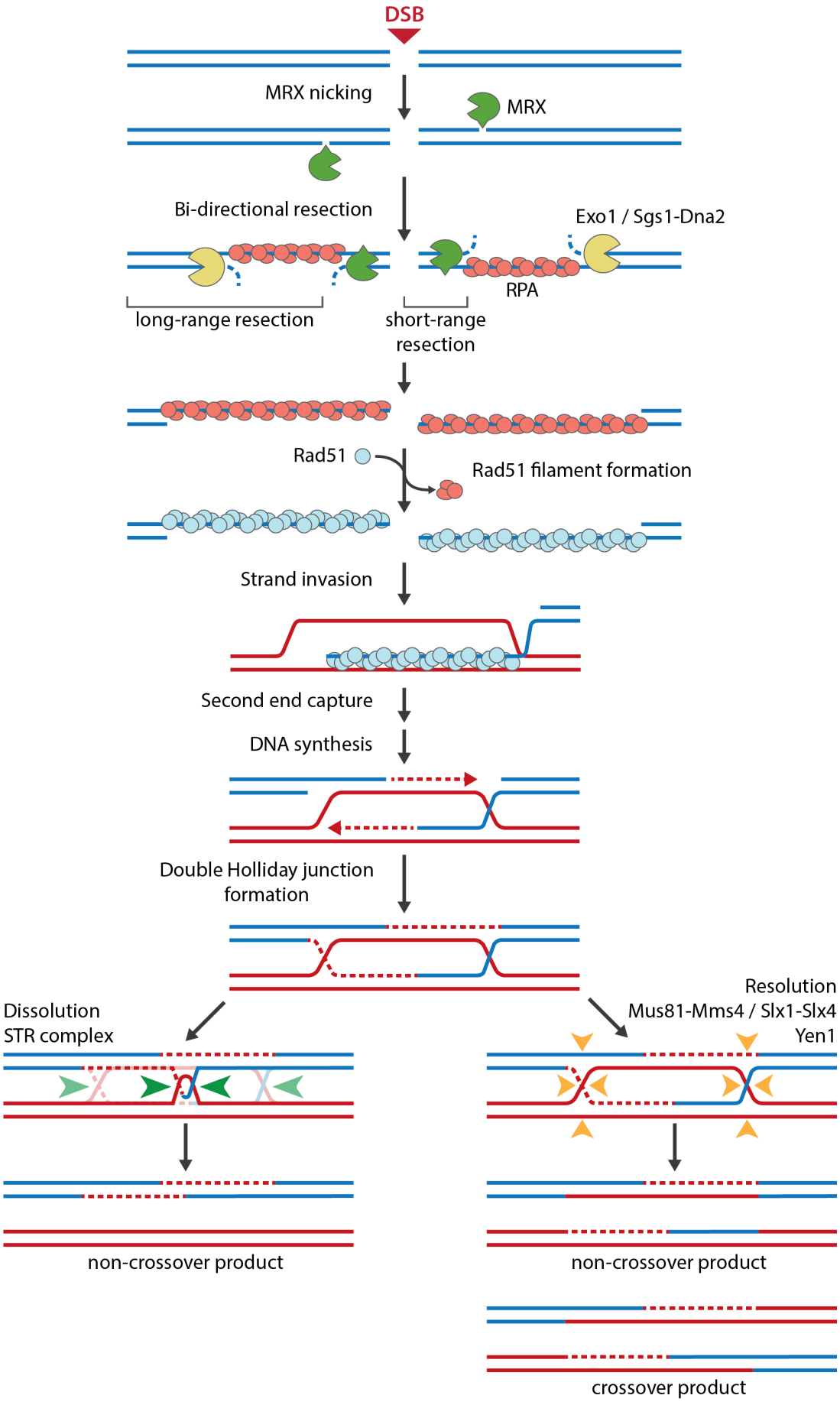
DSB
MRX nicking
MRX
Bi-directional resection
Exo1 / Sgs1-Dna2
RPA
long-range resection
short-range resection
Rad51
Rad51 filament formation
Strand invasion
Second end capture
DNA synthesis
Double Holliday junction formation
Dissolution
STR complex
Resolution
Mus81-Mms4 / Slx1-Slx4
Yen1
non-crossover product
non-crossover product
crossover product

Figure 4. Homogolous recombination mechanism
Schematic representation of the molecular mechanism of homologous recombination. Only *S. cerevisiae* protein nomenclature is shown. HR begins with MRX nicking of the 5'-terminated strands at a DSB, followed by bi-directional resection by MRX, towards the DSB, and Exo1 or Sgs1-Dna2, away from the DSB. Resection results in a long 3' ssDNA overhang that is rapidly coated by RPA. Loading of Rad51 displaces RPA and primes the filament for homology search. Once the homologous sequence is found, the Rad51 filament invades the template duplex. This process is followed by annealing of the second DSB end to the D-loop structure and, subsequently, the two filaments are extended by DNA synthesis. This results in a double Holliday junction, which can be processed by either one of two mechanisms: dissolution and resolution. Dissolution is catalyzed by the STR complex, which promotes branch migration and topological disassociation of the two entangled molecules into exclusively non-crossover products. Resolution is catalyzed by several structure specific endonucleases (Mus81-Mms4, Slx1-Slx4, Yen1), which can produce both crossover or non-crossover products, depending on how ssDNA cuts are introduced at the junctions. For a more detailed description of HR refer to paragraph 1.2.3.

Rad54/RAD54, a member of the Snf2/Swi2 family of superfamily 2 (Sf2) helicases (Flaus et al., 2006) mediates sequence probing during homology search through its dsDNA translocase activity and, possibly, its nucleosome remodeling activity as well (Heyer et al., 2006; Renkawitz et al., 2014). Notably, Rad54/RAD54 appears to be a key factor also in the following steps of homologous recombination, facilitating strand invasion in the template DNA, stabilizing the D-loop structure and removing Rad51/RAD51 from heteroduplex DNA to prompt DNA synthesis (Heyer et al., 2006; Renkawitz et al., 2014; Wright and Heyer, 2014). DNA synthesis further stabilizes the D-loop and restores the information lost at the break site (Figure 4). At this point, recombination can proceed into canonical HR or SDSA that requires D-loop disruption (see Figure 3 and paragraph 1.2.2 for a general description of these mechanisms). Here, the discussion will be focused on the subsequent steps of canonical HR (Figure 4).

In canonical HR, the D-loop is converted into a double Holliday junction (dHJ) after second end capture, a step catalyzed, in yeast, by Rad52 (Nimonkar et al., 2009). In a dHJ, broken and template DNA are intertwined and require specific activities to separate them into two intact molecules. Defects in dHJ processing can lead to aberrant chromosome segregation and genome instability (Wechsler et al., 2011).

Dissolution and resolution are two distinct mechanisms by which HJs are disentangled (Figure 4). Dissolution results in non-crossover products, thus will limit potential loss of heterozygosity (LOH) in vegetatively growing cells, while resolution can lead to both crossover or non-crossover products (Figure 4). The mechanism of dissolution is performed by the Sgs1-Top3-Rmi1 (STR) complex in yeast and by the BLM-TopoIIIα-RMI1-RMI2 (BTRR) complex in human (Bizard and Hickson, 2014). The helicase

Sgs1/BLM catalyzes the migration of the two HJ towards each other (branch migration), together with Top3/TopoIIIα resolving the topological stress arising from this process. The two HJ ultimately converge into a hemicatenated intermediate, a structure where one strand of a DNA molecule is wrapped around one strand of another DNA molecule. These topologically associated molecules are finally separated by Top3/TopoIIIα activity resulting exclusively in non-crossover products (Bizard and Hickson, 2014).

On the other hand, resolution of single and double HJ relies on the coordinated introduction of single-strand cuts at the junction, releasing the entangled molecules into crossover or non-crossover products. Resolution is catalyzed by structure-specific endonucleases (SSE), comprising the yeast Mus81-Mms4 (MUS81-EME1 in human), Slx1-Slx4 (SLX1-SLX4 in human) and Yen1 (GEN1 in human) (Dehé and Gaillard, 2017). Structure-specific endonucleases are able to recognize a variety of structures, specifically Mus81-Mms4 and Slx1-Slx4 act on branched structures and, besides HJ, have been involved in processing of replication forks as well (Ehmsen and Heyer, 2008; Gaillard et al., 2003; Pepe and West, 2014; Rass, 2013; Wyatt et al., 2013). Whereas Yen1/GEN1 displays a preference for HJ cleavage, but recognizes other branched structures as well (Rass, 2013; Rass et al., 2010).

1.3 The role of chromatin in double-strand break repair

In eukaryotes, any DNA transaction, including repair, occurs within chromatin. The basic unit of chromatin is the nucleosome, consisting of about 147 bp of DNA wrapped around an octamer core of histone proteins. Each nucleosome contains two copies of the four core histones H2A, H2B, H3, H4 and can additionally associate with the linker histone H1 or high-mobility group (HMG) proteins, which regulate the DNA length between nucleosomes and contribute to higher order chromatin structure (Luger et al., 1997). Histones and, generally, chromatin proteins are responsible for the different levels of DNA compaction, from the chromatin fiber or “beads on a string” to 3D genome organization found in the nucleus. During evolution, histones acquired a crucial role in gene expression, by regulating the accessibility to the genetic information and serving as a platform for recruitment of other factors. These different functions are achieved through diversification of histone proteins, at the level of post-translational modifications (PTMs) and at the level of histone variants (Soshnev et al., 2016). Moreover, all DNA transactions including transcription and DNA replication, require the activity of chromatin

remodelers, a specialized set of enzymatic machineries that can evict, position and edit nucleosomes (Clapier and Cairns, 2009; Clapier et al., 2017).

It is therefore important to consider DSB repair in the context of chromatin. Indeed, it emerged from numerous studies of the last two decades, that nucleosomes and chromatin remodelers have a prominent role in DNA damage response, DSB repair and repair pathway choice (Clouaire and Legube, 2019; Hauer and Gasser, 2017; Seeber et al., 2013). In this chapter, the discussion will be focused on how chromatin and nucleosome remodelers participate, specifically, in DSB repair.

1.3.1 Histones PTMs in response to DNA double-strand breaks

Generally, histones are subject to post-translational modifications that primarily occur on their N- and C-terminal tails protruding from the nucleosome core. PTMs comprise a variety of chemical modifications, such as phosphorylation, methylation, acetylation, ubiquitylation, SUMOylation and PARylation (Smeenk and van Attikum, 2013), which can confer different properties to the histones or nucleosomes bearing them. Specifically, histone PTMs are able to affect nucleosome stability and compaction level of the chromatin fiber and, in addition, they can provide differential binding sites for effector proteins. Therefore, as for all DNA processes, histone PTMs are crucial also for the DDR. In this chapter, the most relevant histone PTMs involved in DSB repair will be described.

Upon DNA damage, a key mark on chromatin is the phosphorylation of histone H2A on serine 129 (γH2A) in yeast or phosphorylation of histone variant H2A.X on serine 139 (γH2A.X) in mammalian cells. This modification is catalyzed by phosphoinositide-3-kinase-related kinases, specifically ATR, ATM and DNA-PK in mammals and the ATR and ATM orthologues Mec1 and Tel1 in yeast, respectively. Thereby, γH2A/γH2A.X decorate nucleosomes flanking the break and extend over large chromatin domains, guided by 3D genome architecture (Arnould and Legube, 2020; Clouaire and Legube, 2019). The establishment of such chromatin domain is important to elicit an appropriate DNA damage response. Specifically, γH2A/γH2A.X is directly involved in the recruitment of checkpoint and repair proteins. Among these, there are the mammalian checkpoint mediator MDC1 and the yeast Rad9 (53BP1 in human), a checkpoint signaling mediator and regulator of resection (Hammet et al., 2007; Javaheri et al., 2006; Lou et al., 2006). Moreover, also several chromatin remodelers, such as SWR1, INO80 and SWI/SNF have

been found to be recruited to DSBs via interaction with γH2A/γH2A.X (Attikum et al., 2007; van Attikum et al., 2004; Chai et al., 2005; Downs et al., 2004; Morrison et al., 2004). Besides H2A/H2A.X, phosphorylation of other histones has been shown at DSBs. In yeast, phosphorylation of H4 at serine 1 appears to be important for NHEJ and H2B phosphorylation at tyrosine 129 has also been observed at DSBs, however its role in DSB repair is not clear yet (Cheung et al., 2005; Lee et al., 2014).

Histone mono-, di- and tri- methylation is catalyzed by specific enzymes, histone methyltransferases (HMTs) that use S-adenosylmethionine to transfer methyl groups to lysine or arginine residues (Kouzarides, 2002). Generally, histone methylation is associated with heterochromatic sites, characterized by higher level of chromatin compaction and by gene repression. In yeast, H3K79 methylation by Dot1 at DSBs is required, together with γH2A, for Rad9 recruitment (Grenon et al., 2007; Wysocki et al., 2005). While the human Rad9 orthologue, 53BP1, recognizes H4K20 methylation, a mark that is always present in heterochromatin and becomes exposed upon DSB induction (Botuyan et al., 2006).

In contrast to methylation, histone acetylation is a modification generally associated with active gene transcription and open chromatin and it is catalyzed by histone acetyltransferases (HATs) (Eberharter and Becker, 2002). Both in yeast and human cells, several HATs are recruited to DSB sites, where they mediate the acetylation of several lysine residues on different histones. Among human HATs, TIP60, MOF1, CBP and p300 have been involved in DSB repair (Smeenk and van Attikum, 2013). Particularly, recruitment of the SWI/SNF nucleosome remodeler appears to depend on CBP and p300 acetylation of H3K18 and of several H4 lysine residues (Ogiwara et al., 2011). Analogously, acetylation of N-terminal lysines of histone H3 and H4 in yeast have been shown to be important for DSB repair (Bird et al., 2002; Tamburini and Tyler, 2005). Interestingly, activity of the yeast HATs Gcn5 and Esa1 (part of the NuA4 complex) is crucial for SWI/SNF association at DSB sites (Bennett and Peterson, 2015), suggesting that histone acetylation might be a common mechanism to promote SWI/SNF recruitment to DSBs in eukaryotic cells.

Ubiquitylation is another important histone PTM that was shown to coordinate the DNA damage response. For example, in mammalian cells, a ubiquitylation cascade mediated by the ubiquitin (Ub) ligases RNF8/RNF168 and involving the ubiquitylation of H2A, H2A.X and H2B at several residues plays an important role in the recruitment of DNA repair

factors, such as 53BP1 and BRCA1 (Smeenk and van Attikum, 2013; Van and Santos, 2018). Moreover, BRCA1 itself was shown to interact with BARD1, forming a ubiquitin ligase complex that catalyzes H2A ubiquitylation (Densham et al., 2016; Kalb et al., 2014; Witus et al., 2021). Interestingly, BRCA1-BARD1-dependent H2A ubiquitylation at DSBs appears to stimulate HR, likely through the recruitment of SMARCAD1, a chromatin remodeler known for its role in promoting resection (Densham et al., 2016) (discussed in details in 1.3.6). Also in budding yeast, histone ubiquitylation, specifically of H2B on lysine 123, seems to contribute to the DDR via activation of the checkpoint kinase Rad53 (Giannattasio et al., 2005).

Lastly, histone tails can be modified via PARylation, the synthesis of poly(ADP-ribose) (PAR) chains by proteins of the PARP (poly(ADP-ribose) polymerase) family (Messner et al., 2010). Nucleosome PARylation was shown to induce chromatin relaxation (Lagueux et al., 1994; Poirier et al., 1982). Interestingly, studies on mammalian cells have identified this modification to be enriched at DSBs, where it has been proposed to favor chromatin relaxation, possibly in conjunction with the activity of nucleosome remodelers (Smeenk and van Attikum, 2013). Notably, DSB-depended PARylation appears to direct the recruitment of the chromatin remodeler ALC1 to DSBs (Gottschalk et al., 2009; Smeenk and van Attikum, 2013). However, the precise mechanism of recruitment of ALC1 and its subsequent function are still unclear.

1.3.2 Effects of chromatin remodelers on nucleosome organization

In eukaryotic cells, the presence of nucleosomes on DNA requires the activity of specific machineries – ATP-dependent chromatin remodelers – to regulate DNA accessibility during processes like transcription, replication and DNA repair. Typically, cells possess several chromatin remodelers, as protein complexes or single subunits, which have distinct effects on nucleosomes. Specifically, the activities of chromatin remodelers can be divided into (i) nucleosome sliding and eviction, (ii) nucleosome positioning and (iii) nucleosome editing (Figure 5). Despite the variety in their functions, all chromatin remodelers possess an ATPase subunit or domain that belongs to the RecA-like helicase superfamily 2 (SF2) and it is thought to work via closely related mechanisms (Clapier and Cairns, 2009; Clapier et al., 2017). Indeed, to date, evidence suggests that the ATPase domains of chromatin remodelers catalyze, via a shared mechanism, DNA translocation to break histone-DNA interactions and to move DNA along the nucleosome surface

(Clapier and Cairns, 2009; Clapier et al., 2017). According to this model, effects of chromatin remodelers on nucleosomes depend on their accessory subunits and/or substrate specificity, likely mediated by histone modifications, histone variants and by interactions with other factors (Clapier and Cairns, 2009; Clapier et al., 2017). Chromatin remodelers have been divided into several subfamilies based on the conservation of their ATPase subunit and their function (Clapier et al., 2017; Flaus et al., 2006). The most studied of these subfamilies, which are conserved from yeast to humans, comprise ISWI, CHD, SWI/SNF and INO80. This chapter will briefly introduce the different remodeling activities and which subfamilies of remodelers are primarily involved (Figure 5).

Nucleosome positioning consists in the formation of so-called nucleosome arrays, in which nucleosomes are regularly spaced at specific distances from each other. Nucleosome arrays can be found, for example, in the promoter region of actively transcribed genes (Baldi et al., 2020; Lai and Pugh, 2017). This function is mainly carried out by remodelers belonging to the ISWI and CHD subfamilies, namely Chd1, Isw1 and Isw2 in yeast. However, the yeast Ino80-C has also been implicated in nucleosome positioning as well (Gkikopoulos et al., 2011; Krietenstein et al., 2016; Kubik et al., 2019; Oberbeckmann et al., 2021a; Ocampo et al., 2016).

Access to the DNA molecule requires nucleosome sliding along DNA and, possibly, even their eviction to expose, for example, binding sites of transcriptional activators or repressors. In yeast, SWI/SNF and RSC, both belonging to the SWI/SNF subfamily, are the primary remodelers involved in this activity (Clapier and Cairns, 2009; Clapier et al., 2017).

Lastly, nucleosome editing implies the replacement of histone subunits with their canonical form or with one of their variants. Such activity is crucial to establish specialized chromatin domains, such as centromeric regions (Henikoff and Dalal, 2005), and to provide or remove binding sites for other factors. Specifically, H2A/H2A.Z exchange is known to be catalyzed by remodelers of the INO80 subfamily, such as yeast Swr1 and Ino80-C, as well as SRCAP, p400 and INO80-C in human cells (Clapier and Cairns, 2009; Clapier et al., 2017).

A considerable number of studies have found several remodelers to be recruited at DSBs (Attikum et al., 2007; van Attikum et al., 2004; Bantele et al., 2017; Bennett and Peterson, 2015; Bennett et al., 2013; Bird et al., 2002; Chai et al., 2005; Chen et al., 2012; Costelloe et al., 2012; Downs et al., 2004; Eapen et al., 2012; Gnugnoli et al., 2021; Lademann et al.,

2017; Morrison et al., 2004; Shim et al., 2005, 2007; Tsukuda et al., 2005). It is reasonable to assume that chromatin remodelers would promote or regulate DSB repair by carrying out the same activities described above. The role of the chromatin remodelers involved in DSB repair will be analyzed in the next chapters, with a focus on DNA end resection.

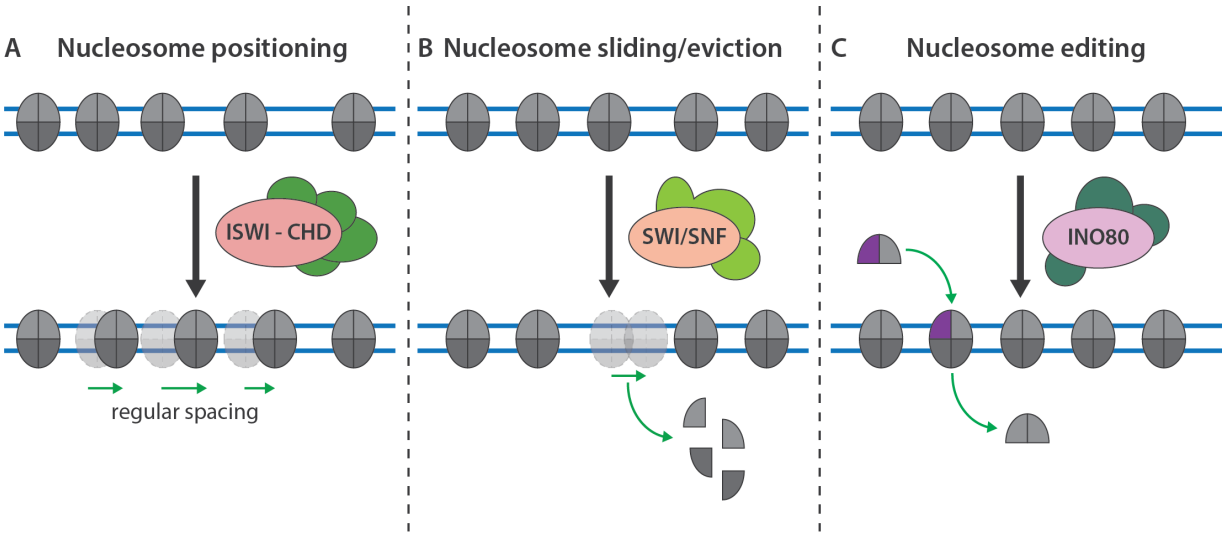

Figure 5. Chromatin remodeler activities and their effects on nucleosomes
The activity of different chromatin remodelers can result in three distinct effects on nucleosomes (in shades of grey): positioning, sliding/eviction and editing. A) Several remodelers have the ability to space nucleosomes at fixed distances from each other (position), forming nucleosome arrays. This activity is primarily catalyzed by remodelers of the ISWI and CHD subfamilies (see 1.3.2 and 1.3.4 for more details). B) Virtually all remodelers can slide nucleosomes, however, mainly the SWI/SNF subfamily members are able to evict nucleosomes by destabilizing histone-DNA contacts. C) Remodelers of the INO80 subfamily can change nucleosome composition by replacing canonical histones (grey) with histone variants (purple) or viceversa.

1.3.3 Nucleosome eviction and resection of double-strand breaks

A crucial step in DSB repair is DNA end resection, not only because it is the first step in homologous recombination, but also because it removes the substrate for NHEJ and, as such, constitutes a fundamental point of control for DSB repair pathway choice. Importantly, the process of DNA end resection requires nucleases to access DNA, which could be prevented by the presence of nucleosomes, thereby constituting an additional layer of control for resection. Consistently, there is evidence suggesting that resection nucleases are specifically inhibited by nucleosomes. In particular, the initial Mre11 endonucleolytic cut appears to preferentially occur in linker DNA, suggesting that nucleosomal DNA may be resistant to Mre11 nicking (Mimitou et al., 2017; Wang et al., 2017). Moreover, we can speculate that the 3'-5' exonucleolytic activity of Mre11 might

be particularly inhibited by nucleosomes located between the initial nick and the DSB. However, further studies are needed to confirm this possibility. Importantly, resection by both long-range resection nucleases, Exo1 and Sgs1-Dna2, appears to be strongly hindered by the presence of nucleosomes (Adkins et al., 2013), indicating that additional factors, such as chromatin remodelers, are required to relieve this barrier. Interestingly, Exo1 was shown to be able to bypass H2A.Z-containing nucleosomes *in vitro* (Adkins et al., 2013), likely due to their reduced stability (Abbott et al., 2001; Jin and Felsenfeld, 2007; Zhang et al., 2005).

Cells could overcome this nucleosome barrier through nucleosome eviction, possibly mediated by chromatin remodelers. Consistent with this hypothesis, nucleosome eviction has been observed around resected DSBs in numerous studies (Attikum et al., 2007; Bantele and Pfander, 2019; Chen et al., 2008; Mimitou et al., 2017; Tsukuda et al., 2005, 2009). Importantly, two remodelers known for their evicting activity, SWI/SNF and RSC, have been shown to locate at DSBs (Bennett and Peterson, 2015; Bennett et al., 2013; Chai et al., 2005; Kent et al., 2007; Liang et al., 2007; Shim et al., 2005, 2007; Wiest et al., 2017), suggesting an involvement in DSB repair. Indeed, Mre11 recruitment to DSBs is impaired in both SWI/SNF and RSC yeast mutants (Shim et al., 2007; Wiest et al., 2017). Currently, it is unclear by which mechanism these remodelers promote MRX binding; whether they do so by sliding or evicting nucleosomes and whether they might also facilitate MRX nucleolytic activity. Nonetheless, in both mutants, nucleosome eviction at DSBs is delayed or reduced, suggesting that they might play an early role in promoting DNA end resection (Shim et al., 2007; Wiest et al., 2017). However, RSC and SWI/SNF recruitment at DSBs seems to follow different kinetics and, accordingly, it appears to occur by distinct pathways. RSC was shown to bind in the proximity of a DSB within 10 minutes after induction and likely before resection initiation (Chai et al., 2005), via an unknown mechanism. In contrast, SWI/SNF recruitment was detected significantly later (Chai et al., 2005), likely via recognition of acetylated histones by its several bromodomains (Bennett and Peterson, 2015; Cheng et al., 2021). Consistently, the histone acetyltransferase NuA4 was shown to be recruited at DSBs (Cheng et al., 2021). Moreover, in agreement with its later recruitment, SWI/SNF was also found to promote long-range resection (Wiest et al., 2017). Altogether, these data point towards a role of RSC and SWI/SNF in facilitating resection in yeast, presumably via their evicting activity.

RSC and SWI/SNF remodelers have been involved in the DDR and in later steps of HR as well (Chai et al., 2005; Kent et al., 2007; Shim et al., 2007; Wiest et al., 2017). In particular, RSC mutants show a decrease in γH2A levels (Kent et al., 2007; Shim et al., 2007), while defective SWI/SNF correlates with reduced activation of Rad53, the DDR effector kinase (Wiest et al., 2017). SWI/SNF and RSC were also found to be required during HR in synapsis formation and in post-synaptic steps, respectively (Chai et al., 2005). However, it is not clear whether they contribute to these processes via a mechanism independent from their evicting activity.

Moreover, the role of SWI/SNF remodelers in DSB repair appears to be conserved in humans as well. Similarly to yeast, BAF (homologue of SWI/SNF) and PBAF (homologue of RSC), are also recruited to DSBs and they facilitate resection (Hays et al., 2020; Park et al., 2006). However, whether this function depends on their nucleosome eviction activity still needs to be tested.

Since remodelers share a common DNA translocation mechanism, it is possible that also other subfamilies of remodelers contribute to nucleosome eviction. Indeed, several studies found that INO80's function is important for resection (Attikum et al., 2007; van Attikum et al., 2004; Gospodinov et al., 2011). Interestingly, this seems to depend on a role of INO80 in promoting nucleosome eviction (Attikum et al., 2007; Tsukuda et al., 2005). Consistently, INO80 has been involved in nucleosome eviction at promoters of actively transcribed genes as well (Qiu et al., 2020). These observations suggest that INO80 might be able to catalyze different remodeling reactions at DSBs (see also 1.3.4 and 1.3.5). Therefore, more studies are needed to elucidate the precise role of INO80 in homologous recombination.

1.3.4 Nucleosome positioning at double-strand breaks

Nucleosome organization has been extensively studied in yeast, particularly in the context of transcribed genes. Typically, promoters are characterized by a nucleosome-free region (NFR) that is followed by a regularly spaced array of nucleosomes over the gene body (Baldi et al., 2020; Weiner et al., 2010; Yuan et al., 2005). To date, four remodelers have been identified to contribute to the specific spacing observed at transcribed genes in yeast: Chd1, Isw1a, Isw2 and Ino80 (Gkikopoulos et al., 2011; Krietenstein et al., 2016; Kubik et al., 2019; Oberbeckmann et al., 2021a; Ocampo et al., 2016). Biochemical and structural studies have showed that these nucleosome remodelers employ intrinsic

molecular rulers and sensing of different DNA shapes to position nucleosomes at fixed distances (Krietenstein et al., 2016; Oberbeckmann et al., 2021a, 2021b; Yamada et al., 2011). In addition to this, positioning remodelers appear to be guided by barrier-factors, like the general regulatory factors Abf1, Rap1 or Reb1 in yeast or CTCF in mammals, which bind to specific DNA sequences located, for example, at gene promoters, replication origins and at other functionally distinct genomic loci (Eaton et al., 2010; Fu et al., 2008; Krietenstein et al., 2016; Kubik et al., 2019; Li et al., 2015; Rossi et al., 2018; Wiechens et al., 2016). Interestingly, a recent *in vitro* study reported that also DSBs are sensed as barrier-factors to which nucleosomes are subsequently phased (Oberbeckmann et al., 2021a). Nucleosome repositioning after DSB induction has been observed *in vivo* as well, but so far only at specific genomic loci such as *MAT* and the *PHO5* gene (Kent et al., 2007; Shim et al., 2007; Tripuraneni et al., 2021; Tsabar et al., 2016). However, whether such repositioning coincides with the formation of nucleosome arrays and involves the activity of positioning remodelers still needs to be determined. Importantly, a considerable amount of studies in yeast and human cells reported a role for remodelers of the ISWI, CHD1 and CHD7 subfamilies in homologous recombination (Casari et al., 2021; Gnugnoli et al., 2021; Kari et al., 2016; Lan et al., 2010; Nakamura et al., 2011; Rother et al., 2020; Smeenk et al., 2012; Toiber et al., 2013; Zhou et al., 2018). Interestingly, several of these remodelers were found to be recruited at DSBs and to promote resection as well (Delamarre et al., 2020; Gnugnoli et al., 2021; Kari et al., 2016; Rother et al., 2020; Smeenk et al., 2012; Toiber et al., 2013). Overall, these data suggest that positioning remodelers have a role in HR. However, it is unclear by which mechanism they act and whether this mechanism involves nucleosome spacing. Moreover, even if this latter hypothesis would be verified, it is still unclear whether nucleosome arrays would facilitate resection or whether they would merely arise as a consequence of the intrinsic nucleosome positioning activity of remodelers recruited to DSBs for other tasks.

1.3.5 Nucleosome editing at double-strand breaks

As described above, changes in the histone composition of a nucleosome can modify its properties, such as stability, the set of post-translational modifications that decorate its histones and its interactions with neighboring nucleosomes or with other factors (Talbert and Henikoff, 2017). In eukaryotes, numerous histone variants with different degrees of conservation can be found. Notably, of these, variants of H2A and H3 are present in nearly

every eukaryote, from yeast to humans (Talbert and Henikoff, 2010). Generally, H3 variants are deposited via *de novo* nucleosome assembly, whereas H2A variants can be directly incorporated in pre-existing nucleosomes via exchange of H2A-H2B dimers (Talbert and Henikoff, 2017). Therefore, it is reasonable to speculate that incorporation of H2A variants may be of relevance at DSBs. Indeed, both in yeast and human cells, a transient increase in H2A.Z incorporation around DSBs has been detected (Alatwi and Downs, 2015; Gursoy-Yuzugullu et al., 2015; Kalocsay et al., 2009; Nishibuchi et al., 2014; Xu et al., 2012). Moreover, SWR1, the remodeler responsible for H2A.Z deposition, was found to be recruited at DSBs in yeast (Attikum et al., 2007; Morillo-Huesca et al., 2010). Interestingly, H2A.Z-containing nucleosomes are less stable than canonical ones (Abbott et al., 2001; Jin and Felsenfeld, 2007; Zhang et al., 2005) and, thus, they may be overcome more easily by resection nucleases (Adkins et al., 2013) or become more easily evicted by chromatin remodelers. This may represent one mechanism by which H2A.Z incorporation could facilitate DNA end resection. Accordingly, the absence of H2A.Z correlates with a strong defect in resection (Kalocsay et al., 2009; Lademann et al., 2017). In addition, H2A.Z could also provide binding sites for the recruitment of HR factors (Xu et al., 2012).

As previously mentioned, also the INO80 complex is involved in H2A/H2A.Z exchange and, specifically, it catalyzes H2A.Z removal and incorporation of canonical H2A, counteracting SWR1 activity (Ayala et al., 2018; Eustermann et al., 2018). Consistently, accumulation of H2A.Z around DSBs was observed in INO80-C deficient cells (Alatwi and Downs, 2015; Lademann et al., 2017; Papamichos-Chronakis et al., 2006). Interestingly, this affected Rad51 filament formation, downstream of resection. Whereas the role of INO80-C in promoting resection seems to be independent from its H2A.Z removal activity (Lademann et al., 2017), in agreement with the proposed function of H2A.Z in resection. These observations suggest that INO80-C might act differently at distinct steps during the HR pathway and, moreover, that INO80-C recruitment at DSBs might serve several functions, including nucleosome eviction, editing and possibly positioning (see discussion above).

The later function of INO80 in HR appears to be conserved in higher eukaryotes as well (Alatwi and Downs, 2015). Indeed, nucleosome editing by INO80 is required in human cells to promote Rad51 binding after resection (Alatwi and Downs, 2015). Overall, it appears that a dynamic exchange of H2A/H2A.Z is necessary for the successful repair of DSBs via homologous recombination.

1.3.6 Alternative roles of chromatin remodelers at double-strand breaks: the antagonism between Fun30 and Rad9

Fun30 and its orthologues Etl1 (mouse) and SMARCAD1 (human) are evolutionarily conserved single subunit remodelers, original members of a distinct subfamily (Flaus et al., 2006). The catalytic mechanism of Fun30 is still not entirely clear (Bantele and Pfander, 2019). A recent study showed that SMARCAD1 can both evict and assemble entire nucleosomes *in vitro* (Markert et al., 2021), whereas yeast Fun30 was found to be able to slide nucleosomes and exchange histone dimers as well (Awad et al., 2010). Notably, despite their possibly different remodeling mechanisms, Fun30 and SMARCAD1 appear to have a conserved function in promoting long-range resection. Fun30 deletion mutants display delayed long-range resection and defects in resection-dependent repair pathways (Bantele et al., 2017; Chen et al., 2012; Costelloe et al., 2012; Eapen et al., 2012). Moreover, Fun30 is specifically recruited to DSBs via a conserved mechanism that involves the 9-1-1 complex, binding at ss-dsDNA junctions at resected DSBs, and requires Fun30 phosphorylation during S and M phases of the cell cycle, when HR and thereby resection are enabled (Bantele et al., 2017; Chen et al., 2016). Interestingly, Exo1 was shown to be unable to process nucleosomal substrates *in vitro* even in the presence of Fun30 (Adkins et al., 2013), suggesting that Fun30's mechanism might not involve simple nucleosome eviction and that it might require other factors. Importantly, it was observed that the resection defect of *FUN30* mutants was rescued by the deletion of *RAD9*, a gene encoding for a well-known resection inhibitor (Bantele et al., 2017; Chen et al., 2012). These results point towards a reciprocal antagonism between Fun30 and Rad9. Interestingly, this mechanism seems to be conserved in humans as well, where SMARCAD1 functions as resection activator and 53BP1, the Rad9 orthologue, as resection inhibitor (Bothmer et al., 2011; Bunting et al., 2010; Costelloe et al., 2012; Densham et al., 2016; Lazzaro et al., 2008). Recruitment of Rad9 and its orthologues at DSBs occurs via the recognition of multiple histone PTMs (Botuyan et al., 2006; Fradet-Turcotte et al., 2013; Grenon et al., 2007; Hammet et al., 2007; Hu et al., 2017; Huyen et al., 2004; Toh et al., 2006; Wilson et al., 2016; Wysocki et al., 2005). Therefore, a potential mechanism by which Fun30 could facilitate resection might involve remodeling of Rad9-bound nucleosomes. Several scenarios are plausible: Fun30 might directly remove Rad9 from nucleosomes, it might slide or evict entirely Rad9-bound nucleosomes or it can catalyze

histone dimer exchange to deplete Rad9 binding sites. Further studies are required to elucidate the function of Fun30 at DSBs.

2. Aim of the study

During homologous recombination (HR), DNA double-strand break ends are converted to single-stranded DNA (ssDNA) overhangs by a dedicated set of nucleases in a process called DNA end resection. In eukaryotic cells, DNA end resection, similarly to any DNA transaction, occurs in the context of chromatin. Seminal studies have revealed that the presence of nucleosomes on DNA constitutes a roadblock for resection nucleases. Consistently, a multitude of chromatin remodelers have been involved in homologous recombination, supporting resection as well as later steps of HR. Nonetheless, the exact fate of nucleosomes during DNA end resection was unclear. In particular, several studies showed evidence for nucleosome eviction, while others suggested that nucleosomes might be present on the ssDNA produced by resection. Technical limitations of previous studies, based on conventional chromatin-IP experiments may have been responsible for these contradictory results.

Therefore, we sought out to establish a ChIP-sequencing technique that, in combination with site-specific induction of DSBs, would allow us to determine whether proteins bound to single-stranded or double-stranded DNA at resected DSBs *in vivo*. Then, we aimed at investigating whether nucleosomes bound to the ssDNA resulting from resection and whether they were evicted in concomitance with resection. Lastly, in case we could obtain evidence for nucleosome eviction, another aim of this project was to identify whether and which nucleosome remodelers were involved in this activity.

3. Results

3.1 Strand-specific ChIP-sequencing

Chromatin immuno-precipitation (ChIP) is, to date, the gold-standard technique to precisely determine chromatin binding of repair proteins at sites of DSBs. However, a caveat of ChIP-based methods is that they can only measure the aggregate of signals arising from the entirety of a cell population. This limitation becomes especially significant in the context of resected DSBs, where resection initiation and elongation are stochastic, even when a single site-specific DSBs is induced simultaneously in a cell ensemble (Zierhut and Diffley, 2008). Therefore, the distinction between the ssDNA and dsDNA compartments of a resected DSB often relies solely on the spatial information provided by the detection of ssDNA-binding proteins (e.g. RPA, Rad51), labelling the area of resection around the DSB. Colocalization of repair proteins with ssDNA binding proteins is used as indicator of binding to resected DNA, but this type of comparison is prone to lead to misinterpretation and controversies: for example, compare the strand-separated plots in Figure 7B and Figure 8 to the forward-plus-reverse plots in Figure 9.

For this reason, we decided to utilize strand-specific ChIP-sequencing to be able to directly visualize if proteins bind to ssDNA or dsDNA at resected DSBs. Strand-specific ChIP-seq utilizes unique steps during library preparation. Indeed, in contrast to classical library preparation protocols, where sequencing adapters are ligated directly to dsDNA molecules (Meyer and Kircher, 2010), here we first denature the DNA and then ligate sequencing adapters to the 3' end of ssDNA in an adaptase-mediated reaction (Figure 6A). In this way, strand identity is retained and protein enrichment can be unequivocally determined for each DNA strand (Figure 6A). Moreover, we avoid the loss of resected ssDNA that would occur during the pre-processing steps (blunting and A-tailing) of standard library preparation methods (Meyer and Kircher, 2010). Adaptase-based library preparation was already employed successfully to analyze parental histone transfer to replicating DNA strands (Gan et al., 2018) and for genome-wide mapping of sites of irreparable DNA damage, marked by ssDNA-bound Rad52 (Costantino and Koshland, 2018).

For this thesis, we combined strand specific ChIP-sequencing with systems in *Saccharomyces cerevisiae* by which we can induce either one or multiple site-specific

DSBs. In such setting, given the specific polarity of resection that leaves 3' ssDNA overhangs at a DSB, we observed ssDNA-binding proteins enriching forward strands upstream of the DSB and reverse strands downstream of the DSB, while dsDNA binding proteins will have no strand preference and equally enrich forward and reverse strands. Additionally, dsDNA-binding proteins are expected to show a decreased signal in the resected area (Figure 6B).

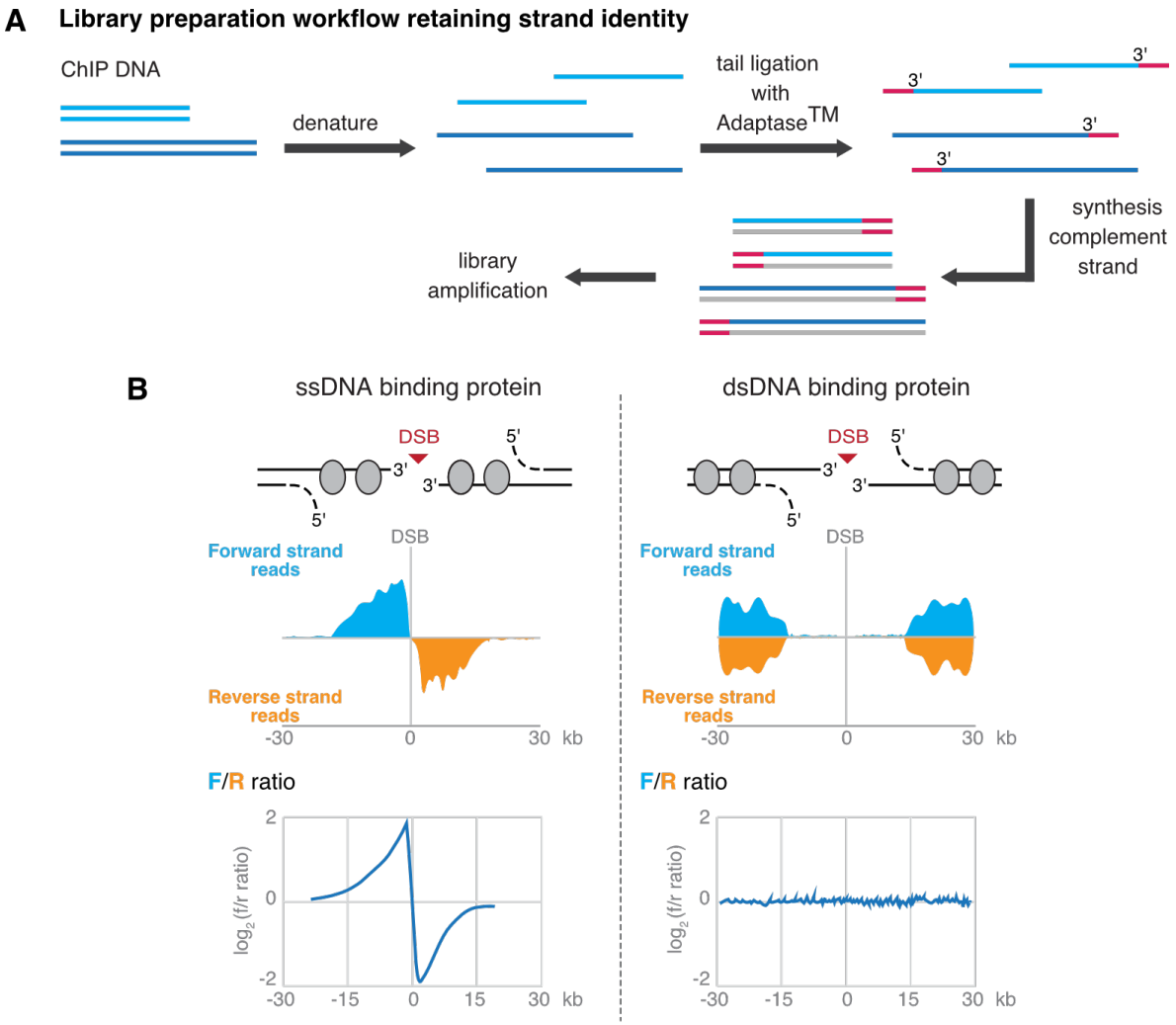

Figure 6. Strand-specific ChIP-sequencing.
A) Workflow of strand-specific ChIP-sequencing. Sonicated and purified DNA resulting from chromatin immunoprecipitation is denatured and sequencing adapters are ligated at the 3' of ssDNA molecules using adaptase (Accel-NGS 1S Plus kit, Swift Biosciences). In the next steps, the complementary strand is synthesized and the resulting dsDNA molecules amplified before sequencing. Forward and reverse reads are then assigned bioinformatically according to read directionality. **B)** Illustration of how strand-specific ChIP-sequencing, combined with site-specific induction of DSBs, would discriminate between ssDNA (left) and dsDNA (right) binding of proteins recruited to DSBs.

3.2 Strand-specific ChIP-sequencing recapitulates RPA binding to ssDNA at resected DSBs

First, we validated strand-specific ChIP-sequencing by measuring the DNA binding profile of RPA, a well-known ssDNA-binding protein that readily binds to ssDNA intermediates during DNA replication and repair (Chen and Wold, 2014). To perform this experiment, we used a budding yeast strain where the expression of the HO endonuclease from the *pGAL1-10* promoter generates a single DSB on chromosome III, in the *MAT* locus (Lee et al., 1998). Yeast cells naturally exploit the HO endonuclease for mating-type switching, which occurs through DSB induction at *MAT* and recombination with homologous loci – *HML* and *HMR* – located on chromosome III (Kostriken et al., 1983). Here, we used a strain where repair of the break is inhibited by the deletion of *HML* and *HMR* (Bantele et al., 2017; di Cicco et al., 2017). To be able to follow resection, we additionally used nocodazole to synchronize cells in mitosis, when they are competent for homologous recombination and thus resection is activated. To observe changes in ongoing resection, we harvested cells at 2 and 4 hours after HO induction.

We observed a progressive signal loss on the forward and reverse strands at the opposite sides of the DSB in the input sample, at 2 and 4 hours after DSB induction, indicating ongoing resection of the 5' strand (Figure 7A, left panel). In addition, we detected strong RPA enrichment on the forward strand upstream of the DSB and on the reverse strand downstream, up to 10 kb at 2 hours and 20 kb at 4 hours (Figure 7B, left panel). Through progression of the leading edge, we can estimate a resection rate of about 5 kb/hour, which is consistent with what has been previously established (Mimitou et al., 2017; Zhu et al., 2008). A similar pattern of RPA binding has also been found at resected DSBs induced by I-PpoI in *S. pombe* (Ohle et al., 2016) and during class switch recombination of immunoglobulin genes (Di Virgilio et al., 2013; Yamane et al., 2013).

To better visualize the strand bias generated by resection, we also plotted the forward to reverse strand ratio for each time point, normalized to the signal in the uninduced sample (Figure 7, right panels). Indeed, for both input and RPA we clearly see a ratio skewed towards forward and reverse strands, upstream and downstream of the DSB, respectively. In summary, we confirmed that strand-specific ChIP-sequencing can visualize the occurrence of ssDNA during resection and its binding by RPA.

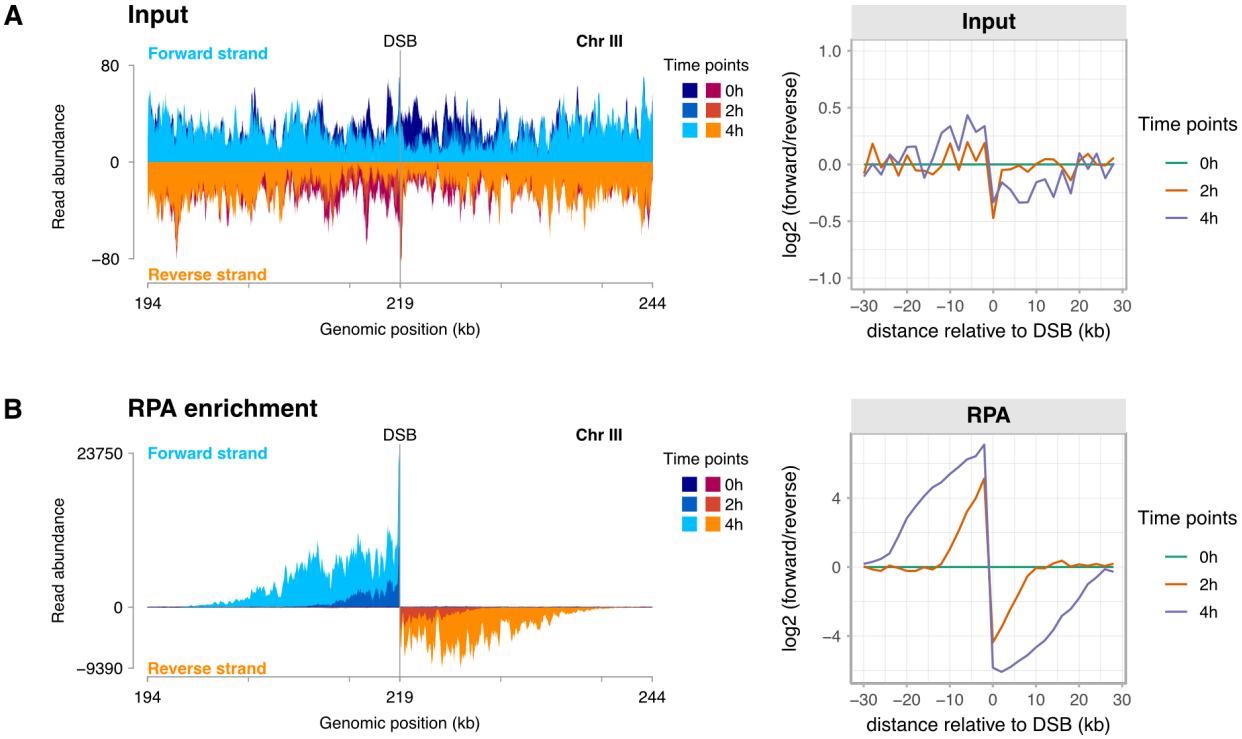

Figure 7. Strand-specific ChIP-sequencing recapitulates ssDNA binding of RPA.
A single DSB on chromosome III at the *MAT* locus was induced in yeast cells arrested in M phase through induction of the HO endonuclease. Samples were collected at 2 and 4 hours after DSB induction. RPA ChIP was performed on the extracted chromatin and the resulting DNA was subjected to strand-specific library preparation and sequencing. Sequencing reads were plotted as forward and reverse strand coverage 25 kb upstream and downstream of the DSB (left) and as $\log_2$ ratio of forward:reverse coverage normalized to the uninduced sample (right) for both input DNA **(A)** and RPA ChIP **(B)**. Strand-specific loss of input reads can be observed in the resected area, while RPA shows strand-specific enrichment, according to resection directionality. Results representative of n = 3 biological replicates.

3.3 Dpb11 and the 9-1-1 complex localize on double-stranded DNA

In eukaryotic cells, formation of ssDNA at DSBs is one of the crucial steps in DSB repair and signaling. Specifically, RPA bound to ssDNA recruits Mec1 (homologue of the human ATR), one of the apical kinases of the DNA damage checkpoint, via interaction with its co-factor Ddc2 (ATRIP in human cells) (Deshpande et al., 2017; Zou and Elledge, 2003). Recruitment of Mec1 at sites of DSB is required for its activation and for phosphorylation of multiple substrates around the break, one of these is the effector kinase Rad53 (Chk2 in human). Rad53 is brought in close proximity to Mec1 by a cascade of phosphorylation-mediated binding events, which requires the loading of the 9-1-1 complex onto DNA and its binding to the scaffold protein Dpb11 (TopBP1 in human) (Majka et al., 2006a; Mordes et al., 2008; Navadgi-Patil and Burgers, 2008, 2009; Pfander and Diffley, 2011; Puddu et al., 2008). The 9-1-1 is a ring-shaped heterotrimeric complex comprising Mec3, Rad17 and Ddc1 subunits and belongs to the PCNA family of sliding clamps. The 9-1-1 complex

is placed on DNA by the RFC-Rad24 clamp loader, which has been shown to directly interact with ssDNA-bound RPA (Majka et al., 2006b; Piya et al., 2015; Zou et al., 2003). RFC-Rad24, together with the RPA-ssDNA filament, is thought to direct loading of the 9-1-1 to 5' ss-dsDNA junctions (Ellison and Stillman, 2003; Majka et al., 2006b; Zou et al., 2003). However, it is unclear whether at sites of resection the 9-1-1 complex would bind and slide onto ssDNA behind the resection machinery or onto dsDNA and move ahead of resection (Bantele et al., 2019; Bekker-Jensen et al., 2006). According to *in vitro* data, 9-1-1 appears to be loaded on ssDNA in proximity of ss-dsDNA junctions, while sliding was shown to occur on dsDNA (Castaneda et al., 2021; Ellison and Stillman, 2003; Majka and Burgers, 2003; Majka et al., 2006b; Zheng et al., 2021). Therefore, we decided to test with our method how the 9-1-1 complex and its interactor Dpb11 would bind at a resected DSB *in vivo*.

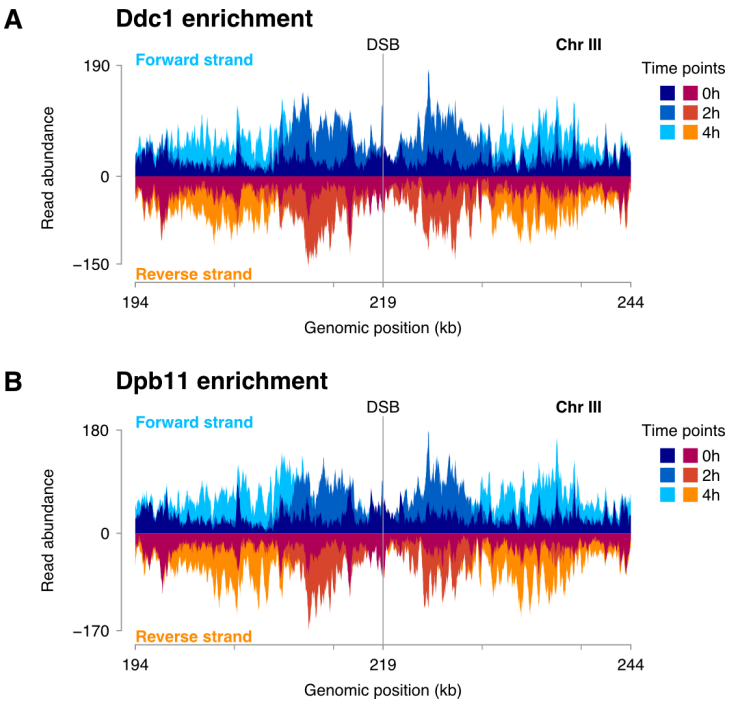

Figure 8. The 9-1-1-Dpb11 axis is associated to dsDNA.
Ddc1^{3FLAG} **(A)** and Dpb11^{3FLAG} **(B)** strand-specific ChIP-sequencing coverage at a HO DSB on chromosome III in yeast cells arrested in M phase and harvested at the indicated time points after HO-induction. Ddc1 and Dpb11 equally enrich forward and reverse strands. Peaks move away from the DSB over time according to resection directionality. In addition, peaks profiles and locations are nearly identical for the two proteins, as it is expected since Ddc1 and Dpb11 directly interact with each other. Results representative of n = 2 biological replicates.

For this experiment, we generated strains endogenously expressing C-terminal 3xFLAG-tagged Ddc1 or Dpb11 (Ddc1^{3FLAG}, Dpb11^{3FLAG}), in addition to the same DSB induction

system described in paragraph 3.2, also the same experimental set-up has been used. We observe an increasing signal intensity for both Ddc1^{3FLAG} and Dpb11^{3FLAG} after DSB induction and equal enrichment of both the forward and reverse strands at all time points, indicating dsDNA binding (Figure 8). In addition, coverage of Ddc1^{3FLAG} and Dpb11^{3FLAG} strand-specific ChIP-seq shows nearly identical profiles for both proteins, peaking at 6 kb (after 2 hours of DSB induction) and at 14 kb (after 4 hours of DSB induction), suggesting that 9-1-1 and its binding partner Dpb11 move along dsDNA, with a similar pace as the resection machinery (Figure 9). Therefore, our data, together with previous *in vitro* results (Ellison and Stillman, 2003; Majka and Burgers, 2003; Majka et al., 2006b; Zou et al., 2003), suggests a model where the 9-1-1 complex, after loading on ssDNA at 5' ss-dsDNA junctions, travels on dsDNA ahead of resection, likely remaining in proximity to the 5'-resected junction (Figure 9).

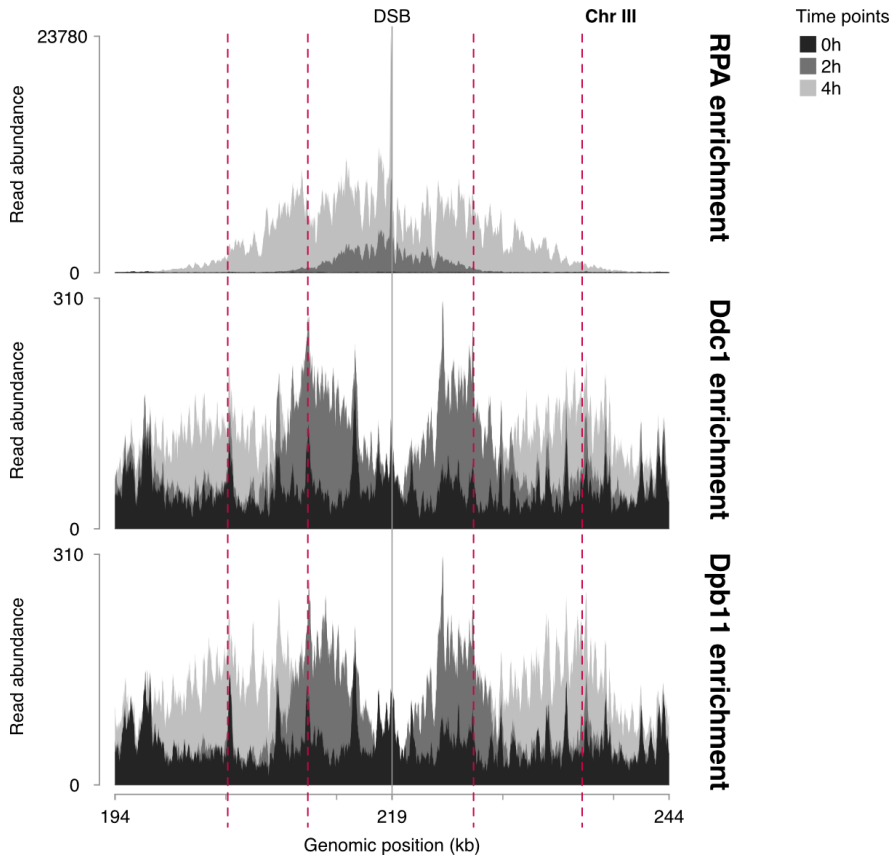

Figure 9. The 9-1-1 complex slides on DNA at the same speed of the resection machinery.
RPA (top), Ddc1^{3FLAG} (middle) and Dpb11^{3FLAG} (bottom) strand-specific ChIP-sequencing data from three individual experiments, shown already as forward vs. reverse strand coverage in Figure 7 and Figure 8. Here, forward and reverse coverage were summed for each time point. Red dashed lines indicate the extent of resection at 2 h and 4 h after HO-induction, which corresponds to peak signals in the Ddc1^{3FLAG} and Dpb11^{3FLAG} plots, indicating that the 9-1-1 complex slides at the same pace of the resection machinery. It is

worth to notice that without the distinction between forward and reverse strand is not possible to assign unequivocally the 9-1-1 complex to the ssDNA or dsDNA compartment (see paragraph 3.1 for discussion).

3.4 Strand-specific ChIP-seq detects Rad51 filaments and homology search intermediates

A core factor of homologous recombination is Rad51, a recombinase belonging to the RecA family. Rad51 is well-known for forming nucleoprotein filaments with ssDNA at resected DSBs and for pairing ssDNA to a homologous dsDNA template. Thereby, it catalyzes the crucial process of homology search, as well as pairing and strand-invasion into the homologous dsDNA (Heyer et al., 2010; San Filippo et al., 2008; Sung and Robberson, 1995). For these reasons, Rad51 can potentially associate with both ssDNA and dsDNA and thus is a very good candidate to test the method of strand-specific ChIP-sequencing at DSBs.

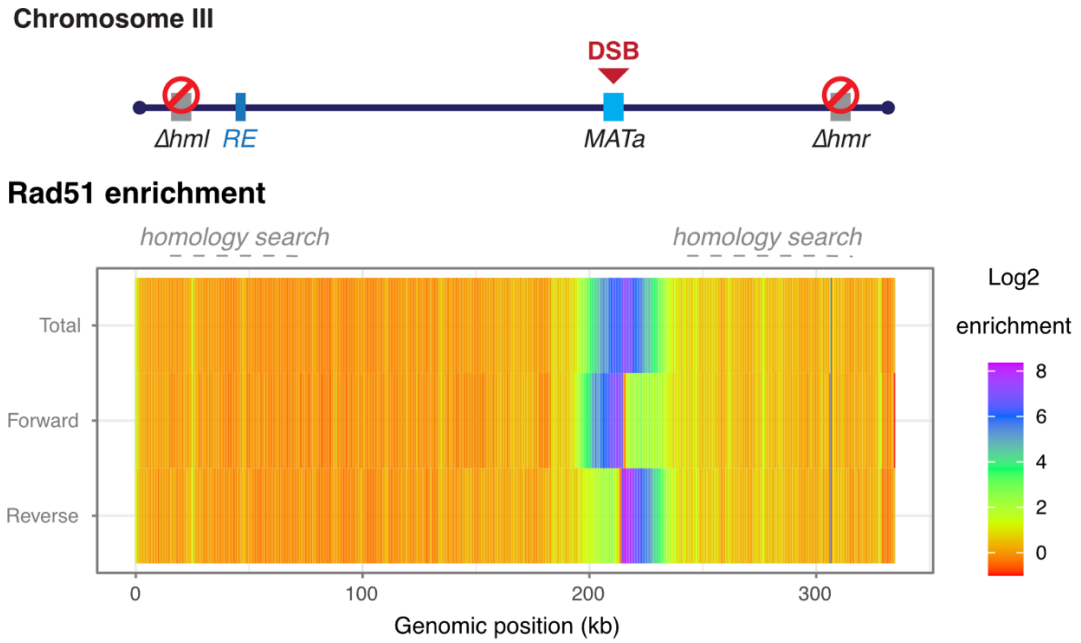

Figure 10. Strand-specific Rad51 ChIP-sequencing reveals Rad51 filament formation on resected ssDNA and homology search on dsDNA.
Top: scheme of chromosome III of the *S. cerevisiae* strain used in the experiment. The strain carries the recombination enhancer (*RE*), which defines chromosome III architecture, and deletions of the *HMR* and *HML* loci, which are the homologous donors of *MAT*, where a single DSB is induced. Bottom: Rad51 enrichment on chromosome III after 4 h of HO induction in M phase arrested cells. Forward, reverse and total coverage was normalized according to the signal of the uninduced sample and plotted in $\log_2$ scale as heatmaps (500 bp bins). Rad51 signal is strand-biased in the vicinity of the DSB, indicating Rad51 filament formation. A second type of Rad51 signal that has no strand-bias is detectable near the recombination enhancer and at the right side of the DSB, indicated by the dashed lines. This signal likely reflects the ongoing homology search on dsDNA. Result representative of n=2 biological replicates.

We observed that, at the resected DSB in the *MAT* locus, Rad51 strongly associates to ssDNA (Figure 10). In addition, we also detected specific Rad51 enrichment further away from the DSB on the right arm of chromosome III and at the recombination enhancer (*RE*) locus, but not elsewhere in the genome (Figure 10 and Figure 11). This signal showed no bias for either strand, indicating that it originates from dsDNA binding and reveals regions of ongoing homology search. Consistently, in a setting similar to what we have used here, Rad51 ChIP-on-chip revealed extensive Rad51 binding outside of the ssDNA area on the broken chromosome, showing that homology search intermediates can be observed *in vivo* using ChIP (Kalocsay et al., 2009; Renkawitz et al., 2013a). With this experiment we could confirm that the previously observed Rad51 homology search signals arise from dsDNA, indicating that these are bona fide intermediates of homology search.

Moreover, the homology search pattern that we observed in this experiment is consistent with the recombination preference of *MATa* cells for the *HML* donor (Renkawitz et al., 2013a). This process was shown to be directed by chromosome architecture (Renkawitz et al., 2013a). Specifically, the recombination enhancer has been characterized as a crucial player in driving the repair towards the *HML* locus. Indeed, *RE* promotes chromosome looping via direct protein-mediated interaction with *MAT*, bringing the homologous donor *HML* in close proximity to the DSB in *MATa* cells to facilitate repair (Li et al., 2012). In addition to Renkawitz et al., our data shows that Rad51 signals distal to the break are associated with dsDNA indicating that they represent Rad51 engagement during homology search. Therefore, our data support a model in which the 3D genome architecture plays a fundamental role in directing homology search and ultimately, repair (Agmon et al., 2013; Lee et al., 2016; Renkawitz et al., 2013a). In addition, it is worth to mention that the 3D architecture of chromosome III has been involved not only in the homology search process, but also in the spreading of H2A phosphorylation (γH2A) – a marker of DNA damage – beyond the DSB domain (Li et al., 2012). In agreement, we can detect a γH2A enrichment pattern on the whole chromosome III similar to Rad51 (compare Figure 10 with Figure 13).

In conclusion, by using strand-specific ChIP-sequencing we can directly visualize and discriminate between two types of Rad51 signals: the first arising from Rad51 binding to the ssDNA generated by the resection machinery at DSBs (the Rad51 nucleoprotein filament), the second deriving by the transient Rad51 probing of dsDNA (the homology search signal).

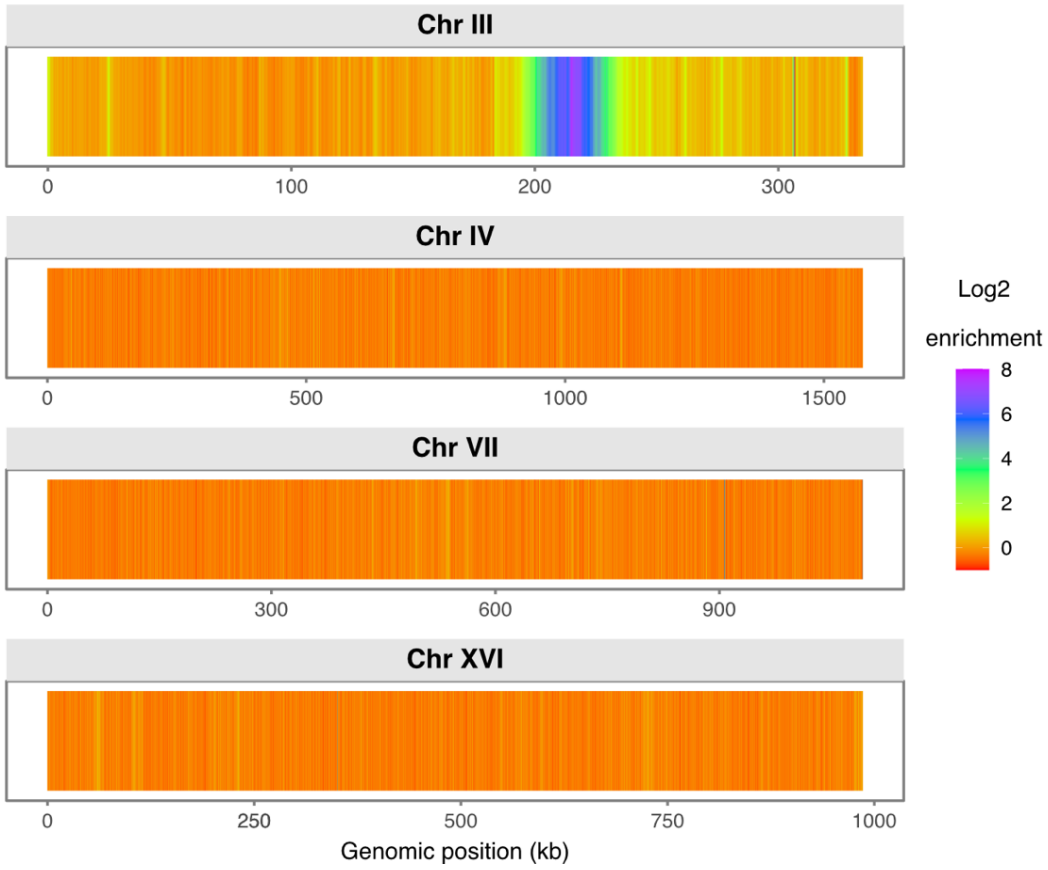

Figure 11. Rad51 enrichment on damaged and undamaged chromosomes.
Rad51 is specifically enriched on the broken chromosome, indicating that homology search preferentially occurs *in cis* and assisted by the peculiar 3D architecture of chromosome III. Strand specific Rad51 ChIP-sequencing data from the same experiment shown in Figure 10. Here, forward-plus-reverse strand coverage for chromosome III, IV, VII and XVI was normalized to the signal of the uninduced sample and plotted in $\log_2$ scale as heatmaps (500 bp bins). We can observe Rad51 enrichment exclusively on chromosome III (bearing the DSB) but not on chromosome IV, VII and XVI, which are representative of all unbroken chromosomes. Result representative of n=2 biological replicates.

3.5 Nucleosome eviction at a resected DSB in the *MAT* locus

In the last two decades, nucleosomes and chromatin remodelers have received increasing attention as relevant factors in the response to DNA damage, specifically in DSB repair (Seeber et al., 2013; Smeenk and van Attikum, 2013). One of the first events occurring after a DSB is the phosphorylation of histone H2A (referred to as γH2A), which is crucial for the recruitment of DNA damage signaling and repair factors (Hauer and Gasser, 2017; Seeber et al., 2013; Smeenk and van Attikum, 2013). Another important aspect that we need to consider is that DSB repair, particularly resection, occurs on a chromatin substrate. It has been shown that nucleosomes act as a barrier for resection nucleases

(Adkins et al., 2013). Therefore, such barrier must be somehow lifted or circumvented to allow the resection machinery to pass through chromatin. Indeed, several laboratories have observed a correlation between nucleosome eviction and resection (Attikum et al., 2007; Bantele et al., 2019; Chen et al., 2008; Tsukuda et al., 2005, 2009). However, recent data suggest that nucleosomes can be found on the ssDNA produced by resection (Adkins et al., 2017; Huang et al., 2018). These data are further supported by the observation that histones can form nucleosome-like particles on ssDNA, at least *in vitro* (Adkins et al., 2017; Palter et al., 1979). In light of these contrasting models, the consequences of resection on chromatin could have extremely different implications in terms of maintenance of epigenetic marks, as well as of DSB signaling and repair. Therefore, it is crucial to understand if nucleosomes are evicted upon resection, if they are retained during resection or assembled *de novo* on resected ssDNA.

Given the ability of strand-specific ChIP-sequencing of discriminating between ssDNA and dsDNA binding modes, we were in the ideal position to answer this question.

3.5.1 γH2A is lost at a resected DSB

Phosphorylation of an evolutionarily highly conserved SQ motif in the C-terminus of H2A (or H2A variants) is one of the primary response to DNA damage in many species (Redon et al., 2002). Specifically, upon DSB induction in yeast and mammals, the apical kinases Mec1/Tel1 and ATM are responsible for H2A Ser-129 and H2A.X Ser-139 phosphorylation, respectively (Burma et al., 2001; Downs et al., 2000; Lee et al., 2014; Shroff et al., 2004). This histone mark can spread over extensive chromatin domains around the DSB, covering about 100-200 kb in yeast and 1-2 Mb in human cells (Lee et al., 2014; Rogakou et al., 1999).

Therefore, since γH2A is highly abundant at DSBs and it is easily detectable using phosphorylation-specific antibodies, we decided to test it in strand-specific ChIP-sequencing. As for the experiments described previously, we induced a single DSB in the *MAT* locus in nocodazole arrested cells and followed γH2A enrichment over a time course of 4 hours. After 2 hours of DSB induction, we observed a large increase in the γH2A signal compared to the uninduced sample, which was further enhanced at the 4-hour time point (Figure 12).

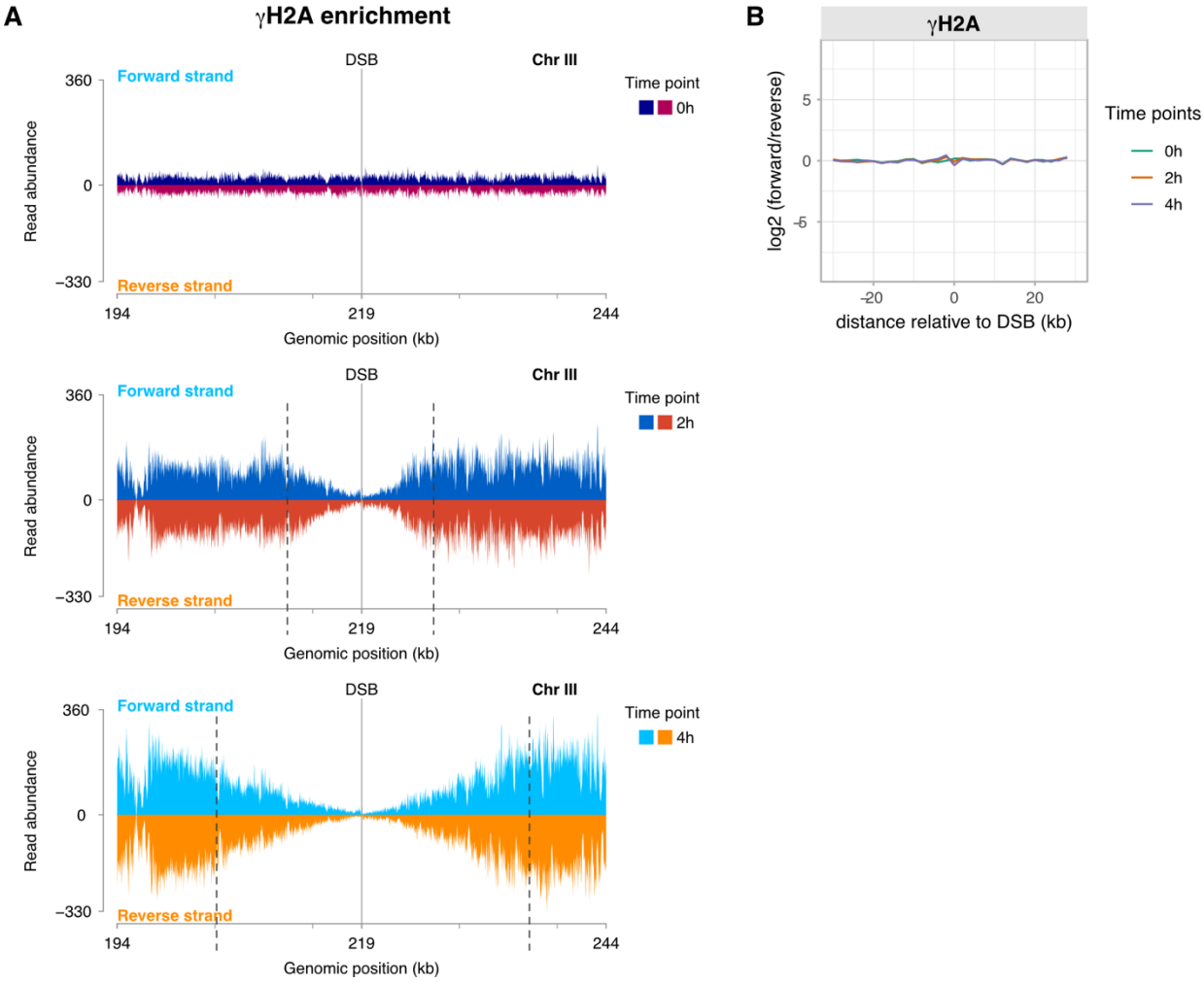

Figure 12. γH2A is lost at resected DSBs.
γH2A is specifically induced by DSBs but lost in the resected area. **A)** γH2A enrichment in strand-specific ChIP-sequencing at 0, 2 and 4 hours after DSB induction in the MAT locus, through HO overexpression, in cells arrested in M phase. Forward and reverse strand coverage are plotted separately in a 50 kb window centered at the DSB. The grey dashed lines indicate RPA signal extension at 2 and 4 hours, derived from the experiment shown in Figure 7. γH2A signal increases over time after the introduction of a DSB, but it is lost in the vicinity of the DSB, following resection dynamics (dashed lines). **B)** $\log_2$ of forward:reverse strand ratio normalized to the uninduced sample as in Figure 7. As visible in A, γH2A ChIP pulls down forward and reverse strands equally, suggesting that γH2A is present only in nucleosomes binding to dsDNA. Results representative of n=2 biological replicates.

However, we detected a considerable decrease of sequencing reads in the vicinity of the DSB, within 5 kb at 2 hours and extending up to about 10-15 kb, following resection spreading, as indicated by the dashed lines in Figure 12. Similarly, γH2A signal loss in the resected area was observed at an HO-induced DSB via ChIP-qPCR (Bantele et al., 2019). Moreover, both forward and reverse strands were equally enriched at any time point in strand-specific ChIP-sequencing, suggesting that phosphorylation of H2A is specifically occurring on nucleosomes bound to dsDNA (Figure 12). The clear reduction of γH2A

signal within the resected area can be explained by different mechanisms: first, phosphorylation might be removed from nucleosomes in the resected area by either phosphatases or by exchanging γH2A with its unmodified version; second, it might be a hint that nucleosomes are evicted to allow resection, as it has been previously suggested (Bantele et al., 2019). Therefore, to determine if the latter hypothesis holds true, we decided to test unmodified canonical histones in strand-specific ChIP-sequencing (see paragraph 3.5.2 and 3.5.3 for discussion of these results).

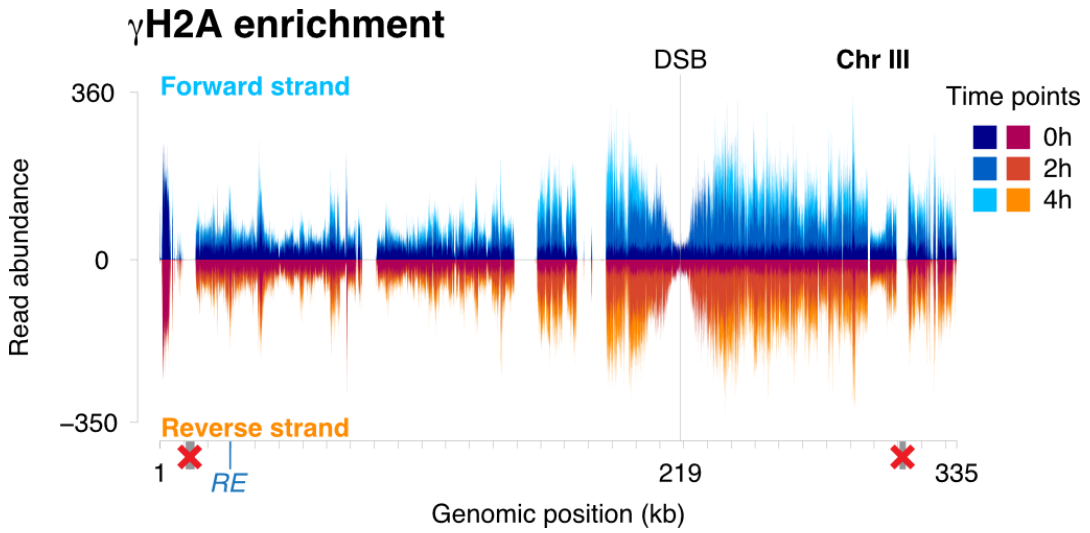

Figure 13. Spreading of γH2A reflects chromosome III architecture.
γH2A strand-specific ChIP-sequencing data from Figure 12 plotted for the entirety of chromosome III. The blue rectangle marked with "RE" delimits the recombination enhancer locus, the grey rectangles marked with a red cross delimit the deleted HML and HMR loci. γH2A is enriched on the broken chromosome after DSB induction, this domain extends for more than 100 kb on both sides of the break. It is interesting to notice that the γH2A pattern of enrichment recapitulates the one seen for Rad51 (compare with Figure 10): we can observe a strong signal on the right arm of the chromosome and a signal corresponding to the recombination enhancer. Results representative of n=2 biological replicates.

When plotting the data of this experiment on the entire chromosome III, we could also observe a pattern of γH2A enrichment that is similar to Rad51 (Figure 13, see paragraph 3.4). More specifically, the γH2A signal is stronger on the right arm of chromosome III and we can detect peaks corresponding to the recombination enhancer locus. The same pattern has been previously observed after HO induction in a *MATa* strain lacking the homologous regions *HML* and *HMR*, similar to the strain that we have used here (Li et al., 2012). Moreover, as evident from Figure 13, γH2A enrichment extends beyond the resected area, over more than 100 kb around the DSB, and it is interspersed with valleys of little or no signal, suggesting that spreading of H2A phosphorylation might be hindered

by local chromatin features and/or assisted by the chromosomal/nuclear architecture. Indeed, it has been observed that γH2A is not only confined to a region or chromosome affected by a DSB, but it can also be detected on other, undamaged chromosomes. For example, when inducing a DSB close to a centromeric region in yeast, γH2A signals are detected also on all of the other centromeres (Lee et al., 2014). Since, in the yeast nucleus, centromeres are clustered together (Duan et al., 2010), this suggest that H2A phosphorylation can spread to regions that physically interact with each other.

3.5.2 Nucleosomes are lost at a DSB upon resection

Then, to determine if the loss of γH2A is caused by nucleosome eviction upon resection, we moved on to analyze the behavior of canonical histones at a single resected DSB. For this, we applied two different strategies: on the one hand, we used antibodies against canonical histones; on the other hand, we used endogenous tagging. Several of the anti-histone antibodies that we have been testing showed unspecific DNA binding, thus confounding the interpretation of strand-specific ChIP-sequencing data (antibody specificity was tested independently, data not shown). Despite this, we could validate the specificity of a frequently used anti-H3 antibody (van Emden et al., 2019; Yu et al., 2019). By using such antibody in strand-specific ChIP-sequencing, we could pull down forward and reverse strands in equal amounts throughout the yeast genome, consistent with the presence of H3-containing nucleosomes on dsDNA (Figure 14).

Moreover, when analyzing the surrounding of an HO-induced DSB, we observed a steady decrease in the signal, over a time course of 4 hours, in the area affected by resection and no association with ssDNA (Figure 15).

Although we detected H3 eviction from the resected area of a DSB, we could envision that H2A/H2B dimers could associate with resected ssDNA. To tackle this question, we generated two different yeast strains bearing an endogenous triple-FLAG (3FLAG) tag at the C-terminus of either H2B (*HTB1*) or H3 (*HHT1*) and then used an anti-FLAG antibody in strand-specific ChIP-sequencing. Also in this case, we could confirm what we have observed previously: both H2B and H3 associate solely with dsDNA and they are evicted upon resection (Figure 15).

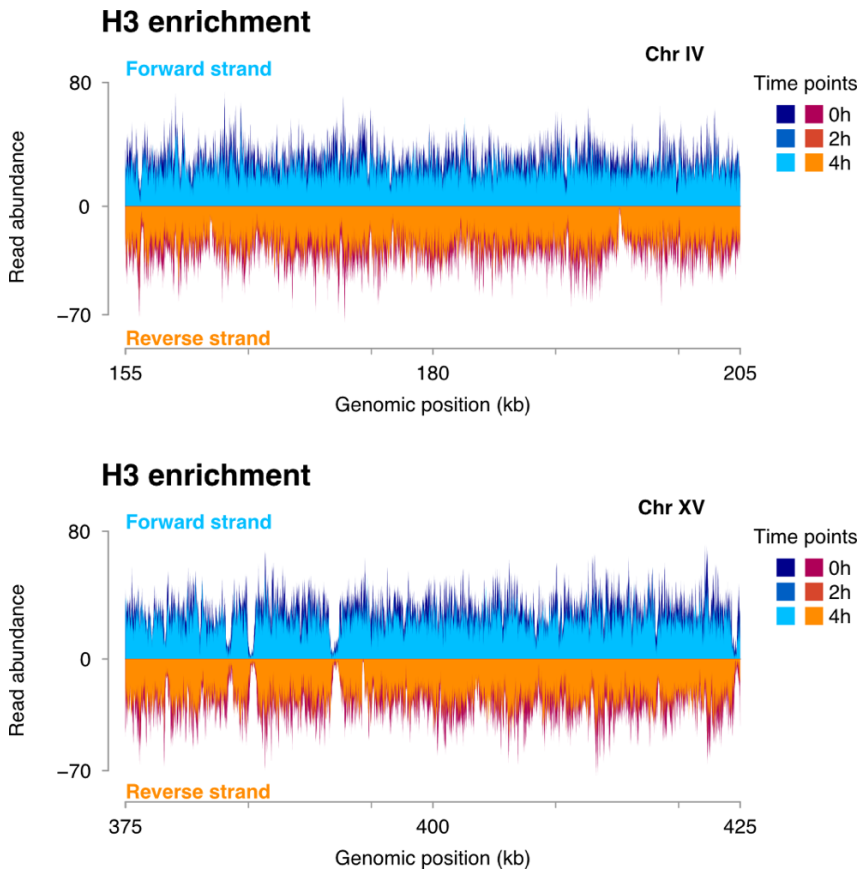

Figure 14. Strand-specific ChIP-seq recapitulates H3 binding to dsDNA.
Strand-specific H3 ChIP-sequencing performed after DSB induction at the *MAT* locus with the HO endonuclease for the indicated time points in M phase arrested cells. The figure shows forward and reverse H3 coverage at two different locations on undamaged chromosome IV (top) and XV (bottom), representative of all undamaged chromosomes. Histone H3 enriches forward and reverse strands, indicating the presence of H3 within nucleosomes bound to dsDNA. Results representative of n=2 biological replicates.

Up to this point, we have done experiments only with cells arrested in M phase, when homologous recombination is upregulated and thus cells are in a resection-proficient state. However, we reasoned that in this cell cycle phase, nucleosome assembly factors may not be present or active as in other cell cycle phases, as in the case of human CAF-1 (Marheineke and Krude, 1998; Polo et al., 2004). As a consequence, we might have overlooked the assembly of nucleosomes or sub-nucleosomal particles on ssDNA. Therefore, we repeated some of the previous experiments in asynchronously growing cells. As expected, DSB induction triggered a checkpoint-dependent cell cycle arrest (Figure 16B) and resection (Figure 16A, see input and RPA). Even in this case, after analyzing strand-specific H3 ChIP-seq data, we observed nucleosome eviction and no binding to ssDNA (Figure 16A, see H3 enrichment).

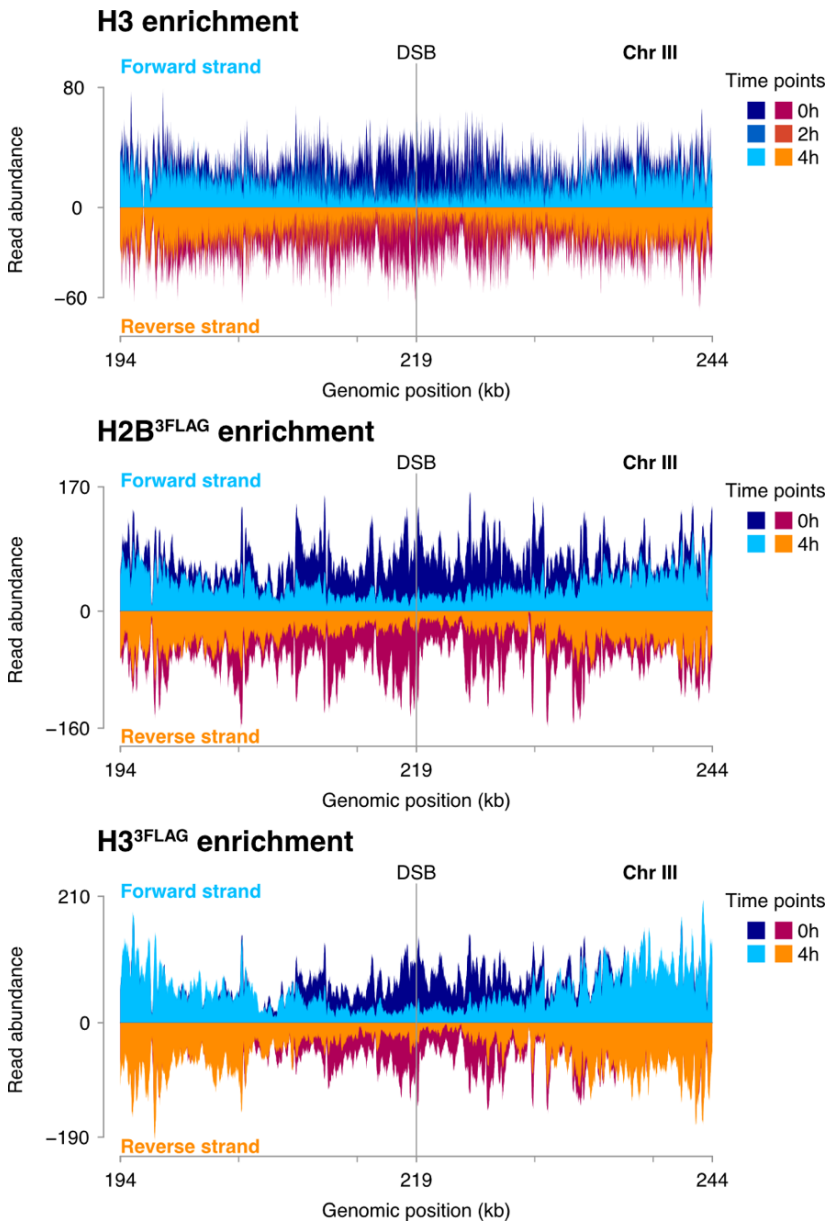

Figure 15. Nucleosomes are lost from resected DNA at a DSB.
Nucleosomes are lost upon resection and exclusively associate with dsDNA. Strand-specific coverage of H3 (same dataset as Figure 14, top panel), H2B^{3FLAG} (middle panel), and H3^{3FLAG} (bottom panel) 50 kb around an HO-induced DSB on chromosome III in nocodazole arrested cells, before and 2, 4 hours after DSB induction. A signal decrease in the area affected by resection can be observed in all three experiments. In addition, forward and reverse strands are equally enriched suggesting dsDNA binding and excluding association of histones with ssDNA. Results representative of n=2 biological replicates.

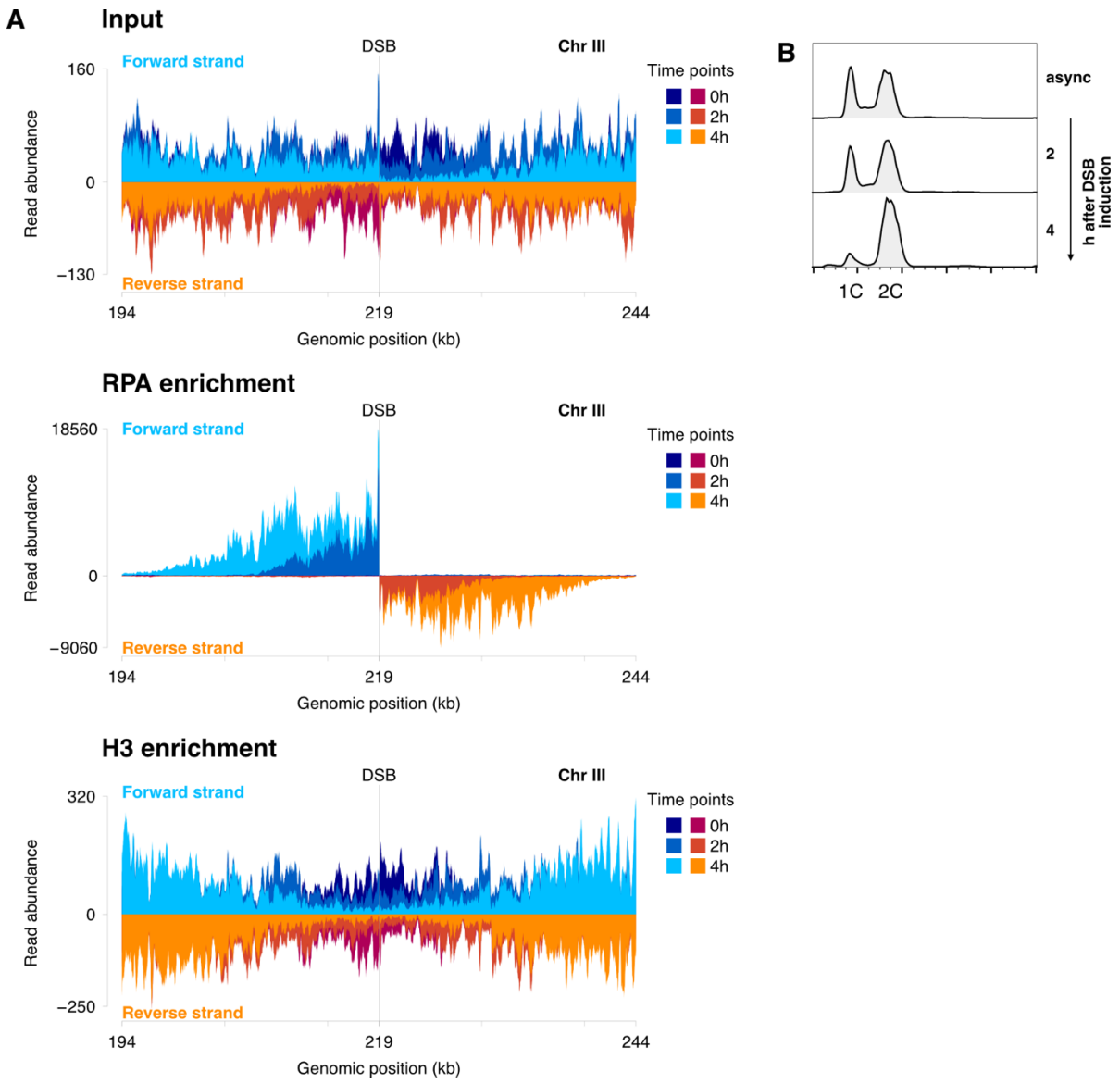

Figure 16. Nucleosomes are lost from a resected DSB in asynchronous cells.
A) Input (top panel), RPA (middle panel) and H3 (bottom panel) forward and reverse coverage 50 kb around a DSB in the *MAT* locus at 0, 2 and 4 hours after HO induction in asynchronous yeast cells. Resection is detectable already after 2 hours from strand-specific DNA loss in the input and from RPA strand-specific enrichment. Consistently, H3 signal decreases in the resected area, suggesting that nucleosomes are lost upon resection. **B)** DNA content measured by flow cytometry in an asynchronous cell population, before and 2, 4 hours after HO DSB induction. Asynchronous cells show arrest of the cell cycle in G2/M after 4 hours of break induction. Results representative of n=2 biological replicates.

Lastly, since resection is initiated stochastically in a cell population, at 4 hours after DSB induction we still observe a substantial amount of dsDNA in the resected area, presumably originating from cells that had not initiated resection. Consequently, we argued that this might limit our ability to detect small fractions of ssDNA-bound nucleosomes, if they existed *in vivo*. Therefore, we decided to push this system to a condition in which the DNA surrounding the DSB would be mostly single-stranded. To

achieve this, we performed a 10-hour time course after DSB induction. As anticipated, after 10 hours we could detect a region of about 10 kb around the DSB at *MAT* that was almost entirely resected (Figure 17). However, strand-specific H3 ChIP-sequencing revealed a considerable signal reduction, but no strand-bias in this area (Figure 17).
In conclusion, we could not find evidence for histones binding to resected single-stranded DNA; thus, we reason that neither ssDNA-bound nucleosomes nor sub-nucleosomal particles do represent major species at a resected DSB in the *MAT* locus.

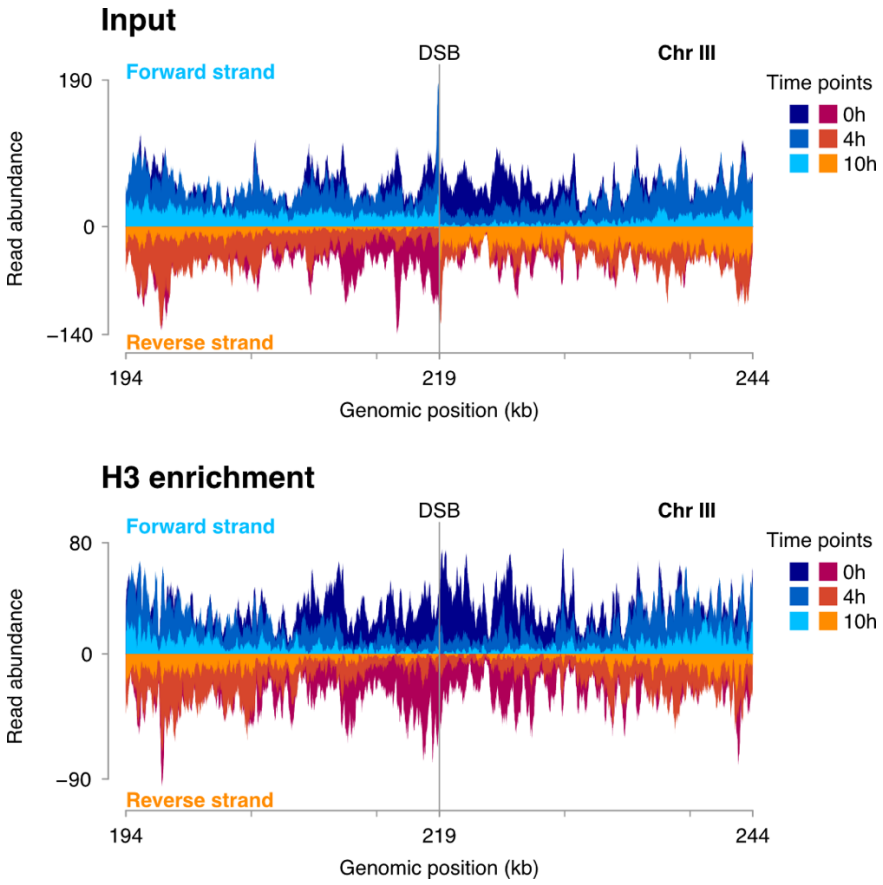

Figure 17. Nucleosomes exclusively bind to dsDNA even after extensive resection.
Input DNA (top) and histone H3 (bottom) strand-separated coverage in a 50 kb window around a HO-induced DSB at the *MAT* locus, before and 4, 10 hours after DSB-induction in nocodazole arrested cells. After 10 hours, extensive resection has occurred, leaving virtually only ssDNA over a 10 kb region surrounding the DSB. H3 ChIP shows eviction in the resected area and H3 binding exclusively to dsDNA, suggesting that nucleosomes do not associate with ssDNA even after extensive resection. Results representative of n=2 biological replicates.

3.5.3 Nucleosomes are fully evicted upon resection

As presented in the previous paragraph, we found evidence that nucleosomes are evicted from the resected area of an HO-induced DSB. However, it has been often argued that

nucleosome displacement is limited at resected DSBs, especially if compared to the substantial histone loss occurring at gene promoters (Papamichos-Chronakis and Peterson, 2013). Specifically, several studies have shown a large decrease in histone levels only within 500 bp from the DSB, while such decrease was frequently more contained in loci further away from the DSB, at time points when resection had produced several kilobases of ssDNA (Papamichos-Chronakis and Peterson, 2013; Sinha and Peterson, 2009). Altogether, these observations have been taken as a hint of the presence of nucleosomes on resected ssDNA (Huang et al., 2018; Papamichos-Chronakis and Peterson, 2013; Sinha and Peterson, 2009). To this regard, it is crucial to highlight that resection initiation and elongation are stochastic in a cell population: this means that, at a specific point after DSB induction, some cells will show ssDNA, others dsDNA. Therefore, in histones ChIP lacking strand information, the signal observed in the resected area possibly originates from a fraction of cells that have not initiated resection (see also discussion in paragraph 3.1). In addition, background DNA binding of antibodies (in this context anti-histone antibodies) used in ChIP can also negatively influence the interpretation of such data. For this reason, we decided to assess the level of background in strand-specific histone ChIP-sequencing, to determine if the residual histone signal that we observed in the resected area after 10 hours of HO-induction reflected background levels. To do this, we designed a strategy in which we could directly compare a strain with endogenously 3xFLAG-tagged H3 – accounting for the ChIP signal – and a strain with no tag – accounting for the background. We mixed, for both strains, undamaged cells with cells that had undergone 10 hours of persistent DSB induction at *MAT* to obtain samples with different amounts of resected ssDNA (Figure 18A). Analyzing a resected area of 10 kb around the DSB, we observed a direct correlation between resection, represented by the loss of input signal, and nucleosome eviction, represented by the decrease in $H3^{3FLAG}$ ChIP signal (Figure 18B). In addition, we measured similar signal intensities in ChIP from $H3^{3FLAG}$ and untagged cells for the "damaged" sample (Figure 18A), suggesting that the residual histone signal that we observe in the resected area simply reflects the background (Figure 18B). Therefore, we conclude that nucleosomes are fully evicted upon resection.

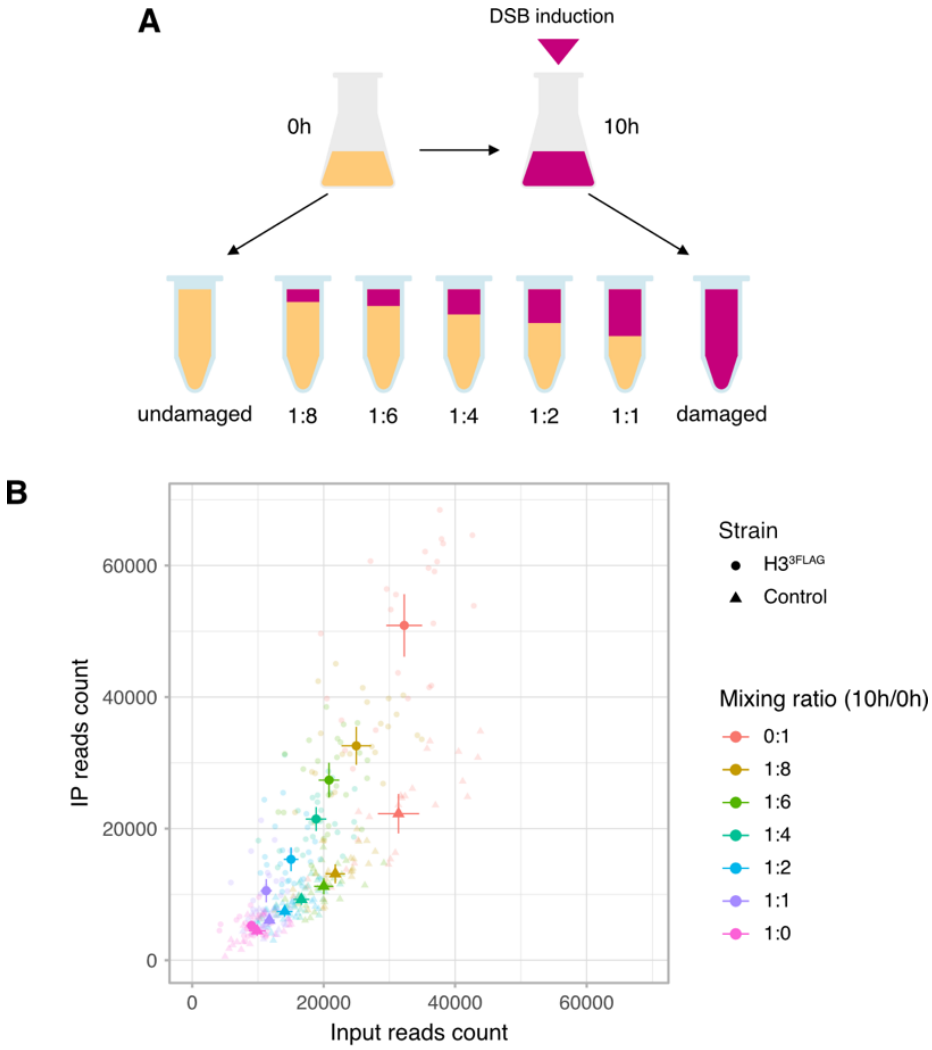

Figure 18. Nucleosomes are fully evicted upon resection.
A) Workflow of the experiment. HO-induction was performed for 10 hours in both H3^{3FLAG} and untagged cells after cell cycle arrest in mitosis. For each strain, damaged and undamaged cells were mixed at the indicated ratios prior to anti-FLAG ChIP. **B)** Reads counts of input versus FLAG IP. Each data point represents reads abundance over 2 kb bins (in pale colours) aggregated over 10 kb surrounding the DSB (in dark colours). At increasing amounts of damaged cells, IP reads count decrease in correlation with input reads count, in both H3^{3FLAG} and control, suggesting full eviction of nucleosomes upon resection. Similar IP reads count for H3^{3FLAG} and control "damaged" sample (pink dot and triangle, respectively) indicate that the residual histone signal in ChIP reflects the background. Average of n = 3 biological replicates, ± standard error of the mean.

3.6 Nucleosome eviction does not depend on genomic location

The results presented so far were all obtained for a single DSB induced at the *MAT* locus. Mating-type switching in budding yeast has been extensively characterized and often taken as a model for the study of homologous recombination (Haber, 2012). Indeed, galactose induction of the HO endonuclease has been used, in the last decades, as a robust system for the introduction of a single, locus specific, DSB (Haber, 2012). However, the

yeast mating type system has been selected by evolution to be prone for repair via HR, thus, it is possible that the chromatin configuration and dynamics at the *MAT* locus could have unique features. For example, it has been shown that the 3D configuration of chromosome III directly depends on a cell's mating type and it is guided by the *RE* locus (Belton et al., 2015). Therefore, to avoid having a biased picture of nucleosome dynamics during resection, we decided to use a second DSB induction system, which employs the AsiSI restriction endonuclease. AsiSI has already been successfully applied to induce DSBs in human cells (Clouaire and Legube, 2019; Iacovoni et al., 2010) and here, for the first time, we adapted the same system in yeast. We generated a strain bearing a codon-optimized version of *AsiSI* harboring a nuclear localization signal and under control of the *pGAL1-10* promoter. The budding yeast genome contains 38 AsiSI recognition sites (Figure 19), thus allowing us to generalize our findings over different genomic locations.

Figure 19. Distribution of AsiSI cut sites in the yeast genome.
Scheme representing *S. cerevisiae* chromosomes (grey) and the 38 AsiSI cut sites positions in the genome (red).

3.6.1 Characterization of the pGAL-AsiSI system in budding yeast

First, we characterized the AsiSI system of DSB induction in yeast. We determined AsiSI cutting efficiency in cells arrested in mitosis and after 6 hours of treatment with galactose. For this, we used a computational approach (similar to Zhu et al., 2019) on DNA input data obtained with strand-specific sequencing. Specifically, we calculated how many reads spanned across each DSB (representing how many DNA molecules remained uncut)

and then divided this number by the average genome coverage. A small ratio will correspond to a high cutting efficiency.

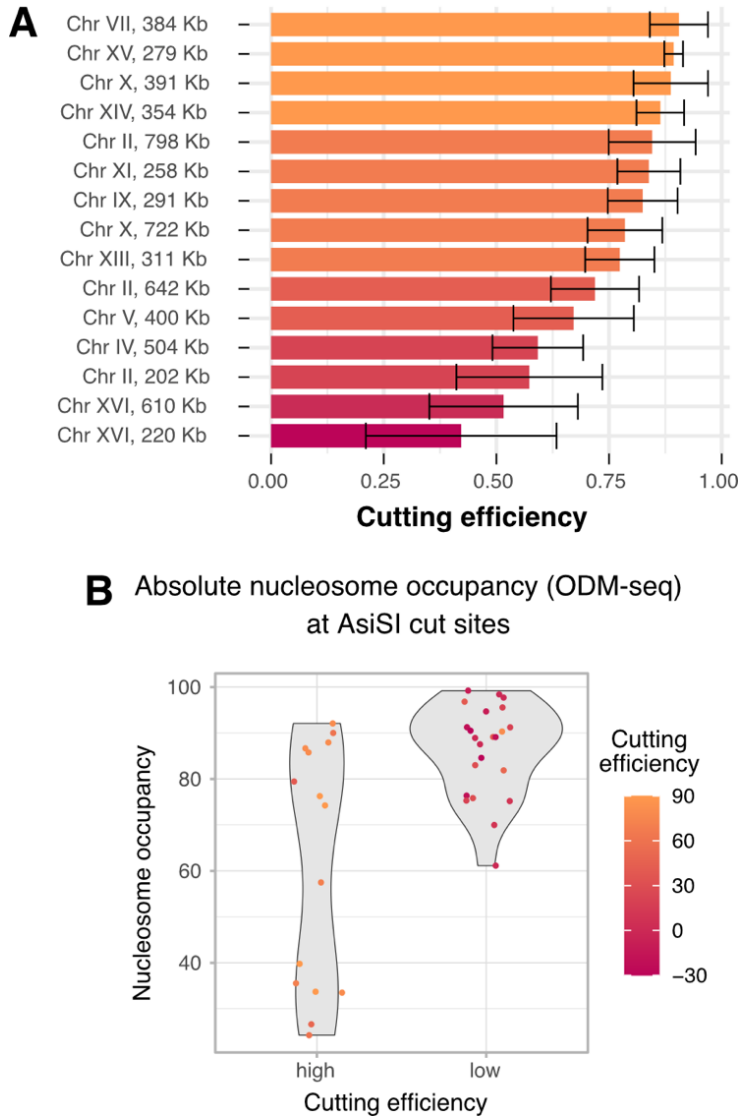

Figure 20. Analysis of AsiSI cutting efficiency.
A) Cutting efficiency of Top15 resected DSBs. Cells were arrested with nocodazole and AsiSI was induced for 6 hours by adding galactose, then strand-specific libraries were prepared from genomic DNA and subjected to high-throughput sequencing. Cutting efficiency was calculated as the ratio between reads spanning a DSB ("uncut" reads) divided by the average genome coverage (Zhu et al., 2019). Average of n = 7 biological replicates, ± standard error of the mean. **B)** Correlation between AsiSI cutting efficiency and absolute nucleosome occupancy (data retrieved from Oberbeckmann et al., 2019, GEO: GSM4193179). AsiSI sites with low cutting efficiency (23) show high nucleosome occupancy, while several AsiSI sites with high cutting efficiency (Top15) show low nucleosome occupancy.

We observed a wide range of cutting efficiencies across the 38 AsiSI restriction sites, with some showing no detectable cut, similar to what was described previously for human cells (Clouaire et al., 2018). A considerable number of AsiSI DSBs showed high cutting

efficiency, ranging from 40% to 90% and, of these, 15 sites displayed also high degrees of resection (Figure 20A and Figure 21). Interestingly, when examining nucleosome occupancy at the different AsiSI cut sites (ODM-seq data from Oberbeckmann et al., 2019), we found that all of the inefficiently cut restriction sites correlated with high nucleosome occupancy, while well-cut (Top15) sites showed different degrees of nucleosome occupancy, with several sites showing low occupancy (Figure 20B). These observations suggest that nucleosome occupancy is presumably a key factor influencing AsiSI cutting.
Next, we measured the level of resection for all AsiSI cut sites by strand-specific RPA ChIP-sequencing. After 6 hours of AsiSI induction, loss of DNA signal in the input and RPA enrichment indicates that the majority of the DSBs was resected (Figure 21). Moreover, for the top 15 DSBs, the extension of RPA enrichment was comparable to what we have observed at the *MAT* locus (Figure 22). Notably, for some of the DSBs, resection spread rather asymmetrically, suggesting that the chromatin state of a given locus or other features could act as a constraint for resection (Figure 21).

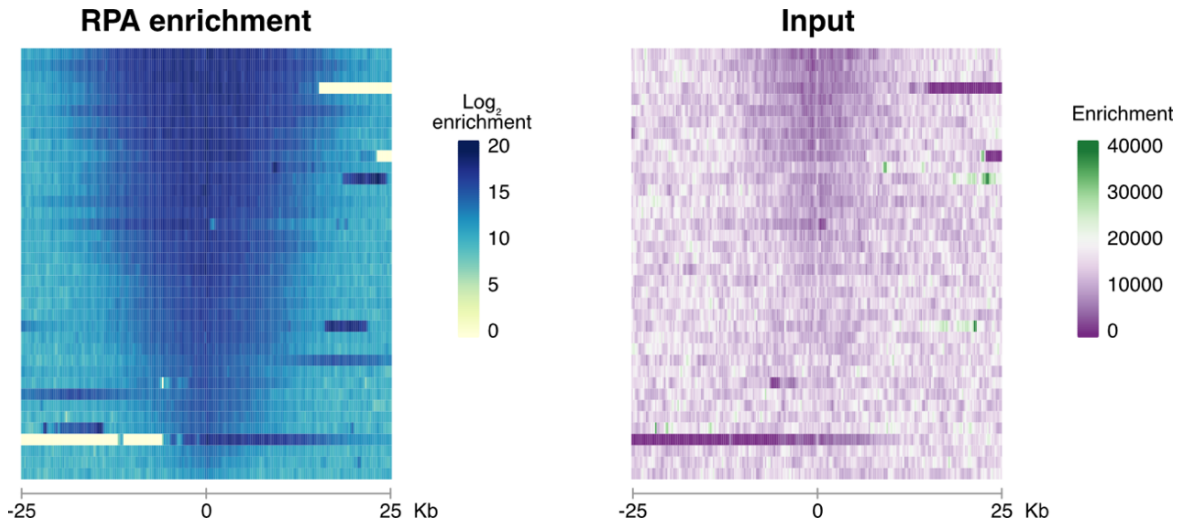

Figure 21. AsiSI DSBs are resected to different extents.
Heatmaps of the sum of forward and reverse strand coverage for RPA enrichment, in log2 scale (left) and for input DNA (right), over a 25 kb window on each side of the breaks (200 bp binning). Heatmaps are ordered from top to bottom according to RPA signal intensity calculated over 40 kb centered around the DSBs. AsiSI induction was performed for 6 hours in cells arrested in mitosis. AsiSI cut sites were resected to different levels throughout the yeast genome, the top 15 breaks showed a higher degree of resection as indicated, not only by RPA enrichment, but also by loss of input signal. Thus, they were used in the following analysis. Results representative of n=2 biological replicates.

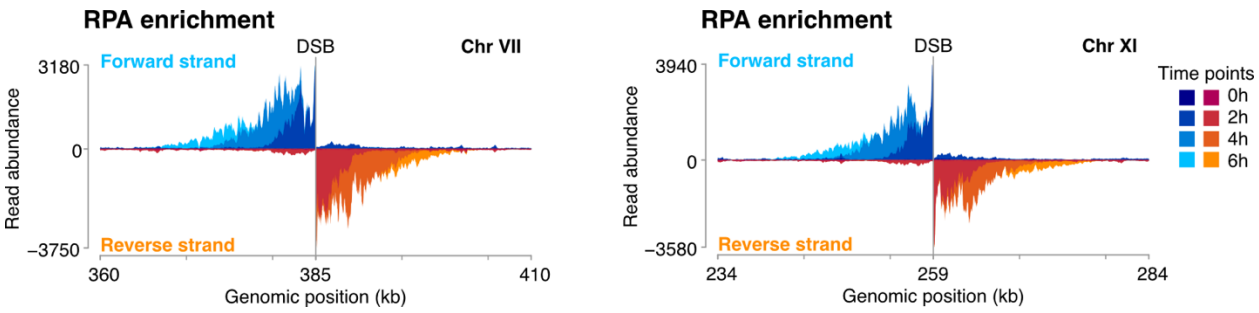

Figure 22. Extension of resection at AsiSI cut sites is comparable to the *MAT* locus.
Forward and reverse strand coverage of strand-specific RPA ChIP-sequencing over a 50 kb window at two of the Top15 AsiSI cut sites. Cells were arrested with nocodazole and galactose was added to the medium for AsiSI induction. Samples were taken before and at 2, 4, and 6 hours after galactose addition. The spread of resection at Chr VII 384,688 bp (left) and Chr XI 258,665 bp (right) is similar to the extent observed at an HO-induced DSB. Same dataset as in Figure 21. Results representative of n=2 biological replicates.

3.6.2 Nucleosome eviction upon resection occurs throughout the yeast genome

Given the efficiency of AsiSI cutting and resection at a substantial amount of DSBs, we moved on to measure histone enrichment. As described previously for DSB induction at the *MAT* locus, we used two complementary strategies: on the one hand anti-histone antibodies, on the other hand endogenously triple-FLAG tagged histones. When comparing H3, H2B^{3FLAG} and H3^{3FLAG} enrichment for all of the 38 AsiSI DSBs with input and RPA enrichment, we observed that a high decrease in histone coverage, indicative of nucleosome eviction, correlated with high levels of resection (Figure 23).

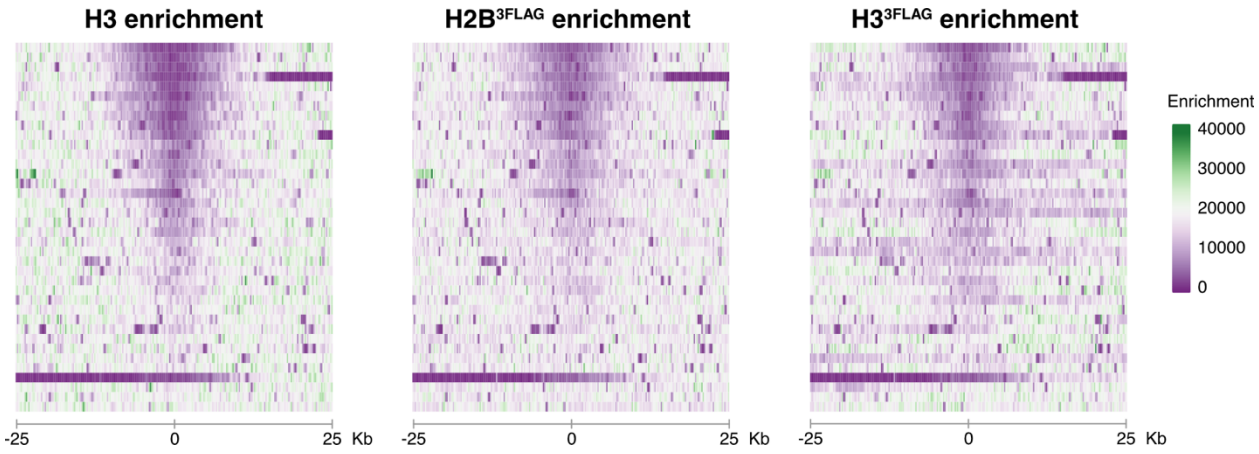

Figure 23. Degree of nucleosome eviction correlate with degree of resection.
Heatmaps of the sum of forward and reverse strand coverage for H3 (left), H2B^{3FLAG} (middle) and H3^{3FLAG} (right) enrichment over a 50 kb window centered at DSBs and measured after 6 hours of AsiSI induction (as in Figure 21) by strand-specific ChIP-sequencing. Coverage was calculated as in Figure 21 and the breaks were sorted by RPA signal intensity. Resection corresponds to nucleosome eviction at individual cut sites. Results representative of n = 2 biological replicates.

Next, we focused our analysis on the Top15 resected AsiSI DSBs and, as anticipated, we detected γH2A, H3, $H2B^{3FLAG}$ and $H3^{3FLAG}$ eviction at individual DSBs (Figure 24). Moreover, by averaging the coverage for forward and reverse strand in input and strand-specific H3 ChIP for Top15 breaks, we confirmed that the extent of nucleosome eviction coincides with resection, which is marked by strand-specific loss of DNA (Figure 25).

When we examined the DNA binding for these different histones, we observed that, even after induction of DSBs, histones enriched both forward and reverse strands equally, as exemplified in Figure 24 by the strand separated coverage plots for one of the Top15 breaks and by the equal loss of H3 coverage on forward and reverse strands in Figure 25. Consistently, when we averaged the ratios of forward to reverse strands of the top 15 resected AsiSI breaks, we observed a strong bias for input DNA and RPA, indicating resection and ssDNA binding of RPA, but only dsDNA binding for all histones (Figure 26). Altogether, we conclude that nucleosome eviction is not exclusive to the *MAT* locus but is rather a widespread mechanism in response to resection throughout the yeast genome.

Lastly, the gold standard technique for mapping nucleosomes is partial digestion of chromatin by micrococcal nuclease (MNase). Therefore, we reasoned that, if nucleosomes would occupy resected ssDNA, they would protect it from MNase digestion and we would be able to detect their footprint by strand-specific ChIP-sequencing. Therefore, we added a MNase digestion step to fragment chromatin prior to histone ChIP and strand-specific library preparation. Remarkably, we could not detect any ssDNA binding of histone H3 even in this experiment and we rather observed additional loss of the 3' resected ssDNA (Figure 27). Importantly, the hypersensitivity of ssDNA to MNase digestion constitutes additional evidence that nucleosomes are neither left nor assembled on ssDNA behind the resection machinery in yeast.

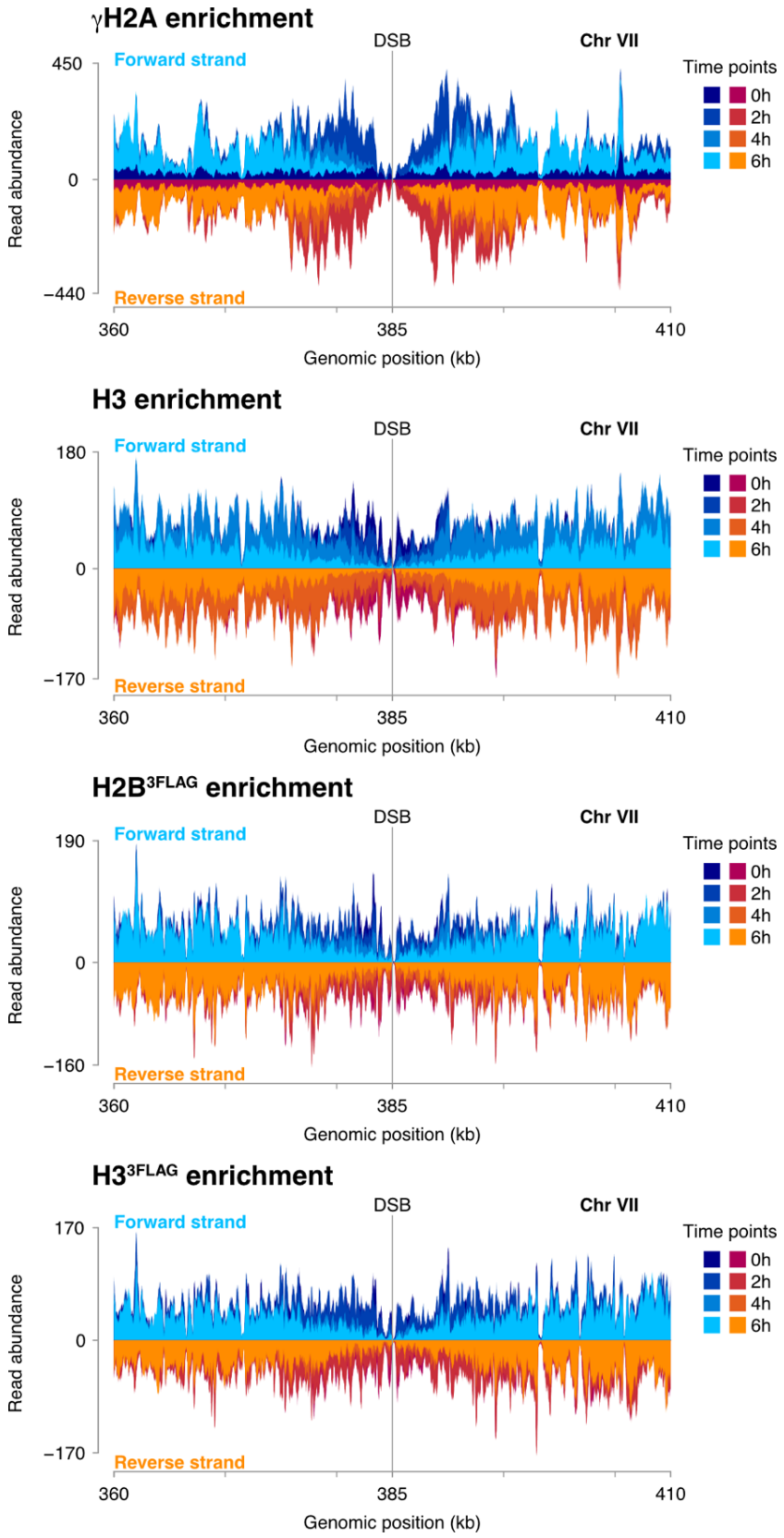

Figure 24. Nucleosome eviction at an AsiSI cut site on chromosome VII.
Strand-specific coverage in a 50 kb window centered at a single AsiSI cut site (chromosome VII, 384.688 bp) of, from top to bottom panel, γH2A, H3, $H2B^{3FLAG}$ and $H3^{3FLAG}$ ChIP before and after 2, 4 and 6 hours of AsiSI induction in cells arrested in nocodazole. Histone eviction and dsDNA binding are visible for all histones analyzed. Same dataset as in Figure 23. Results representative of n=2 biological replicates.

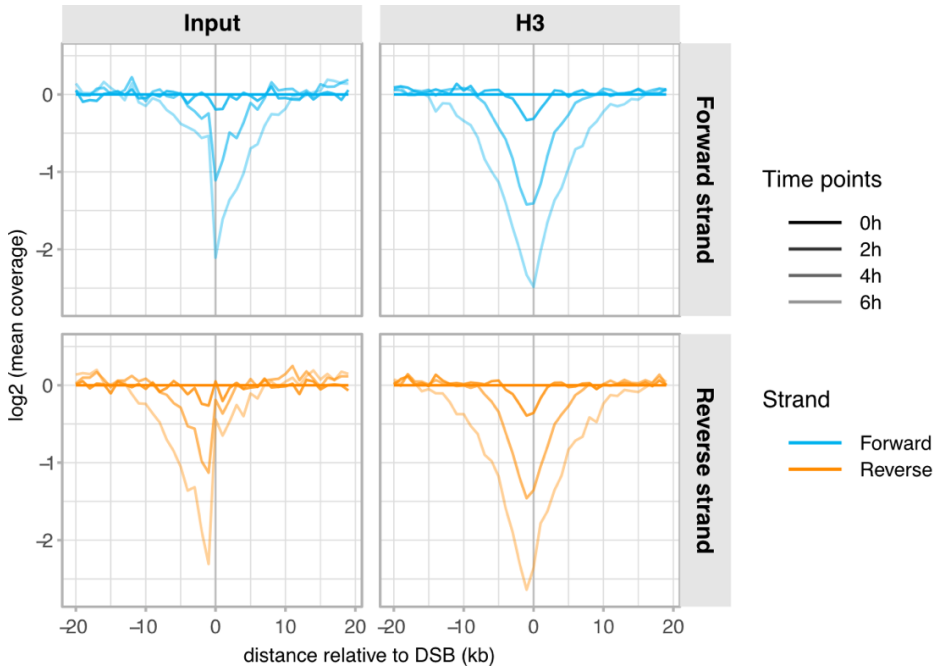

Figure 25. Resection and nucleosome eviction coincide at Top15 AsiSI cut sites.
Strand-separated coverage of input and strand-specific H3 ChIP-seq normalized to uninduced sample and averaged over Top15 AsiSI DSBs (1000 bp binning, $\log_2$ scale) after DSB induction for 0, 2, 4 and 6 hours in cells arrested in M phase. Plots cover a 40 kb window centered at the DSB. Both DNA and H3 signals are lost over the time course upon AsiSI induction. Specifically, the input signal is lost in a biased manner, consistent with the 5' strand being resected, while the histone signal is lost in an equal manner on the forward and reverse strands, indicating nucleosome eviction. It is worth to mention that after 6 hours of break induction there is a limited, but detectable loss of the 3' DNA strand, as it was previously observed (Zierhut and Diffley, 2008). Same dataset as in Figure 23 and Figure 24. Results representative of n=2 biological replicates.

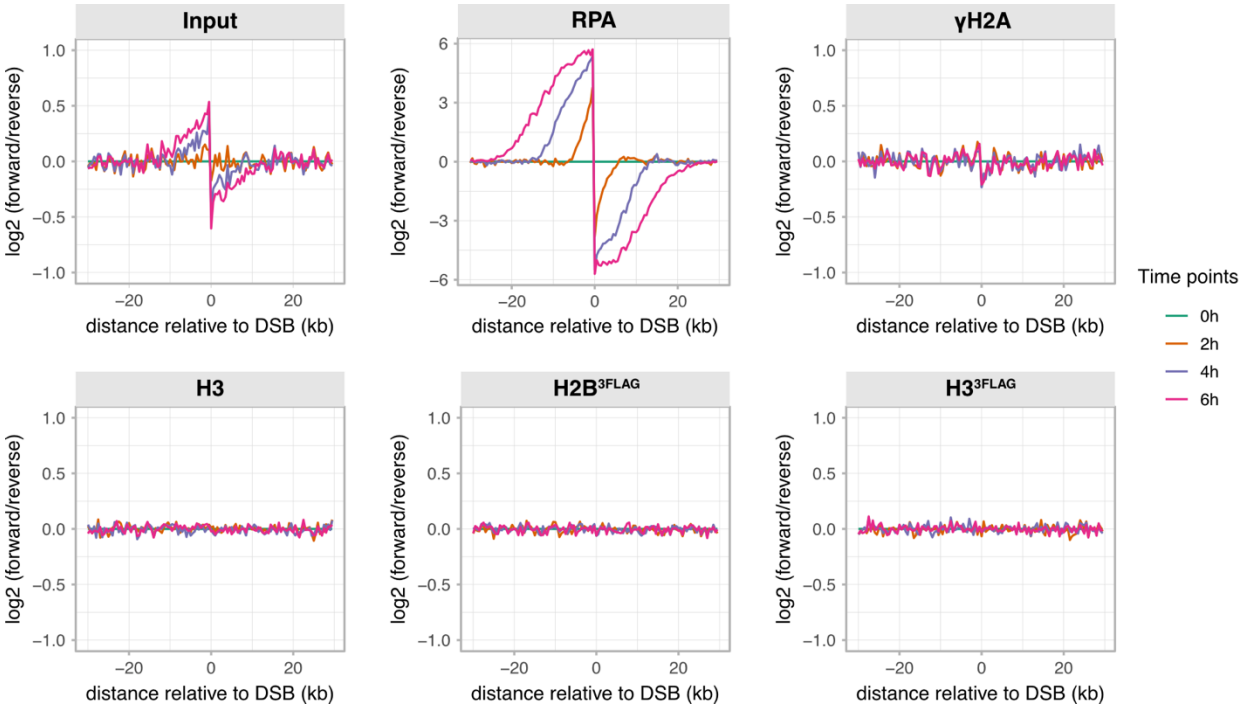

Figure 26. Histones associate exclusively with dsDNA after AsiSI induction.
Log2 ratio of forward to reverse strand coverage normalized to the uninduced sample and averaged over

Top15 AsiSI DSBs (500 bp binning). A 60 kb window centered at the DSB is shown for input DNA, RPA, γH2A, H3, H2B^{3FLAG} and H3^{3FLAG}. Cells were harvested at the indicated time points after AsiSI induction. Strand-bias in input DNA and RPA strand-specific ChIP-sequencing analysis indicate ongoing resection and ssDNA binding by RPA, while histones bind exclusively to dsDNA. Results representative of n=2 biological replicates.

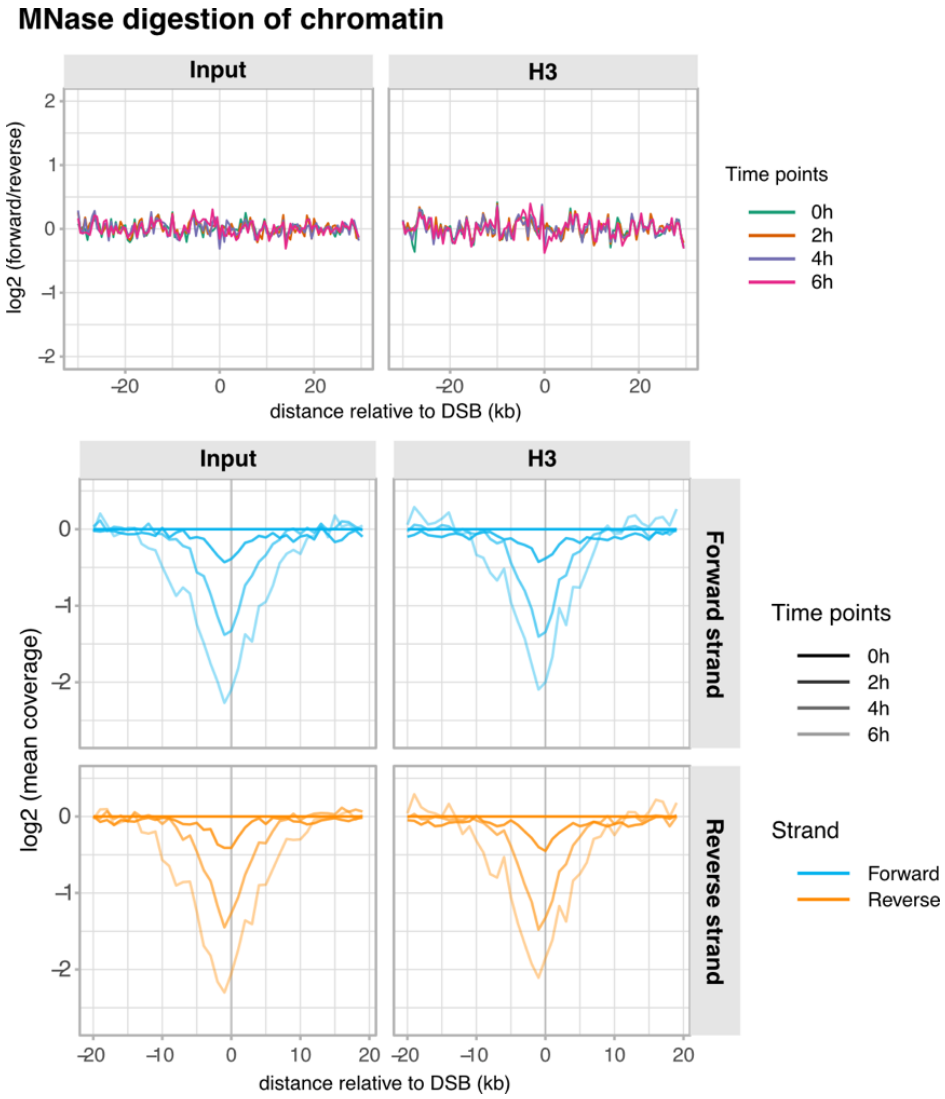

Figure 27. Lack of nucleosomes on resected ssDNA leads to MNase hypersensitivity.
Yeast cells were arrested in mitosis and harvested at 0, 2, 4 and 6 hours after AsiSI induction. Prior to ChIP, DNA was fragmented via MNase treatment. Top panels: Log_2 of forward to reverse strand ratio of input and H3 coverage averaged over Top15 resected AsiSI cut sites. The absence of strand bias suggests dsDNA binding of histones. Bottom panels: Forward and reverse coverage of input and H3 ChIP normalized to uninduced sample and averaged over Top15 DSBs (1000 bp bins, log_2 scale). Plots cover a 40 kb window centered at the DSB. Both input and H3 ChIP coverage show a similar signal loss on forward and reverse strands after AsiSI induction, indicating that the absence of nucleosomes on resected ssDNA causes its hypersensitivity to MNase digestion. Results representative of n = 2 biological replicates.

3.7 Resection and nucleosome eviction are coupled

The data presented so far point towards a model in which resection and eviction are coupled. Even more, nucleosome eviction might be a prerequisite for resection. Therefore, we asked whether nucleosome eviction was the result of an active process, catalyzed by nucleosome remodelers, or whether it is entirely caused by the passage of the resection machinery through chromatin. To date, a large number of chromatin remodelers have been described to take part in DSB repair, some of which are known for their role in promoting resection or later steps in homologous recombination, like Fun30 and Ino80-C (Karl et al., 2022; Seeber et al., 2013). Hence, to answer this question, we sought out the chromatin remodelers that could perform this activity.

3.7.1 Fun30 is dispensable for nucleosome eviction

Fun30 (SMARCAD1 in human) is a remodeler of the Swr1-like family and it is evolutionarily conserved throughout eukaryotes (Flaus et al., 2006). Despite the role of Fun30 and SMARCAD1 in promoting resection is well established (Bantele et al., 2017; Chen et al., 2012, 2016; Costelloe et al., 2012; Eapen et al., 2012), it is still not entirely clear by which mechanism and which effect Fun30/SMARCAD1 has on nucleosomes. To this regard, it has been shown that both Fun30 and SMARCAD1 have an antagonistic relationship with Rad9/53BP1, which are well-known inhibitors of resection (Bantele et al., 2017; Bothmer et al., 2011; Bunting et al., 2010; Chen et al., 2016; Costelloe et al., 2012; Lazzaro et al., 2008). Rad9 and 53BP1 have been shown to be multivalent nucleosome binders and to specifically recognize DNA damage-induced histone PTMs (Botuyan et al., 2006; Bunting et al., 2010; Fradet-Turcotte et al., 2013; Grenon et al., 2007; Hammet et al., 2007; Hu et al., 2017; Huyen et al., 2004; Toh et al., 2006; Wilson et al., 2016; Wysocki et al., 2005). Therefore, one of the proposed mechanism of action of Fun30/SMARCAD1 would be to evict nucleosomes bound by Rad9/53BP1 and hence locally restore a chromatin environment favorable for resection (Bantele and Pfander, 2019; Karl et al., 2022). Indeed, it has recently been shown that SMARCAD1 can evict nucleosomes *in vitro*, which would support this hypothesis (Markert et al., 2021).

Thus, we first decided to test how a *FUN30* deletion would influence nucleosome eviction and resection. For this, we introduced a *FUN30* deletion in a strain bearing the *pGAL-AsiSI* construct. In addition, given the defect of *fun30Δ* cells in resection elongation (Bantele et al., 2017; Chen et al., 2012; Costelloe et al., 2012; Eapen et al., 2012), we also introduced

a deletion of the Fun30 antagonist, *RAD9*, to prevent resection inhibition. After AsiSI induction, we observed that resection spread to a larger extent in the *fun30Δ rad9Δ* strain compared to wild-type, as it was previously described (Bantele et al., 2017; Chen et al., 2012) (Figure 28A).

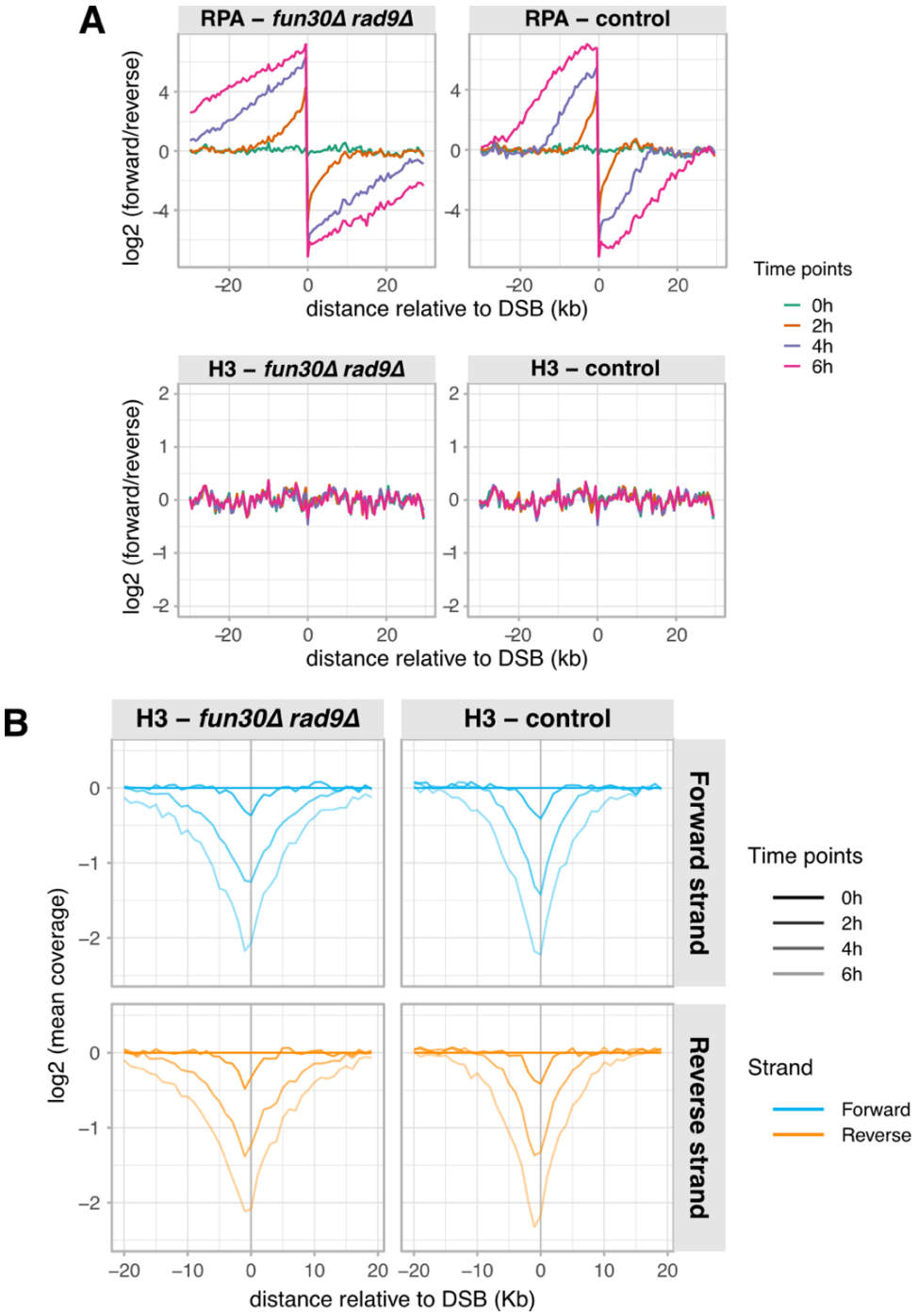

Figure 28. Fun30 is not required for nucleosome eviction at DSBs.
Control (right panels) and *fun30Δ rad9Δ* (left panels) cells were harvested at the indicated time points after AsiSI induction in nocodazole arrested cells. **A)** Log_2 of forward:reverse strands ratios calculated from strand-specific ChIP-sequencing coverage of RPA (top) and H3 (bottom) averaged over Top15 resected AsiSI breaks (500 bp binning). Plots cover a 60 kb window centered at the DSB. RPA strand-biased ratios

showed a more extensive spread of resection in *fun30Δ rad9Δ* cells compared to the control. Moreover, no ssDNA binding was detected in strand-specific H3 ChIP sequencing in neither of the strains. **B)** Log_2 mean of H3 ChIP strand-separated coverage over Top15 AsiSI sites, normalized to uninduced sample (1000 bp bins). A 20 kb window on each side of the DSB is shown. H3 signal loss reflects nucleosome eviction, according to the extent of resection in each strain. Results representative of n=2 biological replicates.

However, *FUN30* deletion did not affect nucleosome eviction in *fun30Δ rad9Δ* cells, but it rather correlated with the degree of resection, similarly to wild-type cells (Figure 28B). Moreover, we also did not find evidence of nucleosomes binding to resected ssDNA in the absence of Fun30 remodeling activity (Figure 28A). Therefore, we conclude that, despite Fun30 is crucial for resection, it is dispensable for nucleosome eviction. In fact, it has been observed that Fun30 is unable to relieve the nucleosomal barrier *in vitro* (Adkins et al., 2013), suggesting that Fun30 and SMARCAD1 may promote resection via different mechanisms.

3.7.2 The INO80 complex is not required for nucleosome eviction

The INO80 complex (INO80-C) is also belonging to the Swr1-like family of remodelers and it is conserved from yeast to human (Flaus et al., 2006). Notably, it has been shown that Ino80 is recruited to DSBs, likely via H2A phosphorylation (van Attikum et al., 2004; Downs et al., 2004; Morrison et al., 2004). Moreover, several reports in the literature linked INO80-C with nucleosome eviction at DSBs and at gene promoters (Attikum et al., 2007; Qiu et al., 2020; Tsukuda et al., 2005). In contrast, INO80-C function is primarily associated with H2A and H2A.Z exchange dynamics (Alatwi and Downs, 2015; Brahma et al., 2017; Lademann et al., 2017; Papamichos-Chronakis et al., 2006, 2011). Specifically, INO80-C was shown to catalyze the exchange of H2A.Z for canonical H2A at DSBs (Alatwi and Downs, 2015; Lademann et al., 2017; Papamichos-Chronakis et al., 2006, 2011). Therefore, we decided to test whether the INO80 complex plays a role in nucleosome eviction using the AsiSI system and, in addition, whether H2A.Z would bind to resected ssDNA in the absence of functional INO80-C. Specifically, we deleted *ARP8*, a gene that encodes for one of its multiple subunits. Deletion of *ARP8* causes the loss of the entire Arp8-module, which results in a defective remodeling activity of the complex (van Attikum et al., 2004, 2004; Brahma et al., 2018; Knoll et al., 2018; Papamichos-Chronakis et al., 2006; Tosi et al., 2013; Tsukuda et al., 2009). After AsiSI induction, we performed strand-specific H2A.Z and H3 ChIP-sequencing.

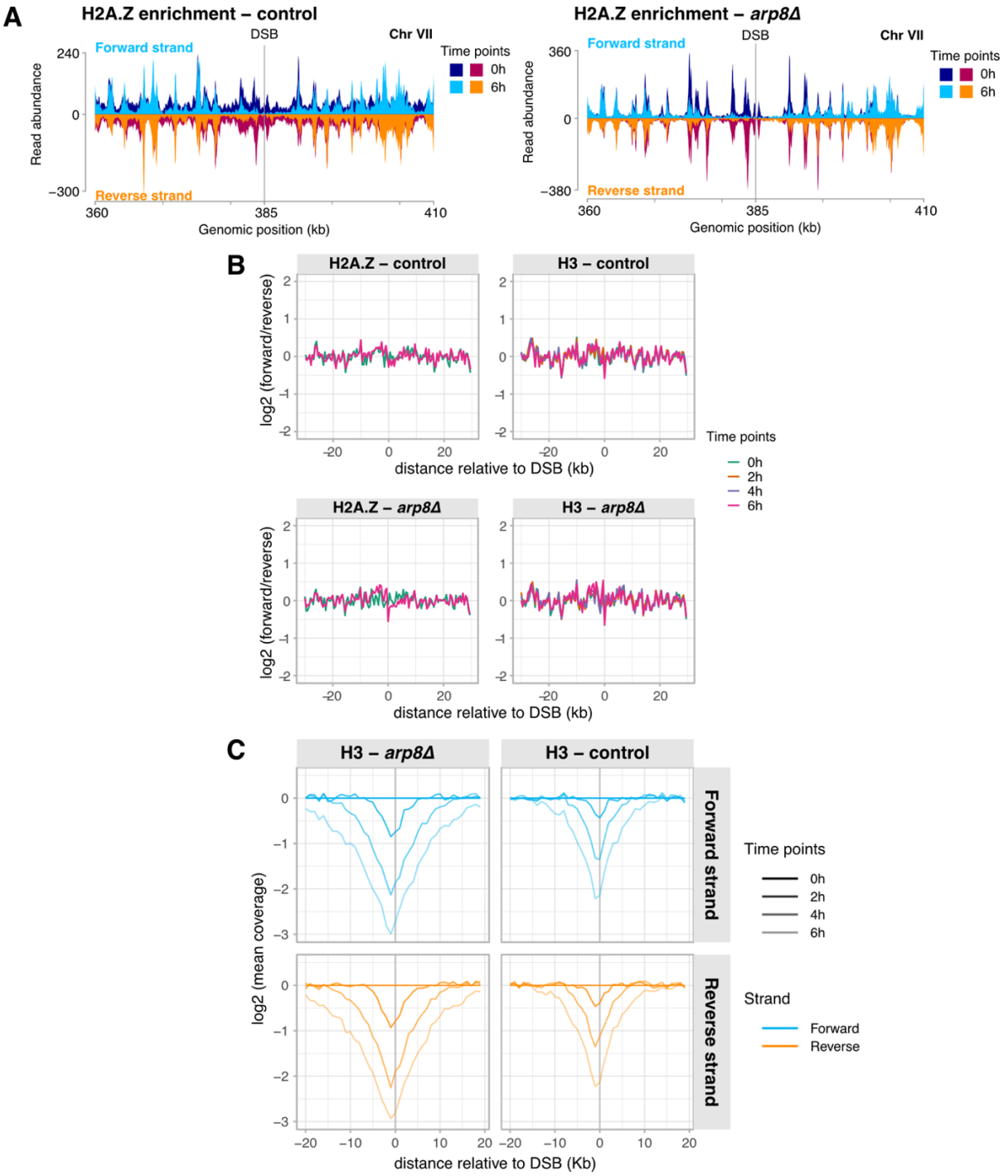

Figure 29. Nucleosome eviction at resected DSB does not depend on INO80-C function.
Cells were arrested in nocodazole and AsiSI was induced for the indicated time points in each panel. **A)** Strand-specific H2A.Z ChIP-sequencing coverage in a 50 kb window centered at one of the Top15 resected AsiSI DSBs (chromosome VII, 384.688 bp). In both control (left) and *arp8Δ* cells (right), H2A.Z shows dsDNA binding and eviction upon resection, in addition, H2A.Z occupancy pattern is similar to already published data (Gu et al., 2015; Lademann et al., 2017). **B)** Forward:reverse strand $\log_2$ ratios of H2A.Z (left panels) and H3 (right panels) coverage in wild-type (top panels) and *arp8Δ* (bottom panels) cells averaged over Top15 AsiSI cut sites (500 bp binning). Plots cover a 60 kb window centered at the DSB. H2A.Z coverage data were subjected to peak calling prior to the calculation. Neither H2A.Z nor H3 ratios provide evidence for ssDNA binding of the respective histone, both in *arp8Δ* and control. **C)** Log_2 mean of strand-separated H3 coverage over Top15 AsiSI breaks, normalized to the uninduced sample (1000 bp binning). A 20 kb window on each side of the DSB is shown. *Arp8Δ* (left panels) and control cells (right panels) show extensive

H3 signal loss, indicative of nucleosome eviction. Decrease of H3 coverage is even higher in the *arp8* mutant. Results representative of n=2 biological replicates.

First, the pattern of H2A.Z peaks that we observed in the control strain reflected already published data of H2A.Z occupancy in cells arrested in mitosis (Gu et al., 2015; Lademann et al., 2017) (Figure 29A). Moreover, *arp8Δ* cells showed no defect in nucleosome eviction when compared to wild-type and rather the H3 ChIP signal loss is increased in the mutant (Figure 29C). This observation suggests that INO80-C is not directly involved in nucleosome eviction at DSBs and its function might even be, to some extent, detrimental for resection. Lastly, for both *arp8Δ* and control strain, we found no evidence of ssDNA binding in H2A.Z and H3 ChIP (Figure 29B). Hence, we reasoned that the function of the INO80-C is not required for resection nor for nucleosome eviction.

3.7.3 RSC and SWI/SNF are crucial for nucleosome eviction and resection

RSC and SWI/SNF remodeling complexes are both part of the Snf2 subfamily of nucleosome remodelers (Flaus et al., 2006). Notably, the main function described for these chromatin remodelers is nucleosome eviction (Clapier and Cairns, 2009; Clapier et al., 2017). In addition, there is strong and increasing evidence in the literature that SWI/SNF and RSC, as well as their human counterparts, BAF and PBAF, are involved in DSBs repair (Bennett and Peterson, 2015; Hays et al., 2020; Kent et al., 2007; Liang et al., 2007; Park et al., 2006; Shim et al., 2007; Wiest et al., 2017). Specifically, they have been shown to promote resection both in yeast (Bennett and Peterson, 2015; Kent et al., 2007; Liang et al., 2007; Shim et al., 2007; Wiest et al., 2017) and in human (Hays et al., 2020). Therefore, they are good candidates for being tested for their role in nucleosome eviction in the AsiSI system. However, since these remodelers seem to share the same nucleosome remodeling activity, we inferred that they may act redundantly. Thus, we generated a yeast strain in which we could deplete both RSC and SWI/SNF simultaneously. To achieve this, we made use of an auxin-inducible degron (AID) system that was previously developed (Morawska and Ulrich, 2013). Briefly, we fused a triple-AID tag to the C-terminus of Sth1 and Snf2, which are the catalytic subunits of RSC and SWI/SNF, respectively. In this way, addition of auxin (IAA) to the culture medium would trigger the degradation of the proteins harboring the degron. Remarkably, when we induced AsiSI in cells where Sth1 and Snf2 were simultaneously depleted, we found a strong defect in nucleosome eviction as well as in resection (Figure 30). This observation suggests that

nucleosome eviction and resection are concurrent events and that they are intrinsically coupled processes. Importantly, suppression of nucleosome eviction by the removal of RSC and SWI/SNF activities affected resection, indicating that nucleosome eviction is a crucial step for resection to occur. This led us to the conclusion that RSC and SWI/SNF remodeling is necessary for the first step of HR and that they represent the major evicting activities at DSBs.

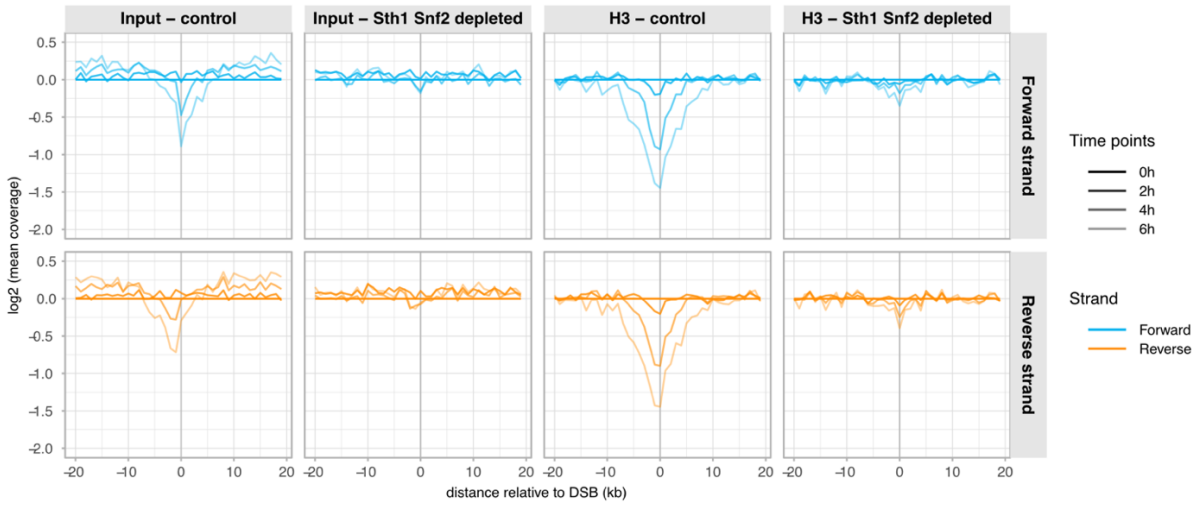

Figure 30. RSC and SWI/SNF are required for nucleosome eviction and resection.
Control and Sth1 Snf2 depleted cells, arrested in mitosis, were harvested at the indicated time points after AsiSI induction. Forward and reverse coverage of input and H3 ChIP, averaged over Top15 AsiSI breaks and normalized to the uninduced sample (1000 bp binning, $\log_2$ scale). A 20 kb window on each side of the DSB is shown. DNA and H3 signal loss in the wild-type strain indicate ongoing resection and nucleosome eviction, respectively. Notably, when RSC and SWI/SNF remodeling function is absent, both nucleosome eviction and resection are abolished. Results representative of n=2 biological replicates.

4. Discussion

4.1 Strand-specific ChIP-sequencing is able to discriminate between ssDNA and dsDNA binding

The first step of DSB repair via homologous recombination (HR) is DNA end resection, the nucleolytic degradation of dsDNA that generates long 3' ssDNA overhangs (Symington and Gautier, 2011). As a result, resection divides the damaged chromatin into distinct ssDNA and dsDNA domains. These domains comprise different sets of DNA repair and checkpoint factors, which can associate either directly to ssDNA or dsDNA or via protein-protein interaction. However, it is unclear how rigid the separation between the two domains is and how factors from different compartments would interact with each other. Consequently, determining the properties and interactions of ssDNA and dsDNA compartments will be crucial to understand the mechanisms underlying DNA damage response and repair. Adequate methodologies are needed to discriminate between these two domains *in vivo*. For example, proteins accumulating at DSBs form so-called foci that can be visualized using microscopy (Bekker-Jensen et al., 2006). Currently, only super-resolution microscopy may provide sufficient resolution to distinguish between the ssDNA and dsDNA compartments and has been exclusively applied to mammalian cells (Chapman et al., 2012; Ochs et al., 2019; Reindl et al., 2017; Whelan and Rothenberg, 2021). Instead, a methodology that is widely used to determine protein binding at DSBs is chromatin immunoprecipitation (ChIP) (Clouaire et al., 2018; Renkawitz et al., 2013a; Shroff et al., 2004; Wang and Haber, 2004). Nevertheless, the outcome of ChIP reflects exclusively the combination of signals emerging from each cell in a population. This means that, considering the stochasticity of resection initiation and elongation, even when inducing a single DSB in a specific genomic locus, only a fraction of cells will show resected ssDNA at a given distance from the DSB (Zierhut and Diffley, 2008). Therefore, the colocalization of a protein of interest with proteins binding to ssDNA or dsDNA is insufficient to infer its association with the ssDNA or dsDNA compartment, respectively. To circumvent this limitation, we established a technique that allows to directly discriminate whether a signal came from ssDNA or dsDNA binding: strand-specific ChIP-sequencing. By generating sequencing libraries from ssDNA using an adaptase-based method, we were able to retain strand identity and, thus, visualize protein enrichment on

forward and reverse strands separately (Figure 6). For example, in Figure 9, where strand specificity of ChIP enrichment was omitted, RPA, Ddc1 and Dpb11 appear to colocalize in the resected area of the DSB. However, when we visualize the sequencing coverage separated in forward and reverse strand (Figure 7B and Figure 8), we can observe that only RPA belongs to the ssDNA compartment, while Ddc1 and Dpb11 are associated with dsDNA. Therefore, our data indicate that strand-specific ChIP-sequencing, in combination with site-specific induction of DSBs, is a powerful technique to determine if proteins associate with ssDNA or dsDNA domains.

4.1.1 Strand-specific ChIP-seq is a powerful method to address any DNA transaction that generates strand asymmetry

Since strand-specific ChIP-sequencing can discriminate between ssDNA and dsDNA binding of proteins, it can be a valid tool to address questions on any chromatin-related process that generates asymmetry between forward and reverse strands. Therefore, strand-specific ChIP-sequencing can be applied to a wide range of biological problems, which will be discussed in this paragraph.

For example, besides resection of DSBs, processing of other types of DNA lesions can lead to the formation of RPA-coated ssDNA (Figure 31). Mismatched base pairs generated by DNA replication or repair are excised during mismatch repair (MMR) leaving a ssDNA patch protected by RPA (Li, 2008). In an analogous mechanism, bulky lesions caused by UV irradiation are removed from DNA in the first step of nucleotide excision repair (NER), which exposes as well a short ssDNA gap bound by RPA (Novarina et al., 2011). ChIP combined with standard sequencing library preparation protocols would not be suitable for the detection of RPA-ssDNA patches in the genome. The reason for this is that the most commonly used library preparation protocols are unable to convert ssDNA into library molecules, since only blunt and A-tailed dsDNA molecules are suitable for adapter ligation (Meyer and Kircher, 2010). Thus, only a method like strand-specific ChIP-sequencing would allow the detection of protein enrichment on ssDNA.

Similarly, transcription is also a potential source of asymmetry, particularly when the RNA product forms a stable duplex with the template DNA, a so-called RNA:DNA hybrid. RNA:DNA hybrids, together with the displaced single-stranded DNA, form three-stranded structures referred to as R-loops (Figure 31), which have been extensively investigated in the last decades (Crossley et al., 2019; Niehrs and Luke, 2020; Rinaldi et al., 2021). There

is an increasing number of studies showing how R-loops are involved in a vast variety of physiological processes, from the regulation of gene expression to DNA repair (Niehrs and Luke, 2020), but they have also been associated with genome instability (Costantino and Koshland, 2018; Rinaldi et al., 2021). In the attempt of understanding the biological role of R-loops, a considerable number of techniques for their detection have been developed (Crossley et al., 2019), however many aspects of R-loop regulation and function still need to be elucidated. For example, it is still unclear whether or not the displaced ssDNA of R-loops is coated by RPA (Rinaldi et al., 2021). In this context, strand-specific ChIP-sequencing can serve as a complementary technique to determine specific protein association to R-loops.

Strand asymmetry is a feature of replication forks as well, since DNA synthesis is continuous on the leading strand, while discontinuous on the lagging strand. This property has been exploited, for example, in the eSPAN method that allows to determine the mechanism of parental histone inheritance or the association of replication factors with leading or lagging strands (Gan et al., 2018; Yu et al., 2014). Moreover, DNA replication is susceptible to perturbations, like DNA lesions, DNA secondary structures or collisions between replication and transcription machineries, that lead to stalling or slowing of the replication fork: a phenomenon referred to as replication stress (Técher and Pasero, 2021; Zeman and Cimprich, 2014). DSBs can be formed through the collapse of replication forks (Figure 31), showing the potential of replication stress to cause genomic instability (Técher and Pasero, 2021; Zeman and Cimprich, 2014). Resection or the uncoupling of DNA polymerase and helicase occurring at stalled forks leads to an accumulation of RPA-coated ssDNA (Figure 31), which is considered a marker of replication stress (Delamarre et al., 2020; Técher and Pasero, 2021; Zeman and Cimprich, 2014; Zou and Elledge, 2003). In this context, strand-specific ChIP-sequencing would be a suitable technique to identify genomic regions affected by replication stress. Indeed, in another project from our group, we used this technique to address the consequences of unscheduled DNA replication in the G1 phase of the cell cycle (Reusswig et al., 2021, Reusswig et al., *in revision*). By using strand-specific RPA ChIP-sequencing we could show that G1 replication causes RPA-ssDNA accumulation during the subsequent S phase, likely as a result of single-end DSBs formation upon collisions between G1 and S replisomes.

In conclusion, strand-specific ChIP-sequencing is a versatile method and we anticipate that it will be useful to interrogate a wide range of DNA transactions.

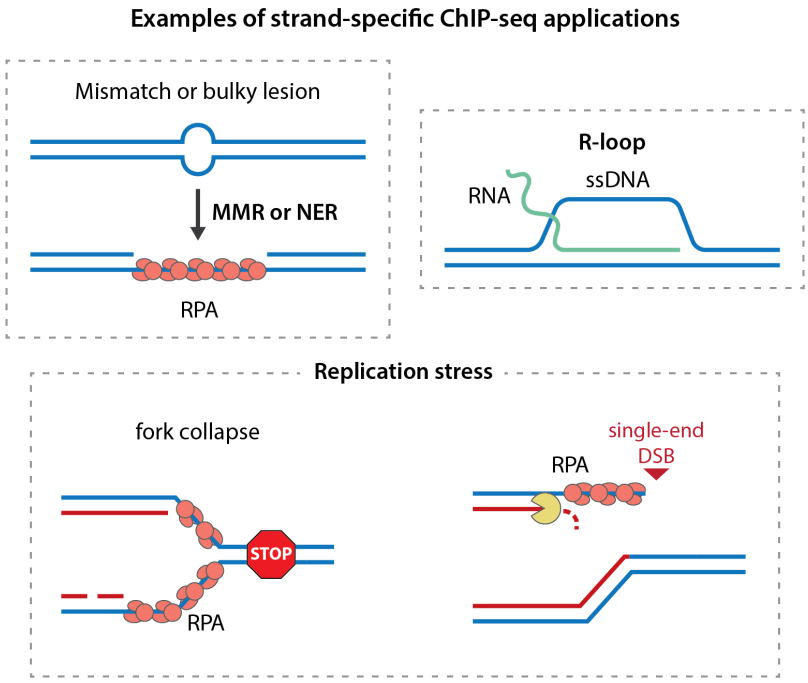

Figure 31. Examples of potential strand-specific ChIP-seq applications.
The figure illustrates DNA transactions that generate strand asymmetry, which can be investigated using strand-specific ChIP-sequencing. Top left panel: DNA mismatches and bulky lesions (such as pyrimidine dimers induced by UV light) are excised during MMR and NER, respectively, exposing ssDNA readily bound by RPA. Top right panel: R-loops can form as a consequence of transcription. Their structure, comprising a hybrid duplex formed by an RNA (green) and a DNA (blue) strand, leaves the second DNA strand displaced. Bottom panel: replication stress generally results in an accumulation of RPA-coated ssDNA, the causes of which can be numerous. For example, uncoupling of DNA polymerase and helicase can lead to fork collapse and RPA-ssDNA accumulation. Furthermore, stalled/collapsed replication forks can be processed by nucleases, generating single-end DSBs (seDSBs) that can be resected to produce RPA-coated ssDNA.

4.2 The 9-1-1 complex and its interactor Dpb11 associate to dsDNA at the leading edge of resection

As discussed in the previous paragraph, RPA-bound ssDNA constitutes a common intermediate of many DNA repair pathways and characterizes stalled replication forks as well. This structure can be considered a general marker of DNA damage and replication stress and, as such, plays a pivotal role in DNA damage sensing and response (Bantele et al., 2019; Rouse and Jackson, 2002; Zou and Elledge, 2003). Specifically, the RPA-ssDNA complex is able to trigger checkpoint activation via the conserved Mec1/ATR pathway. Mec1/ATR is recruited on the RPA-ssDNA platform via its cofactor Ddc2/ATRIP, which recognizes and binds to RPA (Deshpande et al., 2017; Dubrana et al., 2007; Rouse and Jackson, 2002; Zou and Elledge, 2003). Recruitment of Mec1 is crucial for its activation and for the phosphorylation of its targets at damage sites, like histone H2A. However, Mec1 recruitment alone is not sufficient to activate a global checkpoint signaling in the

cell, which rather requires the additional interaction of Mec1/ATR with the 9-1-1 sliding clamp complex (Majka et al., 2006a; Mordes et al., 2008; Navadgi-Patil and Burgers, 2008, 2009; Pfander and Diffley, 2011; Puddu et al., 2008). Indeed, artificial colocalization of Mec1 and 9-1-1 was shown to trigger checkpoint activation even in the absence of DNA damage (Bonilla et al., 2008). The mechanism of 9-1-1 recruitment and loading has been extensively investigated (Castaneda et al., 2021; Ellison and Stillman, 2003; Majka et al., 2006b; Zheng et al., 2021; Zou et al., 2003). According to the latest study, the cryo-EM structure of the RFC-Rad24 clamp loader with DNA shows that its recruitment occurs specifically at 5' ss-dsDNA junctions, where RFC-Rad24 can interact with both ssDNA and dsDNA. Here, the orientation of RFC-Rad24 complex directs the loading of the 9-1-1 clamp on ssDNA (Castaneda et al., 2021; Zheng et al., 2021). Altogether, these observations raise the question of how the 9-1-1 would slide on DNA after its loading. We can envision different possible scenarios. First, the 9-1-1 could remain associated and move on the resected ssDNA. However, it is not clear if the central channel of this ring-shaped complex would be able to accommodate RPA-coated ssDNA. To this point, sliding of PCNA, another clamp of the same family, was shown to be inhibited by RPA (Hedglin and Benkovic, 2017). Second, the 9-1-1 could slide on dsDNA, in analogy with PCNA (De March et al., 2017). In this case, *in vitro* experiments have shown that 9-1-1 sliding occurs on dsDNA (Majka et al., 2006b). Consistently, our results indicate that both 9-1-1 and its binding partner Dpb11 associate with dsDNA at a resected DSB (Figure 8). In addition, not only the coverage profiles of 9-1-1 and Dpb11 are nearly identical, consistent with their interaction, but they also peak in proximity of the leading edge of resection, according to RPA enrichment (Figure 9). This pattern can be explained by the presence of nucleosomes ahead of the resection nucleases, which may hinder the translocation of 9-1-1 on dsDNA away from the resection boundary. Therefore, our data suggest a model in which the 9-1-1 clamp slides on dsDNA after loading, remaining in close proximity of the ss-dsDNA junction and following resection directionality. According to this model, the 9-1-1 complex would travel through chromatin ahead of the resection machinery. Consequently, it is interesting to speculate that the 9-1-1 could have a critical role in the control of resection, serving as a binding platform for the recruitment of DNA repair proteins specifically to dsDNA close to the ssDNA-dsDNA junction. Notably, a previous study from our group has shown that the Fun30 chromatin remodeler is recruited to resected DSB via its interaction with Dpb11 and 9-1-1. Importantly, forced targeting of

Fun30 to DSBs, by fusing it with a subunit of the 9-1-1 complex, resulted in increased resection elongation (Bantele et al., 2017). One possible explanation could be that the remodeling activity of Fun30 on nucleosomes or nucleosome-bound factors, ahead of the resection machinery, would remove the chromatin block hindering the resection nucleases. Interestingly, Fun30 is not required for nucleosome eviction, but appears to promote resection by a different mechanism (see discussion in paragraph 4.4). Future studies will clarify the mechanism of Fun30 remodeling at DSBs.

4.3 The role of genome architecture in DNA repair

4.3.1 Homology search is guided by the chromosomal architecture

A crucial step of DSB repair via homologous recombination is the search of a homologous template. This mechanism is particularly fascinating from a biological point of view, but has also medical relevance, since defects in HR promote genomic instability and thus play a role in cancer development and other diseases. Therefore, the mechanism of homology search has been extensively investigated. The main factor in homology search is Rad51, the eukaryotic homologue of the bacterial RecA recombinase. Rad51 binds to the ssDNA produced by resection forming a nucleoprotein filament that is able to probe chromatin in the search for a homologous sequence (Heyer et al., 2010; San Filippo et al., 2008; Sung and Robberson, 1995). In the following step, strand-invasion and D-loop formation is catalyzed by the Rad51 filament with the aid of Rad54, which stabilizes the 3' end of the filament on the template and promotes its extension by DNA polymerase (Solinger and Heyer, 2001). In yeast, successful engagement of the Rad51 filament with the homologous sequence has been detected one hour after DSB induction (Mehta et al., 2017), but how can cells probe in such short time a large number of possible alignments in the genome? Albeit there is not a complete and definitive answer to this question yet, several aspects of homology search have been experimentally determined. One of these is the role of 3D chromosome architecture in directing the Rad51 filament probing, which was observed in the yeast mating type switch system (Renkawitz et al., 2013a). Mating type genes occupy the *HML* and *HMR* loci on the different arms of chromosome III and contain homology to the *MAT* locus, located between *HML* and *HMR*. Upon DSB induction at *MAT*, depending on the cell's mating type, either *HML* or *HMR* is used as donor for repair via

HR. Renkawitz and colleagues, by using Rad51 ChIP-on-chip, observed that the pattern of Rad51 enrichment recapitulated the specific 3D conformation that chromosome III adopts according to the mating type (Li et al., 2012). Such architecture is directed by the recombination enhancer (*RE*) element that causes chromosome looping (Belton et al., 2015; Li et al., 2012). Importantly, *RE* was able to stimulate homology search *in trans* when inserted on other chromosomes, indicating that physical proximity to the DSB plays a role in the probing mechanism of the Rad51 filament (Renkawitz et al., 2013a). Consistently, by using strand-specific Rad51 ChIP-sequencing we could identify two types of Rad51 signals after DSB induction at *MAT*. The first, representing Rad51 filament formation, originated from ssDNA in the resected area. The second, corresponding to homology search intermediates, derived from dsDNA and showed a pattern of Rad51 enrichment that followed the chromosome III architecture described above. Therefore, our data provide evidence that the Rad51 enrichment observed in Renkawitz et al., 2013 is a bona fide intermediate of homology search. Altogether, our results support a model in which homology search is guided by the 3D chromosome architecture.

Notably, the importance of the 3D environment around a DSB in homology search is valid not only within the mating type switch system, but also for homologous sequences located *in trans* on different chromosomes. Indeed, chromosomes are organized in the yeast nucleus according to a Rabl-like configuration, which involve clustering of centromeres at the spindle pole body and clustering of telomeres near the nuclear periphery. In this way, interactions between loci in the proximity of centromeres or telomeres are facilitated (Bordelet and Dubrana, 2019). Consistently, several studies have shown that homologous recombination occurs efficiently between pericentromeric regions (or subtelomeric regions) of specific chromosomes (Agmon et al., 2013; Brown et al., 2010; Burgess and Kleckner, 1999; Lee et al., 2016). It is interesting to mention that organisms differ in their nuclear organization. Importantly, chromosomes occupy distinct regions of the nucleus in somatic cells of mammals, a configuration that might hinder HR (Cremer and Cremer, 2010; Rao et al., 2014). Moreover, such 3D nuclear organization was shown to be involved in recurrent chromosomal translocations, since it brings in close proximity regions belonging to different chromosomes (Zhang et al., 2012).

4.3.2 γH2A spreading recapitulates the chromosomal architecture

Phosphorylation of histone H2A/H2A.X (γH2A/γH2A.X) is one of the first events occurring at a DSB. This reaction is carried out by the checkpoint kinases Mec1/Tel1 and ATM, in yeast and human respectively (Burma et al., 2001; Downs et al., 2000; Lee et al., 2014; Shroff et al., 2004). A considerable number of studies have observed that γH2A/γH2A.X can spread around a DSB over hundreds of kilobases in yeast and even megabases in mammals (Bantele et al., 2019; Iacovoni et al., 2010; Lee et al., 2014; Renkawitz et al., 2013a; Rogakou et al., 1999; Ström et al., 2004). Consistently, strand-specific ChIP-sequencing revealed extensive γH2A enrichment on chromosome III around the DSB at *MAT*. Interestingly, we also found that the γH2A pattern resembled the Rad51 homology search signal, as it was described previously (Renkawitz et al., 2013a, 2013b). This observation suggests that the principles that govern homology search, particularly the 3D architecture of the nucleus, may be applicable to γH2A distribution as well. Indeed, induction of a DSB near a centromere in yeast leads to spreading of the γH2A signal over the centromeres of unaffected chromosomes (Lee et al., 2014; Renkawitz et al., 2013a). Similarly, γH2A.X distribution in human cells was found to be constrained within the boundaries of topologically associated domains (TADs). In addition, cohesin, a protein complex involved in chromatin loop organization, was found to facilitate γH2A.X spreading at TADs boundaries (Arnould and Legube, 2020; Caron et al., 2012). There is also strong evidence in yeast that cohesin is recruited to DSBs and facilitate recombination between sister chromatids (Piazza et al., 2021; Sjögren and Nasmyth, 2001; Ström et al., 2004; Unal et al., 2007). These observations are not surprising if we consider the role of cohesin in chromatin loop extrusion and sister chromatids cohesion. In agreement, another factor involved in establishing TADs boundaries and insulators, CTCF, was found at the edge of γH2A.X domains with super-resolution microscopy (Natale et al., 2017). Therefore, it appears that proteins involved in the general 3D chromatin organization in the nucleus play pivotal roles in organizing HR and DNA damage response as well.

4.4 Strand-specific ChIP-seq reveals nucleosome dynamics at double-stranded breaks

4.4.1 DNA end resection and nucleosome eviction are intrinsically coupled

DNA lesions and the subsequent repair occur on a chromatin substrate; thus, this raises the question of how repair factors can perform their tasks on DNA that is covered by nucleosomes. This problem has been intensively investigated and, although a lot progress has been made, we still lack a clear and comprehensive view of nucleosome dynamics in DNA repair. In the context of this thesis, the discussion about nucleosome dynamics will be limited to DSB repair. In particular, during HR, the first reaction in which nucleosomes are involved is DNA end resection. Indeed, according to *in vitro* experiments, resection nucleases appear to be inhibited by the presence of nucleosomes (Adkins et al., 2013). This observation suggests that chromatin poses a barrier to resection and, therefore, it needs to be overcome for resection to proceed. Consistently, many groups have observed a decrease in histone ChIP signals around resected DSBs, which has been correlated with nucleosome eviction (Attikum et al., 2007; Bantele et al., 2019; Chen et al., 2008; Tsukuda et al., 2005, 2009). In contrast, a second model has been recently proposed as well. It was argued that nucleosome eviction during resection would occur at a slower pace compared, for example, to nucleosome eviction at the promoter of active genes, suggesting that nucleosomes might associate to the ssDNA produced by resection (Huang et al., 2018; Papamichos-Chronakis and Peterson, 2013; Sinha and Peterson, 2009). This hypothesis was thought to be supported by *in vitro* experiments showing that histone octamers can bind to ssDNA and form particles with similar appearance as canonical nucleosomes, although less stable (Adkins et al., 2017; Palter et al., 1979). Moreover, histones ChIP signals in the region of resection were interpreted to arise from nucleosomes on ssDNA (Huang et al., 2018). In contrast, our data show that nucleosomes do not represent a major species on resected ssDNA and, in contrast, indicate that they are evicted upon resection. These contrasting results between *in vitro* and *in vivo* experiments might be explained by the low affinity of nucleosomes with ssDNA or by the presence of additional factors like RPA on ssDNA, that could prevent re-assembly of nucleosomes on ssDNA *in vivo*, although histones have been detected on ssDNA in the presence of RPA *in vitro* (Adkins et al., 2017).

A consequence of the absence of nucleosomes on resected ssDNA is that ssDNA and dsDNA domains are very different constituents of damaged chromosomes (see also discussion in paragraph 4.1). Indeed, proteins interacting with nucleosomes would be excluded from the ssDNA domain as would be proteins interacting with dsDNA. This poses the question of how factors associated to either one or the other domain would come in contact with each other. One example in this regard is the aforementioned Mec1 kinase, which is recruited to ssDNA upon resection and is also the main kinase responsible for H2A phosphorylation in yeast (Bantele et al., 2019). How can Mec1 reach nucleosomes further away from the resected area, both *in cis* and *in trans*? Mechanisms involving Mec1 diffusion (Li et al., 2020), 3D architecture of the nucleus (Pombo and Dillon, 2015) (see also paragraph 4.3), increased chromatin mobility after DSB induction (Seeber et al., 2018) and/or protein condensates formed via liquid-liquid phase separation (Strom and Brangwynne, 2019) are possible. In addition, if we consider that the 9-1-1 complex is specifically recruited at ssDNA-dsDNA junctions, together with our data suggesting that 9-1-1 remains associated to the leading edge of resection, we can assume that ss-dsDNA junctions may be a focus of interactions between proteins of both domains (see also paragraph 4.2).

Another consequence of nucleosome eviction upon resection is the potential loss of epigenetic marks. This poses a two-fold problem for cells undergoing DNA repair: the first regards how chromatin will be assembled again on DNA after repair, the second regards the restoration of the epigenetic signature of the broken locus. In contrast to DNA replication, where the problem of chromatin assembly has been extensively investigated (Alabert et al., 2017), to date, little is known about the mechanisms behind chromatin restoration after DSB repair (Clouaire and Legube, 2019; Polo and Almouzni, 2015). Therefore, it is unclear if the same network of histone chaperones and chromatin remodelers involved in DNA replication also operates in DSB repair. However, results obtained in mammalian cells after UV-damage suggest that this might be the case (Polo and Almouzni, 2015). Indeed, in yeast, the Asf1 and CAF-1 histone chaperones have been implicated in chromatin restoration and checkpoint recovery after DSB induction (Chen et al., 2008; Diao et al., 2017; Kim and Haber, 2009). Nonetheless, we still have an incomplete picture of how chromatin is restored during DNA repair, particularly of how epigenetic marks are re-established. Importantly, DNA damage has been correlated to epigenetic and transcriptional changes (Oberdoerffer et al., 2008). In this context, we

anticipate that strand-specific ChIP sequencing could be a powerful tool to elucidate these mechanisms if combined with a labeling technique of newly synthesized DNA.

4.4.2 RSC and SWI/SNF act redundantly to promote nucleosome eviction and DNA end resection

Since nucleosomes pose a barrier to resection and our data indicate that this inhibition is overcome by nucleosome eviction, the next question is how eviction occurs at a DSB. There is strong evidence in the literature that chromatin remodelers could be the main actors in this process (Karl et al., 2022; Seeber et al., 2013). For this discussion, it is important to consider that three main activities of chromatin remodelers have been described: sliding/eviction, which leads to translocation of nucleosomes along the DNA and can ultimately result in the eviction of the octamer; positioning, which consists in formation of regularly spaced nucleosome arrays; editing, which refers to the exchange of canonical histones with histone variants and vice-versa. From studies in the context of gene regulation, several remodelers have been ascribed to each one of these activities, suggesting that a certain degree of redundancy is present in the cellular nucleosome remodeling system. Specifically, RSC and SWI/SNF appear to be the main sliders/evictors; Chd1, Isw1, Isw2 and Ino80 have been described as positioners; Swr1 and Ino80 have been described as editors (Karl et al., 2022). Interestingly, all of these remodelers, in addition to Fun30, have been involved in DSB repair in both yeast and human cells and some, importantly, were specifically described to have a role in promoting resection (Attikum et al., 2007; van Attikum et al., 2004; Bantele et al., 2017; Bennett and Peterson, 2015; Bennett et al., 2013; Casari et al., 2021; Chai et al., 2005; Chen et al., 2012; Downs et al., 2004; Eapen et al., 2012; Gnugnoli et al., 2021; Kent et al., 2007; Lademann et al., 2017; Liang et al., 2007; Morrison et al., 2004, 2004; Papamichos-Chronakis et al., 2011; Shim et al., 2005, 2007; Wiest et al., 2017). For this thesis, we concentrated our analysis particularly on Fun30, Ino80, RSC and SWI/SNF in order to understand which of these nucleosome remodelers might be necessary for nucleosome eviction.

Fun30 and its human homologue SMARCAD1 are well-known for specifically promoting resection elongation (Bantele et al., 2017; Chen et al., 2012, 2016; Costelloe et al., 2012; Eapen et al., 2012). One of the proposed mechanism by which Fun30 could stimulate resection is by nucleosome eviction (Bantele and Pfander, 2019; Karl et al., 2022). Notably, SMARCAD1 was recently shown to evict nucleosomes *in vitro* (Markert et al.,

2021). However, our results suggest that Fun30 is dispensable for nucleosome eviction at DSBs. It is possible that Fun30 eviction function could be replaced by other remodelers. Another possibility is that Fun30 activity is necessary at later steps in resection, particularly in counteracting the inhibitory role of Rad9 towards resection. Indeed, in both yeast and human cells, Fun30/SMARCAD1 was described to be an antagonist of Rad9/53BP1 (Bantele et al., 2017; Bothmer et al., 2011; Bunting et al., 2010; Chen et al., 2016; Costelloe et al., 2012; Lazzaro et al., 2008) and, accordingly, another proposed mechanism of Fun30 activity is the removal of Rad9-bound nucleosomes around a DSB. Rad9/53BP1, in fact, can recognize and bind to damage-induced histone PTMs (Botuyan et al., 2006; Bunting et al., 2010; Fradet-Turcotte et al., 2013; Grenon et al., 2007; Hammet et al., 2007; Hu et al., 2017; Huyen et al., 2004; Toh et al., 2006; Wilson et al., 2016; Wysocki et al., 2005). In light of these observations, if we consider that one of the recruitment modes of Fun30 to DSBs is via the 9-1-1 platform located at ss-dsDNA junctions (see paragraph 4.2), we can envision a model in which Fun30 is recruited at the leading edge of resection where it relieves the Rad9 block and allows efficient resection elongation.

The Ino80 complex is, perhaps, the most ambiguous remodeler. Indeed, Ino80 was shown to be involved in nucleosome positioning in gene bodies, but also in nucleosome eviction at gene promoters (Baldi et al., 2020; Qiu et al., 2020). In the context of DSB repair, it has been associated with nucleosome eviction (Attikum et al., 2007; Tsukuda et al., 2005) and, in addition, with removal of H2A.Z and deposition of canonical H2A (Alatwi and Downs, 2015; Lademann et al., 2017; Papamichos-Chronakis et al., 2006, 2011). Our data indicate that Ino80 is not required for nucleosome eviction at DSBs. In contrast, we observed that resection tracts were longer in the *arp8* deletion mutant compared to wild type cells (Figure 29C). This observation suggests that a functional Ino80 complex might even inhibit resection to some extent. A potential explanation may be found in the role of Ino80 in H2A/H2A.Z exchange. It is possible that the H2A/H2A.Z dynamics are impaired when Ino80 function is lacking, leading to an accumulation of H2A.Z in the chromatin surrounding a DSB. Indeed, it has been observed that H2A.Z occupancy increases after DSB induction (Kalocsay et al., 2009). At first, H2A.Z-containing nucleosomes may be incorporated to facilitate resection, since they are more prone to disruption compared to canonical nucleosomes (Abbott et al., 2001; Jin and Felsenfeld, 2007; Zhang et al., 2005). In fact, H2A.Z-containing nucleosomes can be bypassed by the resection nuclease Exo1 *in*

vitro (Adkins et al., 2013). However, persistence of H2A.Z at a DSB when Ino80 is not functional was shown to have detrimental effects on Rad51 filament formation, suggesting that removal of H2A.Z by Ino80 may be required after resection for successful repair (Lademann et al., 2017). Consistently, our data support a model in which Ino80 is dispensable for resection but it may be crucial at later steps of HR.

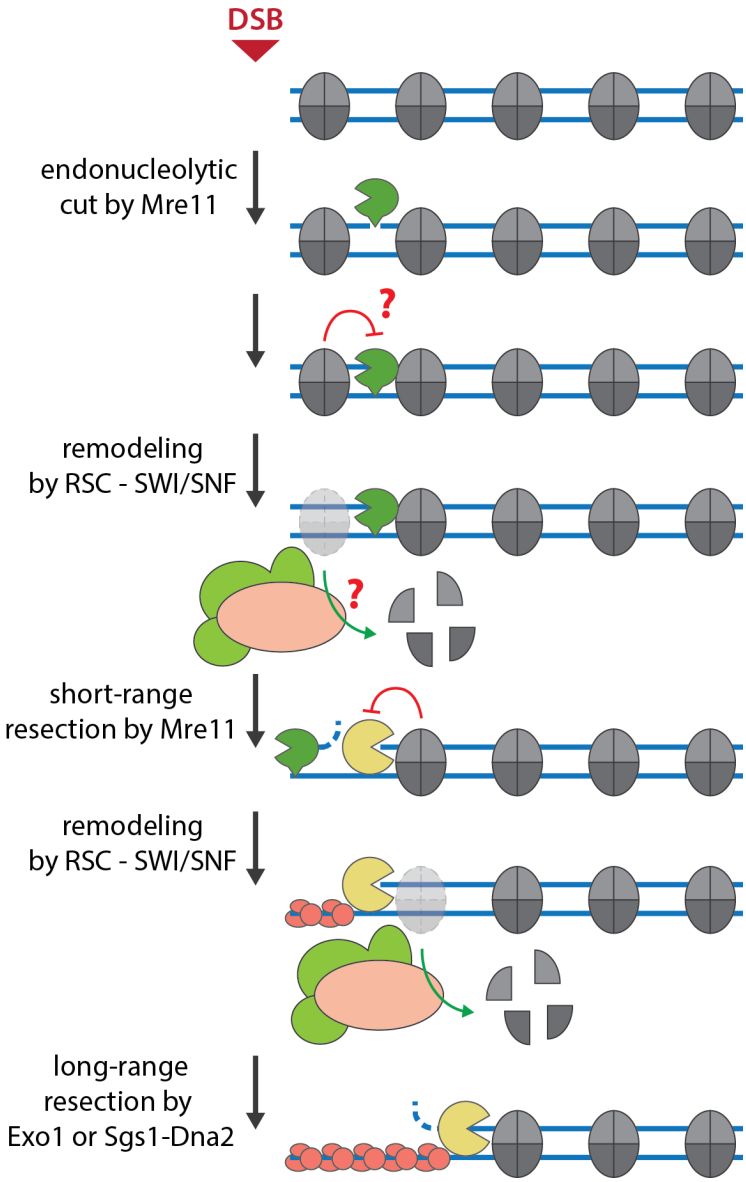

Figure 32. Model for RSC- and SWI/SNF- mediated nucleosome eviction upon resection at DSBs. Previously published data suggest that the endonucleolytic cutting by Mre11 (in dark green) is not affected by the presence of nucleosomes (Mimitou et al., 2017; Myler et al., 2017; Wang et al., 2017). Nonetheless, it is possible that nucleosomes might inhibit the exonucleolytic activity of Mre11. Consequently, RSC and SWI/SNF (in pink and green) might act at this early step to remove the nucleosomal barrier and promote short-range resection. In a later step, RSC and SWI/SNF may promote the nucleolytic activity of long-range resection nucleases (Exo1, Sgs1-Dna2; in yellow) by evicting nucleosomes.

As previously mentioned, both RSC and SWI/SNF display nucleosome eviction activity, suggesting that they may act redundantly. Importantly, both complexes were found to be recruited at DSBs (Bennett and Peterson, 2015; Chai et al., 2005; Cheng et al., 2021; Shim et al., 2005, 2007; Wiest et al., 2017) and, in addition, they appear to promote resection of DSBs both in yeast and in human cells (Bennett and Peterson, 2015; Hays et al., 2020; Kent et al., 2007; Liang et al., 2007; Park et al., 2006; Shim et al., 2007; Wiest et al., 2017). By simultaneously depleting RSC and SWI/SNF, we found that both resection and nucleosome eviction were impaired, suggesting that these processes are intrinsically coupled. Our interpretation is that nucleosome eviction by RSC and SWI/SNF is necessary for resection and that both factors act redundantly. At which step during the resection reaction these factors act is unclear. In agreement with an early role, it has been previously shown that recruitment of Mre11, the nuclease responsible for resection initiation, is impaired in RSC and SWI/SNF single mutants (Shim et al., 2007; Wiest et al., 2017). Mre11 has dual function in resection initiation, on the one hand is able to introduce a single-strand break in the 5' strand (endonucleolytic cutting), on the other hand it catalyzes short-range resection towards the DSB with 3' to 5' directionality (exonucleolytic activity). Interestingly, nucleosomes do not appear to be a barrier for Mre11, which is able to bypass them and reach inter-nucleosomal DNA for endonucleolytic cutting (Mimitou et al., 2017; Myler et al., 2017; Wang et al., 2017). However, the presence of nucleosomes might impair the exonucleolytic activity of Mre11. In this context, it is interesting to speculate that RSC and SWI/SNF might affect one or, perhaps, both of these initial steps performed by Mre11. In light of these considerations, the phenotype that we observe in the double depletion mutant might be caused primarily by a defect in the early steps of resection. Therefore, it will be highly interesting to study the interplay between RSC and SWI/SNF with Mre11.

In addition, we cannot exclude that RSC and SWI/SNF may also have a late role in resection elongation (or long-range resection). Indeed, the nucleases responsible for this step, Exo1 and Sgs1-Dna2, are inhibited by nucleosomes *in vitro* (Adkins et al., 2013), suggesting that nucleosome eviction is required for the processivity of these nucleases. Consistently, a delay in resection elongation was observed in SWI/SNF mutants, possibly due to a defect in nucleosome eviction (Wiest et al., 2017). Both SWI/SNF and RSC were also found to be involved in later steps of HR (Chai et al., 2005). Specifically SWI/SNF appears to be important at the level of strand invasion by the Rad51 filament, while RSC

activity seems to be necessary after the extension of the invading filament (Chai et al., 2005). However, it is still unclear in which way SWI/SNF and RSC may be beneficial to these processes and whether their nucleosome eviction activity is involved. Nonetheless, these observations indicate that RSC and SWI/SNF, beyond facilitating resection, may play also other roles during repair via HR.

5. Materials and Methods

Unless stated otherwise, chemicals and reagents were purchased from: Active Motif, Agrisera Sweden, Beckman Coulter, BD Lifesciences, Bio-Rad, Cayman Chemicals, Greiner, Invitrogen, Merck-Millipore, Quantabio, Roche, Roth, Santa Cruz Biotechnology, Serva, Sigma-Aldrich, Swift Biosciences, Thermo Fisher Scientific, VWR, Worthington Biochemical.

Microbiological, molecular biological and biochemical methods used for this thesis are based on standard procedures or on the instructions provided by the manufacturer. In all experiments reported here, sterile flasks, sterile solutions and media as well as sterile and deionized water were used.

5.1 Microbiology methods

5.1.1 E. coli techniques

Cultivation of *E. coli* cells

XL-1 blue (Stratagene) and Stellar (Clontech) *E. coli* strains were used for preparation of plasmid DNA and cloning, respectively. *E. coli* cells were grown overnight on agar plates at 37 °C and kept at 4 °C for short-term storage. For liquid cultures, single clones were inoculated in LB medium, supplemented with antibiotics for selection, and incubated overnight at 37 °C on a shaking platform.

Transformation of *E. coli* cells

50 µl aliquots of chemically competent *E. coli* cells were thawed on ice, mixed with 2 µl of a cloning reaction or with 1 µl of plasmid and incubated for 15 minutes on ice. Cells were subjected to heat-shock at 42 °C for 45 seconds, incubated 5 minutes on ice and then recovered in LB medium at 37 °C for 1 hour. Afterwards, cells were plated on selective plates

5.1.2 S. cerevisiae techniques

S. cerevisiae media and buffers

YP medium (plates)	1%	yeast extract
	2%	bacto-peptone
	2%	glucose / galactose / raffinose
	(2%	agar)
	for selection:	200 mg/l geniticin G418
		500 mg/l hygromycin B
		100 mg/l nourseothricin
SC medium (plates)	0.67%	yeast nitrogen base
	0.133%	master mix-8
	2%	glucose / galactose / raffinose
	as required	*Ade (22.5 mg/l), Leu (175 mg/l), His, Lys, Met, Arg, Ura, Trp (87.5 mg/l)*
	(2%	agar)
master mix -8	25 g	Ala, Asn, Asp, Cys, Gln, Glu, Gly, Ile, Phe, Pro, Ser, Thr, Tyr, Val
	25 g	myo-inositol
	2.5 g	para-aminobenzoic acid
SORB buffer	100 mM	lithium acetate
	10 mM	Tris-HCl pH 8.0
	1 mM	EDTA pH 8.0
	1 M	sorbitol
PEG buffer	100 mM	lithium acetate
	10 mM	Tris-HCl, pH 8.0
	1 mM	EDTA pH 8.0
	40% (w/v)	PEG-3350
sporulation plates	0.2%	yeast extract
	1.2%	potassium acetate
	0.08%	glucose
	1.6%	agar
	1000 mg/l	Phe
	400 mg/l	Ade, Ura
	200 mg/l	His, Leu, Lys, Trp, Met, Arg
	80 mg/l	Tyr
zymolyase solution	0.5 mg/ml	zymolyase
	0.9 M	sorbitol
	100 mM	EDTA pH 8.0
	100 mM	Tris-HCl pH 8.0
	50 mM	dithiothreitol

FACS buffer	70% 50 mM	ethanol Tris-HCl pH 8.0
RNaseA buffer	50 mM 0.38 mg/ml 0.38 mM	Tris-HCl pH 8.0 RNase A magnesium chloride
Proteinase K buffer	50 mM 1 mg/ml 5% 2.5 mM	Tris-HCl pH 8.0 proteinase K glycerol calcium chloride
SYTOX buffer	50 mM 5 µM	Tris-HCl pH 8.0 SYTOX green

***S. cerevisiae* strains**

Strain	Genotype	Reference
W303a	*MATa ade2-1 ura3-1 his3-11,15 trp1-1 leu2-3,112 can1-100*	(Rothstein, 1983)
RH448	*MATa leu2 his4 lys2 ura3 bar1*	Jentsch lab
RC757	*MATα his6 met1 can1 cyh2 sst2-1*	Jentsch lab
YSB517	*W303a hmlΔ::prS hmrΔ::pRS bar1Δ::TRP1 pGAL-HO::ADE3*	(Bantele et al., 2017)
YSB958	*W303a pGAL-AsiSI-2HA::URA3*	This study (Susanne C. S. Bantele)
YMP41 YMP42	*W303a hmlΔ::prS hmrΔ::pRS bar1Δ::TRP1 pGAL-HO::ADE3 HTB1-3FLAG::hphNT1*	This study
YMP43 YMP44 YMP45	*W303a hmlΔ::prS hmrΔ::pRS bar1Δ::TRP1 pGAL-HO::ADE3 HHT1-3FLAG::hphNT1*	This study
YSB812	*W303a hmlΔ::prS hmrΔ::pRS bar1Δ::TRP1 pGAL-HO::ADE3 DPB11-3FLAG::kanMX4*	This study (Susanne C. S. Bantele)
YMP100	*W303a hmlΔ::prS hmrΔ::pRS bar1Δ::TRP1 pGAL-HO::ADE3 DDC1-3FLAG::hphNT1*	This study
YMP91 YMP93	*W303a pGAL-AsiSI-2HA::URA3 HTB1-3FLAG::hphNT1*	This study

YMP94 YMP95	*W303a pGAL-AsiSI-2HA::URA3 HHT1-3FLAG::hphNT1*	This study
YMP88 YMP90	*W303a pGAL-AsiSI-2HA::URA3 arp8Δ::natNT2*	This study
YMP111	*W303a pGAL-AsiSI-2HA::URA3 fun30Δ::kanMX4 rad9Δ::hphNT1*	This study
YKR1894 YKR1895	*W303a pGAL-AsiSI-2HA::URA3 STH1-3AID-9MYC::hphNT1 SNF2-3AID-9MYC::natNT2 pGPD-OsTIR1-3MYC::LEU2*	This study (Karl-Uwe Reusswig)

S. cerevisiae plasmids

Plasmid	Description	Reference
pCL096	YIplac211 *pGAL-AsiSI-2HA*	This study (Claudio Lademann)
pMP10	pRS305 *pGPD-OsTIR1-3myc*	This study
pKR586	pFA6a-hph-NT1 *3aid*-9myc*	This study
pKR588	pFA6a-nat-NT2 *3aid*-9myc*	This study

Cultivation and storage of *S. cerevisiae*

Yeast cells were cultivated either on agar plates or in liquid cultures at 30 °C. Cells were streaked from glycerol stocks on agar plates with a sterile toothpick. Yeast cells growing on agar plates were used to inoculate small-scale (5-10 ml) overnight liquid cultures, from which large-scale (up to 2 L) cultures were derived for each experiment. All experiments were performed on exponentially growing cultures (OD600 0.5 – 0.7).

Agar plates were kept at 4 °C for short-term storage. For long-term storage, stationary cultures were supplemented with 0.5 volumes of 50% glycerol and stored at -80 °C.

Preparation of competent *S. cerevisiae* cells

Competent yeast cells were prepared from cultures grown to mid-log phase in YP medium supplemented with 2% glucose (YPD). Cells were harvested by centrifugation (500 g, 5 min), and washed first with sterile water, then with SORB buffer. Cells were resuspended in SORB buffer mixed with denatured herring sperm DNA in a 10:1 ratio. Competent cells were then either aliquoted and stored at -80 °C or directly used for transformation.

Transformation of *S. cerevisiae* cells

For transformation, 100 µl of competent yeast cells were mixed with 10 µl of precipitated PCR product or 1 µg of linearized plasmid and 6 volumes of PEG buffer. Cells were incubated for 30 minutes shaking at room temperature and then supplemented with DMSO to a final concentration of 10% prior to heat-shock at 42 °C for 15 minutes. After centrifugation, cells were resuspended in YPD medium and recovered for 3 hours shaking at 30 °C, then plated on selective plates. The recovery step was omitted for transformations based on auxotrophic markers. Subsequently, single colonies were isolated, streaked on selective plates and genotyped via colony PCR.

Genetic manipulation of *S. cerevisiae*

Gene deletions and tagging were performed using a standard PCR-based strategy (Janke et al., 2004; Knop et al., 1999). Plasmid integration was carried out by transforming yeast cells with linearized integrative plasmids. Presence of the desired genetic construct was first assessed by plating on selective media and then confirmed by colony PCR.

Mating, sporulation and tetrad dissection

Overnight cultures of strains with opposite mating types were mixed, spotted on warm YPD plates and incubated for at least 3 hours at 30 °C. Zygotes were picked using the micromanipulator of a tetrad microscope (Singer MSM 300 system) and incubated at 30 °C until they formed visible colonies. Sporulation was performed by streaking diploids on sporulation plates followed by incubation at 30 °C for at least 3 days. Asci from sporulation plates were resuspended in water and mixed 1:1 with a zymolyase solution, then incubated for 10 minutes at room temperature to release the tetrads. Tetrads were dissected (Singer MSM 300 system) on YPD plates and incubated at 30 °C. Genotype and mating type of each spore was determined by replica-plating on selective plates and mating type tester plates.

Drugs used in *S. cerevisiae* liquid cultures

Yeast cells were arrested in M phase by treating exponentially growing cultures (OD600 0.5-0.7) with 5 µg/ml nocodazole for 2-3 hours. Cell cycle arrest was verified using a microscope and by measuring DNA content with flow cytometry. One hour before DSB induction, degradation of Sth1 and Snf2 coupled to an auxin-inducible degron (AID) was

performed by addition of indole-3-acetic acid (IAA) to a final concentration of 1 mM in the culture medium (Morawska and Ulrich, 2013).

DSB induction, crosslinking and harvesting

Expression of the HO endonuclease or the AsiSI restriction enzyme was achieved by addition of galactose to the culture medium to a final concentration of 2%. After each indicated time point, cells were crosslinked with 1% formaldehyde for 16 minutes at room temperature on a shaking platform. Formaldehyde was quenched by adding glycine to a final concentration of 400 mM. Cells were harvested by centrifugation (3500xg at 4°C) and washed with cold PBS. Pellets were flash frozen in liquid nitrogen and stored at -80 °C until further processing.

Cell cycle analysis by flow cytometry

Samples for flow cytometry were prepared from 1 OD of yeast cells harvested by centrifugation, resuspended in FACS buffer and stored at 4 °C before further processing. Pellets were washed with 50 mM Tris pH 8.0, then subjected to RNase A treatment overnight at 37 °C and proteinase K treatment for 30 minutes at 50 °C, with the respective buffers. Subsequently, cells were resuspended in 50 mM Tris pH 8.0 and sonicated. DNA staining was performed by diluting cells 1:20 with SYTOX buffer. Lastly, samples were measured on a MACSquant Analyzer 10 flow cytometer (Miltenyi Biotec) and data analyzed using FlowJo v.10.5.3 (FlowJo LLC).

5.2 Molecular biology methods

5.2.1 Standard molecular biology techniques

Buffers and solutions

TAE buffer	40 mM	Tris-HCl pH 7.6
	20 mM	acetic acid
	1 mM	EDTA pH 8.0
DNA loading buffer (5x)	0.5%	SDS
	0.25%	orange G
	25%	glycerol
	25 mM	EDTA pH 8.0

Preparation of plasmid DNA from *E. coli*

A single *E. coli* colony was inoculated in 5 ml LB medium and grown overnight at 37 °C. Plasmid DNA was extracted using the AccuPrep Plasmid Mini Extraction Kit (Bioneer) following the instructions of the manufacturer.

Ethanol precipitation of DNA

DNA fragments amplified by PCR were purified by adding 2.5 volumes of 95% ethanol and 0.1 volumes of 3 M sodium acetate before incubating for at least 1 hour at -20 °C. The precipitated DNA was retrieved by centrifugation (14.000 rpm in a tabletop centrifuge), air-dried and then resuspended in sterile water.

Polymerase chain reaction (PCR)

PCR reactions were performed to amplify cassettes for gene deletions or tagging, as well as for yeast genotyping. The standard reaction and programs used are listed below.

Standard PCR reaction
2 µl template
3.2 µl primer 1 (10 µM)
3.2 µl primer 2 (10 µM)
1.75 µl dNTPs (10 mM)
10 µl HF-buffer
1 µl DMSO
0.5 µl Phusion polymerase
28.35 µl water

PCR program Phusion
1) 98 °C for 30 sec
2) 98 °C for 30 sec
3) 58 °C for 30 sec
4) 72 °C for 2 min
repeat steps 2 to 4 for 35 cycles
5) 72 °C for 5 min
6) hold at 4 °C

PCR program CASTORP
1) 95 °C for 4 min
2) 95 °C for 1 min
3) 45 °C for 30 sec
4) 72 °C for 2 min
repeat steps 2 to 4 for 10 cycles
5) 95 °C for 1 min
6) 54 °C for 30 sec
7) 72 °C for 2 min
repeat steps 5 to 7 for 20 cycles
8) hold at 4 °C

Agarose gel electrophoresis

DNA samples were mixed with DNA loading buffer and separated on 1% agarose gels containing ethidium bromide (2 µl for 50 ml) in TAE buffer. DNA bands were visualized using an UV-light detection system.

Agarose gel purification

Bands of interest were excised from the agarose gel using a scalpel and purified with a gel extraction kit (NucleoSpin Gel and PCR Clean-up, Macherey Nagel) following the manufacturer's instructions.

Cloning

Inserts of interest were amplified by PCR using plasmids or yeast genomic DNA as template. 5 µg of vector were digested with two restriction enzymes overnight at 37 °C. Afterwards, amplified inserts and vector were separated on an agarose gel and purified. Cloning was performed using the InFusion HD Cloning Kit according to the manufacturer's instructions. Briefly, 50 ng of insert and 50 ng of vector were mixed with the InFusion enzyme mix and incubated for 1 hour at 50 °C. Competent *E. coli* cells were transformed with 2 µl of the cloning reaction and then plated on selective plates. Plasmid DNA extracted from single colonies was sequenced to confirm correct integration of the insert.

Sanger sequencing

Samples were prepared according to the instructions of the Mix2seq kit and sent to Eurofins Genomics for sanger sequencing. Sequences were analyzed using the SnapGene software.

5.2.2 Strand-specific ChIP-sequencing

Buffers and solutions

FA lysis buffer	50 mM	HEPES-KOH pH 7.5
	150 mM	NaCl
	1 mM	EDTA pH 8.0
	1%	Triton X-100
	0.1%	Na-deoxycholate
	0.1%	SDS

protease inhibitors	10 mM 1 cOmplete protease inhibitor (Roche) tablet per 50 ml buffer	Pefabloc SC (Sigma-Aldrich)
MNase buffer	15 mM 10 mM 1.4 mM 0.2 mM	Tris pH 8.0 NaCl CaCl2 EDTA pH 8.0
Adjust buffer	75 mM 200 mM 1.5% 0.2%	HEPES pH 7.5 NaCl Triton X-100 Na-deoxycholate
FA lysis buffer 500 (high salt)	50 mM 500 mM 1 mM 1% 0.1% 0.1%	HEPES-KOH pH 7.5 NaCl EDTA pH 8.0 Triton X-100 Na-deoxycholate SDS
ChIP wash	10 mM 250 mM 1 mM 0.5% 0.5%	Tris-Cl pH 8.0 LiCl EDTA pH 8.0 NP-40 0.5% Na-deoxycholate
TE buffer	10 mM 1 mM	Tris-Cl pH 8.0 EDTA pH 8.0
ChIP elution	50 mM 10 mM 1%	Tris-HCl pH 7.5 EDTA pH 8.0 SDS

List of ChIP antibodies

Antibody	Description	Identifier	Source
anti-FLAG	Mouse monoclonal (M2), coupled to magnetic beads	M8823	Sigma-Aldrich
anti-RFA	Rabbit polyclonal	AS07-214	Agrisera Sweden
anti-Rad51	Rabbit polyclonal	sc-33626	Santa Cruz Biotechnology
anti-H2A phospho Ser129	Rabbit polyclonal	07-745	Millipore
anti-H3	Mouse monoclonal	61475	Active Motif

anti-H2A.Z	Rabbit polyclonal	39647	Active Motif

Chromatin extraction

Equal amounts of cells (100-150 OD) were used for each time point and condition for chromatin extraction. 800 µl of cold FA lysis buffer, supplemented with protease inhibitors, and silica beads were added to the pellets. Then, cells were lysed at 4 °C using a bead beater (MM301, Retsch GmbH) for 6 cycles of 3 minutes ON/3 minutes OFF. The extract was eluted and the insoluble fraction (chromatin) precipitated by centrifugation (14.000 rpm, 15 minutes, 4 °C). The chromatin pellet was resuspended in 1 ml of cold FA lysis buffer with inhibitors and subjected to sonication using Diagenode Bioruptor UCD-200 to reach a fragment size of 200-500 bp. Sonicated chromatin was cleared by centrifugation (6150 g, 30 minutes, 4°C) and diluted 1:1 with FA lysis buffer. Extracts were either immediately used for ChIP or flash frozen and stored at -80 °C.

MNase digestion

The additional step of MNase digestion was performed during chromatin extraction. Briefly, chromatin pellets, retrieved after cell lysis, were resuspended in MNase buffer and digested at 37°C for 30 minutes with 300 U of MNase (lyophilized powder was diluted in MNase buffer with 30% glycerol to a stock concentration of 25U/µl). The reaction was stopped by adding EDTA to a final concentration of 25mM. The digested chromatin was then subjected to sonication as described before. Cleared chromatin extracts were then diluted 1:1 with adjust buffer.

Chromatin immunoprecipitation (ChIP)

Chromatin extracts were used directly after preparation or quickly thawed at 25 °C. 1% of the extract was taken as input and 40% was used for immunoprecipitation. ChIP was performed by incubating chromatin with one of the antibodies listed above, rotating for 2 hours at 4 °C. For all antibodies, except for the magnetic beads-coupled anti-FLAG, ChIP was followed by 30 minutes incubation with Protein A Dynabeads™ (20 µl of slurry for each sample). Afterwards, beads were washed 3x with FA lysis buffer, 1x with high salt FA lysis buffer, 1x with ChIP wash buffer and 1x with TE. To elute the immunoprecipitated complexes, 110 µl of ChIP elution buffer were added to the beads prior to incubation for 10 minutes at 65 °C. Afterwards, proteins were degraded with a final concentration of 1 µg/µl Proteinase K (3 hours, 42 °C) and crosslinks reversed (8 hours, 65 °C). Phenol-

chloroform extraction was used to purify DNA. Briefly, the DNA-containing solution was mixed 1:1 with phenol/chloroform/isoamyl alcohol (25:24:1) and phenol-chloroform residues were removed from the aqueous solution using phase lock gel tubes. DNA was then precipitated with pure ethanol at -20 °C for at least 1 hour. DNA concentration was determined using the Qubit™ dsDNA HS assay kit with a Qubit™ 3.0 fluorometer.

Strand-specific library preparation

Accel-NGS® 1S Plus Library Kit was used to prepare strand-specific ChIP-seq libraries, according to the manufacturer's instructions. 1-3 ng of DNA were used for each library and amplification was performed with 10-12 cycles of PCR. Clean-up steps were carried out with SPRIselect beads. Quality of each library (size distribution, concentration) was assessed using high sensitivity DNA Chips with Bioanalyzer 2100 (Agilent Genomics). DNA was paired-end sequenced either on an Illumina HiSeq 1500 sequencer with 50 cycles per read (LAFUGA, GeneCenter, LMU Munich) or on an Illumina NextSeq 500 sequencer with 75 cycles per read (MPIB sequencing facility). All experiments were performed in biological replicates as indicated in each figure. We considered as biological replicates either independent experiments with the same set of strains or different yeast strains with the same genotype.

Data analysis

Sequencing data analysis was performed in collaboration with Tobias Straub (BMC, Core Facility Bioinformatics, LMU).

Bowtie2 (version 2.2.9) with default parameters was used to map sequencing reads to the *S. cerevisiae* genome. Specifically, the *S. cerevisiae* LYZE00000000.1 assembly from (Matheson et al., 2017) was used for HO experiments (Figure 7 - 18), whereas the *S. cerevisiae* R64 (sacCer3) assembly was used for AsiSI experiments (Figure 20 - 30). Multiple mapping reads were excluded with SAMtools. All plots were generated using RStudio (2021.09.0 Build 351) and R (4.1.0).

Protein enrichment or input were plotted as forward and reverse strand coverage calculated over a 25 kb window on both sides of a HO-induced DSB (Figure 7 - 9; Figure 12 - 17) or of a single AsiSI cut site (Figure 22, 24, 29).

Forward/reverse ratio (Figure 7, 12; Figure 26 - 29) was calculated from forward and reverse strand coverage in a 60 kb window spanning over the break, for AsiSI

experiments the mean ratio of Top15 cut and resected sites was plotted. Each figure legend specifies the data binning.

Plots reporting the mean coverage over Top15 AsiSI DSBs (Figure 25; Figure 27 - 30) were generated for each sample as follows: first, strand specific coverage was normalized to the genome average coverage, then, these values were divided by the normalized coverage of the uninduced sample, lastly the mean of these values between the Top15 breaks was plotted in a 40 kb window centered at the break.

To verify a correlation between nucleosome eviction and DNA end resection (Figure 18), sequencing reads from different samples were first normalized to the same sequencing depth. Read counts were calculated over 2 kb bins along a 10 kb window on both sides of the DSB. For each condition, input and IP read counts, calculated merging "left" and "right" sides of the DSB, was averaged over 3 biological replicates. Error bars represent standard error defined using the ggerr package.

AsiSI cutting efficiency (Figure 20) was determined by using data of wild-type strains uninduced (0 hours) and after 6 hours of DSB induction. Forward and reverse reads overlapping each break site were counted (countOverlaps function of the Genomic Ranges package), setting a minimum overlap of 40 bp. The number of overlapping reads was then normalized to the total number of reads for each sample. Cutting efficiency calculated for the 6 hours time-point was divided by the cutting efficiency of the 0 hours time-point. Average and standard deviation for seven independent experiments was shown.

Absolute nucleosome occupancy values for AsiSI DSBs (Figure 20) were obtained from GEO dataset GSE141051 (Oberbeckmann et al., 2019).

AsiSI heatmap matrices (Figure 21, 23) were generated by using the sum of forward and reverse reads coverage for each break and ordered according to RPA enrichment that was determined by RPA signal intensity over 10 kb window on both sides of each break.

5.3 Biochemistry methods

Buffers and solutions

HU buffer	8 M	urea
	5%	SDS
	200 mM	Tris-HCl pH 6.8
	1.5%	DTT
	traces	bromophenolblue

MOPS buffer	50 mM 50 mM 0.1% 1 mM	MOPS Tris base SDS EDTA pH 8.0 adjust to pH 7.7
MES buffer	50 mM 50 mM 0.1% 1 mM	MES Tris base SDS EDTA pH 8.0
TA buffer	50 mM 50 mM 0.1%	Tris Tricine SDS adjusted to pH 8.2
transfer buffer	48 mM 39 mM 0.0375% 20%	Tris base glycine SDS methanol
TBS	25 mM 137 mM 2.6 mM	Tris-HCl pH 7.5 NaCl KCl
superblotto	2.5% 0.5% 0.5% 0.1%	skim milk powder in TBS bovine serum albumin NP-40 Tween-20
western wash buffer	0.2%	NP-40 in TBS

List of antibodies used for WB

Antibody	Description	Identifier	Source
anti-FLAG	Mouse monoclonal (M2), coupled to HRP	A8592	Sigma-Aldrich
anti-MYC	Mouse monoclonal (4A6)	05-724	Millipore
anti-miniAID	Mouse monoclonal	M214-3	MBL/Biozol
anti-HA	Mouse monoclonal (16B12)	MMS-101R	Covance
anti-H2B	Rabbit polyclonal	39237	Active Motif
anti-H3	Rabbit polyclonal	ab1791	Abcam

TCA precipitation of proteins

1 OD of cells were harvested by centrifugation, flash frozen in liquid nitrogen and store at -80 °C until further processing. Pellets were resuspended in 1 ml of cold water mixed with 150 µl 1.85 M NaOH and 7.5% β-mercaptoethanol, then incubated for 15 minutes at 4 °C. Afterwards, 150 µl 55% tri-chloroacetic acid (TCA) were added and samples incubated for 10 min at 4 °C. Proteins were precipitated by centrifugation and the pellets resuspended in 50 µl HU buffer, before incubation for 10 minutes at 65 °C. Samples were stored at -20 °C.

Gel electrophoresis

Different proteins were separated using different types of gels: NuPAGE 12% (histones) and 4-12% Bis-Tris acrylamide gels, NuPAGE 3-8% Tris-Acetate gels (remodelers). NuPAGE 12% Bis-Tris acrylamide gels were run using using MES buffer for 30 minutes at 200 V. NuPAGE 4-12% Bis-Tris acrylamide gels were run using MOPS buffer for 1 hour at 180 V. NuPAGE 3-8% Tris-Acetate gels were run with TA buffer for 1 hour at 180 V.

Western blot

Proteins were transferred from the gel to a nitrocellulose membrane (Amersham Protran Premium 0.45 µm NC) using transfer buffer at 4 °C, for 90 minutes at 90 V. Membranes were incubated overnight at 4 °C with a primary antibody diluted in superblotto. After washing the membranes 3x with wash buffer, they were incubated with an HRP-coupled secondary antibody (1:3000 in superblotto) for 2 hours at room temperature. Afterwards, membranes were washed 5x with wash buffer prior to incubation with Pierce ECL western blotting substrate (ThermoFisher) according to manufacturer's instruction. Protein bands were detected with a LAS-300 CCD camera system (FujiFilm).

Appendix

Abbreviations

3D	3-dimensional
9-1-1	Rad9-Hus1-Rad1 complex
AID	auxin-inducible degron
ATP	adenosine triphosphate
BIR	break-induced replication
BSA	bovine serum albumin
CHD	Chromodomain-Helicase DNA-binding
ChIP	Chromatin Immunoprecipitation
Chr	chromosome
DDR	DNA damage response
dHJ	double holliday junction
DMSO	dimethyl sulfoxide
DNA	deoxyribonucleic acid
DSB	double-strand break
dsDNA	double stranded DNA
DTT	dithiothreitol
EDTA	ethylenediaminetetraacetic acid
FACS	fluorescence-activated cell sorting
G	guanine
GAL	galactose
HEPES	4-(2-hydroxyethyl)-1-piperazineethanesulfonic acid
HR	homologous recombination
HRP	horseradish peroxidase
HU	hydroxyurea
IAA	indole-3-acetic acid
INO80	Inositol-requiring mutant 80
IP	immunoprecipitation
IR	ionizing radiation
ISWI	Imitation SWItch
LB	lysogeny broth
log	logarithmic
MES	2-(N-morpholino)ethanesulfonic acid
MMEJ	microhomology-mediated end joining
MMR	mismatch repair
MOPS	3-(N-morpholino)propanesulfonic acid)
MRN	MRE11-RAD50-NBS1
MRX	Mre11-Rad50-Xrs2
MS	mass spectrometry
NBS1	Nijmegen breakage syndrome 1

NER	nucleotide excision repair
NGS	next-generation sequencing
NHEJ	non homologous end joining
OD	optical density
PAR	Poly(ADP-Ribose)
PARP	Poly(ADP-Ribose) polymerase
PBS	phosphate-buffered saline
PCNA	proliferating cell nuclear antigen
PCR	polymerase chain reaction
PEG	polyethylene glycol
Pol	polymerase
PTM	post-translational modification
qPCR	quantitative PCR
raff	raffinose
ROS	reactive oxygen species
RPA	replication protein A
RSC	Remodeling the Structure of Chromatin
SC	synthetic complete
SDS	sodium dodecyl sulfate
SDSA	synthesis-dependent strand annealing
SSA	single-strand annealing
ssDNA	single-stranded DNA
SUMO	small ubiquitin-like modifier
SWI/SNF	Switch/Sucrose non-fermentable
TAD	topologically associated domain
TBS	Tris-buffered saline
TMEJ	Theta-mediated end joining
Tris	Tri(hydroxymethyl)aminomethane
UV	ultra violet
WT	wild-type
YP	yeast extract/peptone
γH2A	Histone H2A phosphorylated on serine 129 (*S. cerevisiae*)
γH2A.X	Histone H2A.X phosphorylated on serine 139 (*H. sapiens*)

References

Abbott, D.W., Ivanova, V.S., Wang, X., Bonner, W.M., and Ausió, J. (2001). Characterization of the Stability and Folding of H2A.Z Chromatin Particles: implications for transcriptional activation. J. Biol. Chem. *276*, 41945–41949. https://doi.org/10.1074/jbc.M108217200.

Adkins, N.L., Niu, H., Sung, P., and Peterson, C.L. (2013). Nucleosome dynamics regulates DNA processing. Nat. Struct. Mol. Biol. *20*, 836–842. https://doi.org/10.1038/nsmb.2585.

Adkins, N.L., Swygert, S.G., Kaur, P., Niu, H., Grigoryev, S.A., Sung, P., Wang, H., and Peterson, C.L. (2017). Nucleosome-like, Single-stranded DNA (ssDNA)-Histone Octamer Complexes and the Implication for DNA Double Strand Break Repair. J. Biol. Chem. *292*, 5271–5281. https://doi.org/10.1074/jbc.m117.776369.

Agmon, N., Liefshitz, B., Zimmer, C., Fabre, E., and Kupiec, M. (2013). Effect of nuclear architecture on the efficiency of double-strand break repair. Nat. Cell Biol. *15*, 694–699. https://doi.org/10.1038/ncb2745.

Aguilera, A., and García-Muse, T. (2012). R loops: from transcription byproducts to threats to genome stability. Mol. Cell *46*, 115–124. https://doi.org/10.1016/j.molcel.2012.04.009.

Ahrabi, S., Sarkar, S., Pfister, S.X., Pirovano, G., Higgins, G.S., Porter, A.C.G., and Humphrey, T.C. (2016). A role for human homologous recombination factors in suppressing microhomology-mediated end joining. Nucleic Acids Res. *44*, 5743–5757. https://doi.org/10.1093/nar/gkw326.

Alabert, C., Jasencakova, Z., and Groth, A. (2017). Chromatin Replication and Histone Dynamics. In DNA Replication: From Old Principles to New Discoveries, H. Masai, and M. Foiani, eds. (Singapore: Springer), pp. 311–333.

Alatwi, H.E., and Downs, J.A. (2015). Removal of H2A.Z by INO80 promotes homologous recombination. EMBO Rep. *16*, 986–994. https://doi.org/10.15252/embr.201540330.

Anand, R., Ranjha, L., Cannavo, E., and Cejka, P. (2016). Phosphorylated CtIP Functions as a Co-factor of the MRE11-RAD50-NBS1 Endonuclease in DNA End Resection. Mol. Cell *64*, 940–950. https://doi.org/10.1016/j.molcel.2016.10.017.

Arnould, C., and Legube, G. (2020). The Secret Life of Chromosome Loops upon DNA Double-Strand Break. J. Mol. Biol. *432*, 724–736. https://doi.org/10.1016/j.jmb.2019.07.036.

Attikum, H. van, Fritsch, O., and Gasser, S.M. (2007). Distinct roles for SWR1 and INO80 chromatin remodeling complexes at chromosomal double-strand breaks. EMBO J. *26*, 4113–4125. https://doi.org/10.1038/sj.emboj.7601835.

van Attikum, H., Fritsch, O., Hohn, B., and Gasser, S.M. (2004). Recruitment of the INO80 Complex by H2A Phosphorylation Links ATP-Dependent Chromatin Remodeling with DNA Double-Strand Break Repair. Cell *119*, 777–788. https://doi.org/10.1016/j.cell.2004.11.033.

Awad, S., Ryan, D., Prochasson, P., Owen-Hughes, T., and Hassan, A.H. (2010). The Snf2 homolog Fun30 acts as a homodimeric ATP-dependent chromatin-remodeling enzyme. J. Biol. Chem. *285*, 9477–9484. https://doi.org/10.1074/jbc.M109.082149.

Ayala, R., Willhoft, O., Aramayo, R.J., Wilkinson, M., McCormack, E.A., Ocloo, L., Wigley, D.B., and Zhang, X. (2018). Structure and regulation of the human INO80-nucleosome complex. Nature *556*, 391–395. https://doi.org/10.1038/s41586-018-0021-6.

Bae, S.H., Choi, E., Lee, K.H., Park, J.S., Lee, S.H., and Seo, Y.S. (1998). Dna2 of Saccharomyces cerevisiae possesses a single-stranded DNA-specific endonuclease activity that is able to act on double-stranded DNA in the presence of ATP. J. Biol. Chem. *273*, 26880–26890. https://doi.org/10.1074/jbc.273.41.26880.

Baldi, S., Korber, P., and Becker, P.B. (2020). Beads on a string - nucleosome array arrangements and folding of the chromatin fiber. Nat. Struct. Mol. Biol. *27*, 109–118. https://doi.org/10.1038/s41594-019-0368-x.

Bantele, S.C.S., and Pfander, B. (2019). Nucleosome Remodeling by Fun30SMARCAD1 in the DNA Damage Response. Front. Mol. Biosci. *6*. .

Bantele, S.C.S., Ferreira, P., Gritenaite, D., Boos, D., and Pfander, B. (2017). Targeting of the Fun30 nucleosome remodeller by the Dpb11 scaffold facilitates cell cycle-regulated DNA end resection. ELife *6*. https://doi.org/10.7554/eLife.21687.

Bantele, S.C.S., Lisby, M., and Pfander, B. (2019). Quantitative sensing and signalling of single-stranded DNA during the DNA damage response. Nat. Commun. *10*, 944. https://doi.org/10.1038/s41467-019-08889-5.

Barnard, S., Bouffler, S., and Rothkamm, K. (2013). The shape of the radiation dose response for DNA double-strand break induction and repair. Genome Integr. *4*, 1. https://doi.org/10.1186/2041-9414-4-1.

Bebenek, K., Garcia-Diaz, M., Patishall, S.R., and Kunkel, T.A. (2005). Biochemical properties of Saccharomyces cerevisiae DNA polymerase IV. J. Biol. Chem. *280*, 20051–20058. https://doi.org/10.1074/jbc.M501981200.

Bebenek, K., Pedersen, L.C., and Kunkel, T.A. (2014). Structure-function studies of DNA polymerase λ. Biochemistry *53*, 2781–2792. https://doi.org/10.1021/bi4017236.

Bekker-Jensen, S., Lukas, C., Kitagawa, R., Melander, F., Kastan, M.B., Bartek, J., and Lukas, J. (2006). Spatial organization of the mammalian genome surveillance machinery in response to DNA strand breaks. J. Cell Biol. *173*, 195–206. https://doi.org/10.1083/jcb.200510130.

Belton, J.-M., Lajoie, B.R., Audibert, S., Cantaloube, S., Lassadi, I., Goiffon, I., Baù, D., Marti-Renom, M.A., Bystricky, K., and Dekker, J. (2015). The conformation of yeast chromosome III is mating type-dependent and controlled by the recombination enhancer. Cell Rep. *13*, 1855–1867. https://doi.org/10.1016/j.celrep.2015.10.063.

Bennett, G., and Peterson, C.L. (2015). SWI/SNF recruitment to a DNA double-strand break by the NuA4 and Gcn5 histone acetyltransferases. DNA Repair *30*, 38–45. https://doi.org/10.1016/j.dnarep.2015.03.006.

Bennett, G., Papamichos-Chronakis, M., and Peterson, C.L. (2013). DNA repair choice defines a common pathway for recruitment of chromatin regulators. Nat. Commun. *4*, 2084–2084. https://doi.org/10.1038/ncomms3084.

Berti, M., Cortez, D., and Lopes, M. (2020). The plasticity of DNA replication forks in response to clinically relevant genotoxic stress. Nat. Rev. Mol. Cell Biol. *21*, 633–651. https://doi.org/10.1038/s41580-020-0257-5.

Bhargava, R., Onyango, D.O., and Stark, J.M. (2016). Regulation of Single-Strand Annealing and its Role in Genome Maintenance. Trends Genet. TIG *32*, 566–575. https://doi.org/10.1016/j.tig.2016.06.007.

Bird, A.W., Yu, D.Y., Pray-Grant, M.G., Qiu, Q., Harmon, K.E., Megee, P.C., Grant, P.A., Smith, M.M., and Christman, M.F. (2002). Acetylation of histone H4 by Esa1 is required for DNA double-strand break repair. Nature *419*, 411–415. https://doi.org/10.1038/nature01035.

Bizard, A.H., and Hickson, I.D. (2014). The Dissolution of Double Holliday Junctions. Cold Spring Harb. Perspect. Biol. *6*, a016477. https://doi.org/10.1101/cshperspect.a016477.

Bonilla, C.Y., Melo, J.A., and Toczyski, D.P. (2008). Colocalization of Sensors Is Sufficient to Activate the DNA Damage Checkpoint in the Absence of Damage. Mol. Cell *30*, 267–276. https://doi.org/10.1016/j.molcel.2008.03.023.

Bordelet, H., and Dubrana, K. (2019). Keep moving and stay in a good shape to find your homologous recombination partner. Curr. Genet. *65*, 29–39. https://doi.org/10.1007/s00294-018-0873-1.

Bothmer, A., Robbiani, D.F., Di Virgilio, M., Bunting, S.F., Klein, I.A., Feldhahn, N., Barlow, J., Chen, H.-T., Bosque, D., Callen, E., et al. (2011). Regulation of DNA End Joining, Resection, and Immunoglobulin Class Switch Recombination by 53BP1. Mol. Cell *42*, 319–329. https://doi.org/10.1016/j.molcel.2011.03.019.

Botuyan, M.V., Lee, J., Ward, I.M., Kim, J.-E., Thompson, J.R., Chen, J., and Mer, G. (2006). Structural Basis for the Methylation State-Specific Recognition of Histone H4-K20 by 53BP1 and Crb2 in DNA Repair. Cell *127*, 1361–1373. https://doi.org/10.1016/j.cell.2006.10.043.

Bouwman, B.A.M., and Crosetto, N. (2018). Endogenous DNA Double-Strand Breaks during DNA Transactions: Emerging Insights and Methods for Genome-Wide Profiling. Genes *9*, 632. https://doi.org/10.3390/genes9120632.

Brahma, S., Udugama, M.I., Kim, J., Hada, A., Bhardwaj, S.K., Hailu, S.G., Lee, T.-H., and Bartholomew, B. (2017). INO80 exchanges H2A.Z for H2A by translocating on DNA proximal to histone dimers. Nat. Commun. *8*, 15616. https://doi.org/10.1038/ncomms15616.

Brahma, S., Ngubo, M., Paul, S., Udugama, M., and Bartholomew, B. (2018). The Arp8 and Arp4 module acts as a DNA sensor controlling INO80 chromatin remodeling. Nat. Commun. *9*. https://doi.org/10.1038/s41467-018-05710-7.

Branzei, D., and Foiani, M. (2010). Maintaining genome stability at the replication fork. Nat. Rev. Mol. Cell Biol. *11*, 208–219. https://doi.org/10.1038/nrm2852.

Brown, C.A., Murray, A.W., and Verstrepen, K.J. (2010). Rapid Expansion and Functional Divergence of Subtelomeric Gene Families in Yeasts. Curr. Biol. *20*, 895–903. https://doi.org/10.1016/j.cub.2010.04.027.

Bunting, S.F., Callén, E., Wong, N., Chen, H.-T., Polato, F., Gunn, A., Bothmer, A., Feldhahn, N., Fernandez-Capetillo, O., Cao, L., et al. (2010). 53BP1 inhibits homologous recombination in Brca1-deficient cells by blocking resection of DNA breaks. Cell *141*, 243–254. https://doi.org/10.1016/j.cell.2010.03.012.

Burgess, S.M., and Kleckner, N. (1999). Collisions between yeast chromosomal loci in vivo are governed by three layers of organization. Genes Dev. *13*, 1871–1883. .

Burma, S., Chen, B.P., Murphy, M., Kurimasa, A., and Chen, D.J. (2001). ATM Phosphorylates Histone H2AX in Response to DNA Double-strand Breaks. J. Biol. Chem. *276*, 42462–42467. https://doi.org/10.1074/jbc.C100466200.

Cannan, W.J., and Pederson, D.S. (2016). Mechanisms and Consequences of Double-strand DNA Break Formation in Chromatin. J. Cell. Physiol. *231*, 3–14. https://doi.org/10.1002/jcp.25048.

Cannavo, E., and Cejka, P. (2014). Sae2 promotes dsDNA endonuclease activity within Mre11-Rad50-Xrs2 to resect DNA breaks. Nature *514*, 122–125. https://doi.org/10.1038/nature13771.

Caron, P., Aymard, F., Iacovoni, J.S., Briois, S., Canitrot, Y., Bugler, B., Massip, L., Losada, A., and Legube, G. (2012). Cohesin protects genes against γH2AX Induced by DNA double-strand breaks. PLoS Genet. *8*, e1002460. https://doi.org/10.1371/journal.pgen.1002460.

Casari, E., Gobbini, E., Gnugnoli, M., Mangiagalli, M., Clerici, M., and Longhese, M.P. (2021). Dpb4 promotes resection of DNA double-strand breaks and checkpoint activation by acting in two different protein complexes. Nat. Commun. *12*, 4750. https://doi.org/10.1038/s41467-021-25090-9.

Castaneda, J.C., Schrecker, M., Remus, D., and Hite, R.K. (2021). Mechanisms of loading and release of the 9-1-1 checkpoint clamp. 2021.09.13.460164. https://doi.org/10.1101/2021.09.13.460164.

Ceccaldi, R., Liu, J.C., Amunugama, R., Hajdu, I., Primack, B., Petalcorin, M.I.R., O'Connor, K.W., Konstantinopoulos, P.A., Elledge, S.J., Boulton, S.J., et al. (2015). Homologous-recombination-deficient tumours are dependent on Polθ-mediated repair. Nature *518*, 258–262. https://doi.org/10.1038/nature14184.

Chai, B., Huang, J., Cairns, B.R., and Laurent, B.C. (2005). Distinct roles for the RSC and Swi/Snf ATP-dependent chromatin remodelers in DNA double-strand break repair. Genes Dev. *19*, 1656–1661. https://doi.org/10.1101/gad.1273105.

Chang, H.H.Y., Pannunzio, N.R., Adachi, N., and Lieber, M.R. (2017). Non-homologous DNA end joining and alternative pathways to double-strand break repair. Nat. Rev. Mol. Cell Biol. *18*, 495–506. https://doi.org/10.1038/nrm.2017.48.

Chapman, J.R., Sossick, A.J., Boulton, S.J., and Jackson, S.P. (2012). BRCA1-associated exclusion of 53BP1 from DNA damage sites underlies temporal control of DNA repair. J. Cell Sci. *125*, 3529–3534. https://doi.org/10.1242/jcs.105353.

Chen, J., and Stubbe, J. (2005). Bleomycins: towards better therapeutics. Nat. Rev. Cancer *5*, 102–112. https://doi.org/10.1038/nrc1547.

Chen, R., and Wold, M.S. (2014). Replication protein A: Single-stranded DNA's first responder. BioEssays *36*, 1156–1161. https://doi.org/10.1002/bies.201400107.

Chen, X., and Tomkinson, A.E. (2011). Yeast Nej1 is a key participant in the initial end binding and final ligation steps of nonhomologous end joining. J. Biol. Chem. *286*, 4931–4940. https://doi.org/10.1074/jbc.M110.195024.

Chen, C.-C., Carson, J.J., Feser, J., Tamburini, B., Zabaronick, S., Linger, J., and Tyler, J.K. (2008). Acetylated Lysine 56 on Histone H3 Drives Chromatin Assembly after Repair and Signals for the Completion of Repair. Cell *134*, 231–243. https://doi.org/10.1016/j.cell.2008.06.035.

Chen, L., Trujillo, K., Ramos, W., Sung, P., and Tomkinson, A.E. (2001). Promotion of Dnl4-catalyzed DNA end-joining by the Rad50/Mre11/Xrs2 and Hdf1/Hdf2 complexes. Mol. Cell *8*, 1105–1115. https://doi.org/10.1016/s1097-2765(01)00388-4.

Chen, X., Cui, D., Papusha, A., Zhang, X., Chu, C.-D., Tang, J., Chen, K., Pan, X., and Ira, G. (2012). The Fun30 nucleosome remodeller promotes resection of DNA double-strand break ends. Nature *489*, 576–580. https://doi.org/10.1038/nature11355.

Chen, X., Niu, H., Yu, Y., Wang, J., Zhu, S., Zhou, J., Papusha, A., Cui, D., Pan, X., Kwon, Y., et al. (2016). Enrichment of Cdk1-cyclins at DNA double-strand breaks stimulates Fun30 phosphorylation and DNA end resection. Nucleic Acids Res. *44*, 2742–2753. https://doi.org/10.1093/nar/gkv1544.

Cheng, X., Côté, V., and Côté, J. (2021). NuA4 and SAGA acetyltransferase complexes cooperate for repair of DNA breaks by homologous recombination. PLOS Genet. *17*, e1009459. https://doi.org/10.1371/journal.pgen.1009459.

Cheung, W.L., Turner, F.B., Krishnamoorthy, T., Wolner, B., Ahn, S.-H., Foley, M., Dorsey, J.A., Peterson, C.L., Berger, S.L., and Allis, C.D. (2005). Phosphorylation of Histone H4 Serine 1 during DNA Damage Requires Casein Kinase II in S. cerevisiae. Curr. Biol. *15*, 656–660. https://doi.org/10.1016/j.cub.2005.02.049.

Ciccia, A., and Elledge, S.J. (2010). The DNA Damage Response: Making It Safe to Play with Knives. Mol. Cell *40*, 179–204. https://doi.org/10.1016/j.molcel.2010.09.019.

di Cicco, G., Bantele, S.C.S., Reusswig, K.-U., and Pfander, B. (2017). A cell cycle-independent mode of the Rad9-Dpb11 interaction is induced by DNA damage. Sci. Rep. *7*. https://doi.org/10.1038/s41598-017-11937-z.

Clapier, C.R., and Cairns, B.R. (2009). The Biology of Chromatin Remodeling Complexes. Annu. Rev. Biochem. *78*, 273–304. https://doi.org/10.1146/annurev.biochem.77.062706.153223.

Clapier, C.R., Iwasa, J., Cairns, B.R., and Peterson, C.L. (2017). Mechanisms of action and regulation of ATP-dependent chromatin-remodelling complexes. Nat. Rev. Mol. Cell Biol. *18*, 407–422. https://doi.org/10.1038/nrm.2017.26.

Clerici, M., Mantiero, D., Guerini, I., Lucchini, G., and Longhese, M.P. (2008). The Yku70-Yku80 complex contributes to regulate double-strand break processing and checkpoint activation during the cell cycle. EMBO Rep. *9*, 810–818. https://doi.org/10.1038/embor.2008.121.

Clouaire, T., and Legube, G. (2019). A Snapshot on the Cis Chromatin Response to DNA Double-Strand Breaks. Trends Genet. *35*, 330–345. https://doi.org/10.1016/j.tig.2019.02.003.

Clouaire, T., Rocher, V., Lashgari, A., Arnould, C., Aguirrebengoa, M., Biernacka, A., Skrzypczak, M., Aymard, F., Fongang, B., Dojer, N., et al. (2018). Comprehensive Mapping of Histone Modifications at DNA Double-Strand Breaks Deciphers Repair Pathway Chromatin Signatures. Mol. Cell *72*, 250-262.e6. https://doi.org/10.1016/j.molcel.2018.08.020.

Costantino, L., and Koshland, D. (2018). Genome-wide Map of R-Loop-Induced Damage Reveals How a Subset of R-Loops Contributes to Genomic Instability. Mol. Cell *71*, 487-497.e3. https://doi.org/10.1016/j.molcel.2018.06.037.

Costelloe, T., Louge, R., Tomimatsu, N., Mukherjee, B., Martini, E., Khadaroo, B., Dubois, K., Wiegant, W.W., Thierry, A., Burma, S., et al. (2012). The yeast Fun30 and human SMARCAD1 chromatin remodellers promote DNA end resection. Nature *489*, 581–584. https://doi.org/10.1038/nature11353.

Cremer, T., and Cremer, M. (2010). Chromosome Territories. Cold Spring Harb. Perspect. Biol. *2*, a003889. https://doi.org/10.1101/cshperspect.a003889.

Crossley, M.P., Bocek, M., and Cimprich, K.A. (2019). R-Loops as Cellular Regulators and Genomic Threats. Mol. Cell *73*, 398–411. https://doi.org/10.1016/j.molcel.2019.01.024.

Daley, J.M., and Wilson, T.E. (2008). Evidence that base stacking potential in annealed 3' overhangs determines polymerase utilization in yeast nonhomologous end joining. DNA Repair *7*, 67–76. https://doi.org/10.1016/j.dnarep.2007.07.018.

Daley, J.M., Palmbos, P.L., Wu, D., and Wilson, T.E. (2005). Nonhomologous end joining in yeast. Annu. Rev. Genet. *39*, 431–451. https://doi.org/10.1146/annurev.genet.39.073003.113340.

De March, M., Merino, N., Barrera-Vilarmau, S., Crehuet, R., Onesti, S., Blanco, F.J., and De Biasio, A. (2017). Structural basis of human PCNA sliding on DNA. Nat. Commun. *8*, 13935. https://doi.org/10.1038/ncomms13935.

Dehé, P.-M., and Gaillard, P.-H.L. (2017). Control of structure-specific endonucleases to maintain genome stability. Nat. Rev. Mol. Cell Biol. *18*, 315–330. https://doi.org/10.1038/nrm.2016.177.

Delamarre, A., Barthe, A., Saint-André, C. de la R., Luciano, P., Forey, R., Padioleau, I., Skrzypczak, M., Ginalski, K., Géli, V., Pasero, P., et al. (2020). MRX Increases Chromatin Accessibility at Stalled Replication Forks to Promote Nascent DNA Resection and Cohesin Loading. Mol. Cell *77*, 395-410.e3. https://doi.org/10.1016/j.molcel.2019.10.029.

Deng, S.K., Gibb, B., de Almeida, M.J., Greene, E.C., and Symington, L.S. (2014). RPA antagonizes microhomology-mediated repair of DNA double-strand breaks. Nat. Struct. Mol. Biol. *21*, 405–412. https://doi.org/10.1038/nsmb.2786.

Densham, R.M., Garvin, A.J., Stone, H.R., Strachan, J., Baldock, R.A., Daza-Martin, M., Fletcher, A., Blair-Reid, S., Beesley, J., Johal, B., et al. (2016). Human BRCA1-BARD1 ubiquitin ligase activity counteracts chromatin barriers to DNA resection. Nat. Struct. Mol. Biol. *23*, 647–655. https://doi.org/10.1038/nsmb.3236.

Desai-Mehta, A., Cerosaletti, K.M., and Concannon, P. (2001). Distinct Functional Domains of Nibrin Mediate Mre11 Binding, Focus Formation, and Nuclear Localization. Mol. Cell. Biol. *21*, 2184–2191. https://doi.org/10.1128/MCB.21.6.2184-2191.2001.

Deshpande, R.A., and Wilson, T.E. (2007). Modes of interaction among yeast Nej1, Lif1 and Dnl4 proteins and comparison to human XLF, XRCC4 and Lig4. DNA Repair *6*, 1507–1516. https://doi.org/10.1016/j.dnarep.2007.04.014.

Deshpande, I., Seeber, A., Shimada, K., Keusch, J.J., Gut, H., and Gasser, S.M. (2017). Structural Basis of Mec1-Ddc2-RPA Assembly and Activation on Single-Stranded DNA at Sites of Damage. Mol. Cell *68*, 431-445.e5. https://doi.org/10.1016/j.molcel.2017.09.019.

Deshpande, R.A., Lee, J.-H., Arora, S., and Paull, T.T. (2016). Nbs1 Converts the Human Mre11/Rad50 Nuclease Complex into an Endo/Exonuclease Machine Specific for Protein-DNA Adducts. Mol. Cell *64*, 593–606. https://doi.org/10.1016/j.molcel.2016.10.010.

Deweese, J.E., and Osheroff, N. (2009). The DNA cleavage reaction of topoisomerase II: wolf in sheep's clothing. Nucleic Acids Res. *37*, 738–748. https://doi.org/10.1093/nar/gkn937.

Di Virgilio, M., Callen, E., Yamane, A., Zhang, W., Jankovic, M., Gitlin, A.D., Feldhahn, N., Resch, W., Oliveira, T.Y., Chait, B.T., et al. (2013). Rif1 Prevents Resection of DNA Breaks and Promotes Immunoglobulin Class Switching. Science *339*, 711–715. https://doi.org/10.1126/science.1230624.

Diao, L.-T., Chen, C.-C., Dennehey, B., Pal, S., Wang, P., Shen, Z.-J., Deem, A., and Tyler, J.K. (2017). Delineation of the role of chromatin assembly and the Rtt101Mms1 E3 ubiquitin ligase in DNA damage checkpoint recovery in budding yeast. PLOS ONE *12*, e0180556. https://doi.org/10.1371/journal.pone.0180556.

Dion, V., and Gasser, S.M. (2013). Chromatin movement in the maintenance of genome stability. Cell *152*, 1355–1364. https://doi.org/10.1016/j.cell.2013.02.010.

Doherty, A.J., Jackson, S.P., and Weller, G.R. (2001). Identification of bacterial homologues of the Ku DNA repair proteins. FEBS Lett. *500*, 186–188. https://doi.org/10.1016/S0014-5793(01)02589-3.

Downs, J.A., Lowndes, N.F., and Jackson, S.P. (2000). A role for Saccharomyces cerevisiae histone H2A in DNA repair. Nature *408*, 1001–1004. https://doi.org/10.1038/35050000.

Downs, J.A., Allard, S., Jobin-Robitaille, O., Javaheri, A., Auger, A., Bouchard, N., Kron, S.J., Jackson, S.P., and Côté, J. (2004). Binding of Chromatin-Modifying Activities to Phosphorylated Histone H2A at DNA Damage Sites. Mol. Cell *16*, 979–990. https://doi.org/10.1016/j.molcel.2004.12.003.

Duan, Z., Andronescu, M., Schutz, K., McIlwain, S., Kim, Y.J., Lee, C., Shendure, J., Fields, S., Blau, C.A., and Noble, W.S. (2010). A three-dimensional model of the yeast genome. Nature *465*, 363–367. https://doi.org/10.1038/nature08973.

Dubrana, K., van Attikum, H., Hediger, F., and Gasser, S.M. (2007). The processing of double-strand breaks and binding of single-strand-binding proteins RPA and Rad51 modulate the formation of ATR-kinase foci in yeast. J. Cell Sci. *120*, 4209–4220. https://doi.org/10.1242/jcs.018366.

Eapen, V.V., Sugawara, N., Tsabar, M., Wu, W.-H., and Haber, J.E. (2012). The Saccharomyces cerevisiae Chromatin Remodeler Fun30 Regulates DNA End Resection and Checkpoint Deactivation. Mol. Cell. Biol. https://doi.org/10.1128/MCB.00566-12.

Eaton, M.L., Galani, K., Kang, S., Bell, S.P., and MacAlpine, D.M. (2010). Conserved nucleosome positioning defines replication origins. Genes Dev. *24*, 748–753. https://doi.org/10.1101/gad.1913210.

Eberharter, A., and Becker, P.B. (2002). Histone acetylation: a switch between repressive and permissive chromatin. Second in review series on chromatin dynamics. EMBO Rep. *3*, 224–229. https://doi.org/10.1093/embo-reports/kvf053.

Eccles, L.J., O'Neill, P., and Lomax, M.E. (2011). Delayed repair of radiation induced clustered DNA damage: Friend or foe? Mutat. Res. Mol. Mech. Mutagen. *711*, 134–141. https://doi.org/10.1016/j.mrfmmm.2010.11.003.

Ehmsen, K.T., and Heyer, W.-D. (2008). Saccharomyces cerevisiae Mus81-Mms4 is a catalytic, DNA structure-selective endonuclease. Nucleic Acids Res. *36*, 2182–2195. https://doi.org/10.1093/nar/gkm1152.

Ellison, V., and Stillman, B. (2003). Biochemical Characterization of DNA Damage Checkpoint Complexes: Clamp Loader and Clamp Complexes with Specificity for 5′ Recessed DNA. PLOS Biol. *1*, e33. https://doi.org/10.1371/journal.pbio.0000033.

van Emden, T.S., Forn, M., Forné, I., Sarkadi, Z., Capella, M., Martín Caballero, L., Fischer-Burkart, S., Brönner, C., Simonetta, M., Toczyski, D., et al. (2019). Shelterin and subtelomeric DNA sequences control nucleosome maintenance and genome stability. EMBO Rep. *20*, e47181. https://doi.org/10.15252/embr.201847181.

Eustermann, S., Schall, K., Kostrewa, D., Lakomek, K., Strauss, M., Moldt, M., and Hopfner, K.-P. (2018). Structural basis for ATP-dependent chromatin remodelling by the INO80 complex. Nature *556*, 386–390. https://doi.org/10.1038/s41586-018-0029-y.

Flaus, A., Martin, D.M.A., Barton, G.J., and Owen-Hughes, T. (2006). Identification of multiple distinct Snf2 subfamilies with conserved structural motifs. Nucleic Acids Res. *34*, 2887–2905. https://doi.org/10.1093/nar/gkl295.

Fradet-Turcotte, A., Canny, M.D., Escribano-Díaz, C., Orthwein, A., Leung, C.C.Y., Huang, H., Landry, M.-C., Kitevski-LeBlanc, J., Noordermeer, S.M., Sicheri, F., et al. (2013). 53BP1 is a reader of the DNA-damage-induced H2A Lys 15 ubiquitin mark. Nature *499*, 50–54. https://doi.org/10.1038/nature12318.

Fu, D., Calvo, J.A., and Samson, L.D. (2012). Balancing repair and tolerance of DNA damage caused by alkylating agents. Nat. Rev. Cancer *12*, 104–120. https://doi.org/10.1038/nrc3185.

Fu, Y., Sinha, M., Peterson, C.L., and Weng, Z. (2008). The Insulator Binding Protein CTCF Positions 20 Nucleosomes around Its Binding Sites across the Human Genome. PLoS Genet. *4*, e1000138. https://doi.org/10.1371/journal.pgen.1000138.

Furuse, M., Nagase, Y., Tsubouchi, H., Murakami-Murofushi, K., Shibata, T., and Ohta, K. (1998). Distinct roles of two separable in vitro activities of yeast Mre11 in mitotic and meiotic recombination. EMBO J. *17*, 6412–6425. https://doi.org/10.1093/emboj/17.21.6412.

Gaillard, P.-H.L., Noguchi, E., Shanahan, P., and Russell, P. (2003). The endogenous Mus81-Eme1 complex resolves Holliday junctions by a nick and counternick mechanism. Mol. Cell *12*, 747–759. https://doi.org/10.1016/s1097-2765(03)00342-3.

Gan, H., Serra-Cardona, A., Hua, X., Zhou, H., Labib, K., Yu, C., and Zhang, Z. (2018). The Mcm2-Ctf4-Polα Axis Facilitates Parental Histone H3-H4 Transfer to Lagging Strands. Mol. Cell *72*, 140-151.e3. https://doi.org/10.1016/j.molcel.2018.09.001.

García-Muse, T., and Aguilera, A. (2016). Transcription–replication conflicts: how they occur and how they are resolved. Nat. Rev. Mol. Cell Biol. *17*, 553–563. https://doi.org/10.1038/nrm.2016.88.

Giannattasio, M., Lazzaro, F., Plevani, P., and Muzi-Falconi, M. (2005). The DNA Damage Checkpoint Response Requires Histone H2B Ubiquitination by Rad6-Bre1 and H3 Methylation by Dot1. J. Biol. Chem. *280*, 9879–9886. https://doi.org/10.1074/jbc.M414453200.

Gkikopoulos, T., Schofield, P., Singh, V., Pinskaya, M., Mellor, J., Smolle, M., Workman, J.L., Barton, G.J., and Owen-Hughes, T. (2011). A Role for Snf2-Related Nucleosome-Spacing Enzymes in Genome-Wide Nucleosome Organization. Science *333*, 1758–1760. https://doi.org/10.1126/science.1206097.

Gnugnoli, M., Casari, E., and Longhese, M.P. (2021). The chromatin remodeler Chd1 supports MRX and Exo1 functions in resection of DNA double-strand breaks. PLOS Genet. *17*, e1009807. https://doi.org/10.1371/journal.pgen.1009807.

Goodarzi, A.A., Yu, Y., Riballo, E., Douglas, P., Walker, S.A., Ye, R., Härer, C., Marchetti, C., Morrice, N., Jeggo, P.A., et al. (2006). DNA-PK autophosphorylation facilitates Artemis endonuclease activity. EMBO J. *25*, 3880–3889. https://doi.org/10.1038/sj.emboj.7601255.

Gospodinov, A., Vaissiere, T., Krastev, D.B., Legube, G., Anachkova, B., and Herceg, Z. (2011). Mammalian Ino80 Mediates Double-Strand Break Repair through Its Role in DNA End Strand Resection. Mol. Cell. Biol. *31*, 4735–4745. https://doi.org/10.1128/MCB.06182-11.

Gottlieb, T.M., and Jackson, S.P. (1993). The DNA-dependent protein kinase: requirement for DNA ends and association with Ku antigen. Cell *72*, 131–142. https://doi.org/10.1016/0092-8674(93)90057-w.

Gottschalk, A.J., Timinszky, G., Kong, S.E., Jin, J., Cai, Y., Swanson, S.K., Washburn, M.P., Florens, L., Ladurner, A.G., Conaway, J.W., et al. (2009). Poly(ADP-ribosyl)ation directs recruitment and activation of an ATP-dependent chromatin remodeler. Proc. Natl. Acad. Sci. *106*, 13770–13774. https://doi.org/10.1073/pnas.0906920106.

Grenon, M., Costelloe, T., Jimeno, S., O'Shaughnessy, A., FitzGerald, J., Zgheib, O., Degerth, L., and Lowndes, N.F. (2007). Docking onto chromatin via the Saccharomyces cerevisiae Rad9 Tudor domain. Yeast *24*, 105–119. https://doi.org/10.1002/yea.1441.

Gu, J., Li, S., Zhang, X., Wang, L.-C., Niewolik, D., Schwarz, K., Legerski, R.J., Zandi, E., and Lieber, M.R. (2010). DNA-PKcs regulates a single-stranded DNA endonuclease activity of Artemis. DNA Repair *9*, 429–437. https://doi.org/10.1016/j.dnarep.2010.01.001.

Gu, M., Naiyachit, Y., Wood, T.J., and Millar, C.B. (2015). H2A.Z marks antisense promoters and has positive effects on antisense transcript levels in budding yeast. BMC Genomics *16*. https://doi.org/10.1186/s12864-015-1247-4.

Gursoy-Yuzugullu, O., Ayrapetov, M.K., and Price, B.D. (2015). Histone chaperone Anp32e removes H2A.Z from DNA double-strand breaks and promotes nucleosome reorganization and DNA repair. Proc. Natl. Acad. Sci. U. S. A. *112*, 7507–7512. https://doi.org/10.1073/pnas.1504868112.

Haber, J.E. (2012). Mating-Type Genes and MAT Switching in Saccharomyces cerevisiae. Genetics *191*, 33–64. https://doi.org/10.1534/genetics.111.134577.

Halazonetis, T.D., Gorgoulis, V.G., and Bartek, J. (2008). An Oncogene-Induced DNA Damage Model for Cancer Development. Science *319*, 1352–1355. https://doi.org/10.1126/science.1140735.

Hammet, A., Magill, C., Heierhorst, J., and Jackson, S.P. (2007). Rad9 BRCT domain interaction with phosphorylated H2AX regulates the G1 checkpoint in budding yeast. EMBO Rep. *8*, 851–857. https://doi.org/10.1038/sj.embor.7401036.

Hamperl, S., and Cimprich, K.A. (2016). Conflict resolution in the genome: how transcription and replication make it work. Cell *167*, 1455–1467. https://doi.org/10.1016/j.cell.2016.09.053.

Hamperl, S., Bocek, M.J., Saldivar, J.C., Swigut, T., and Cimprich, K.A. (2017). Transcription-Replication Conflict Orientation Modulates R-Loop Levels and Activates Distinct DNA Damage Responses. Cell *170*, 774-786.e19. https://doi.org/10.1016/j.cell.2017.07.043.

Hanson, S.J., and Wolfe, K.H. (2017). An Evolutionary Perspective on Yeast Mating-Type Switching. Genetics *206*, 9–32. https://doi.org/10.1534/genetics.117.202036.

Hauer, M.H., and Gasser, S.M. (2017). Chromatin and nucleosome dynamics in DNA damage and repair. Genes Dev. *31*, 2204–2221. https://doi.org/10.1101/gad.307702.117.

Hays, E., Nettleton, E., Carter, C., Morales, M., Vo, L., Passo, M., and Vélez-Cruz, R. (2020). The SWI/SNF ATPase BRG1 stimulates DNA end resection and homologous recombination by reducing nucleosome density at DNA double strand breaks and by promoting the recruitment of the CtIP nuclease. Cell Cycle *19*, 3096–3114. https://doi.org/10.1080/15384101.2020.1831256.

Hedglin, M., and Benkovic, S.J. (2017). Replication Protein A Prohibits Diffusion of the PCNA Sliding Clamp along Single-Stranded DNA. Biochemistry *56*, 1824–1835. https://doi.org/10.1021/acs.biochem.6b01213.

Heller, R.C., and Marians, K.J. (2006). Replisome assembly and the direct restart of stalled replication forks. Nat. Rev. Mol. Cell Biol. *7*, 932–943. https://doi.org/10.1038/nrm2058.

Henikoff, S., and Dalal, Y. (2005). Centromeric chromatin: what makes it unique? Curr. Opin. Genet. Dev. *15*, 177–184. https://doi.org/10.1016/j.gde.2005.01.004.

Herrmann, G., Lindahl, T., and Schär, P. (1998). Saccharomyces cerevisiae LIF1: a function involved in DNA double-strand break repair related to mammalian XRCC4. EMBO J. *17*, 4188–4198. https://doi.org/10.1093/emboj/17.14.4188.

Heyer, W.-D., Li, X., Rolfsmeier, M., and Zhang, X.-P. (2006). Rad54: the Swiss Army knife of homologous recombination? Nucleic Acids Res. *34*, 4115–4125. https://doi.org/10.1093/nar/gkl481.

Heyer, W.-D., Ehmsen, K.T., and Liu, J. (2010). Regulation of Homologous Recombination in Eukaryotes. Annu. Rev. Genet. *44*, 113–139. https://doi.org/10.1146/annurev-genet-051710-150955.

Hills, S.A., and Diffley, J.F.X. (2014). DNA Replication and Oncogene-Induced Replicative Stress. Curr. Biol. *24*, R435–R444. https://doi.org/10.1016/j.cub.2014.04.012.

Hoeijmakers, J.H.J. (2009). DNA Damage, Aging, and Cancer. N. Engl. J. Med. *361*, 1475–1485. https://doi.org/10.1056/NEJMra0804615.

Hopfner, K.-P., Karcher, A., Shin, D.S., Craig, L., Arthur, L.M., Carney, J.P., and Tainer, J.A. (2000). Structural Biology of Rad50 ATPase: ATP-Driven Conformational Control in DNA Double-Strand Break Repair and the ABC-ATPase Superfamily. Cell *101*, 789–800. https://doi.org/10.1016/S0092-8674(00)80890-9.

Hopfner, K.-P., Craig, L., Moncalian, G., Zinkel, R.A., Usui, T., Owen, B.A.L., Karcher, A., Henderson, B., Bodmer, J.-L., McMurray, C.T., et al. (2002). The Rad50 zinc-hook is a structure joining Mre11 complexes in DNA recombination and repair. Nature *418*, 562–566. https://doi.org/10.1038/nature00922.

Howard, S.M., Yanez, D.A., and Stark, J.M. (2015). DNA damage response factors from diverse pathways, including DNA crosslink repair, mediate alternative end joining. PLoS Genet. *11*, e1004943. https://doi.org/10.1371/journal.pgen.1004943.

Hu, Q., Botuyan, M.V., Cui, G., Zhao, D., and Mer, G. (2017). Mechanisms of Ubiquitin-Nucleosome Recognition and Regulation of 53BP1 Chromatin Recruitment by RNF168/169 and RAD18. Mol. Cell *66*, 473-487.e9. https://doi.org/10.1016/j.molcel.2017.04.009.

Huang, J., and Dynan, W.S. (2002). Reconstitution of the mammalian DNA double-strand break end-joining reaction reveals a requirement for an Mre11/Rad50/NBS1-containing fraction. Nucleic Acids Res. *30*, 667–674. https://doi.org/10.1093/nar/30.3.667.

Huang, T.-H., Fowler, F., Chen, C.-C., Shen, Z.-J., Sleckman, B., and Tyler, J.K. (2018). The Histone Chaperones ASF1 and CAF-1 Promote MMS22L-TONSL-Mediated Rad51 Loading onto ssDNA during Homologous Recombination in Human Cells. Mol. Cell *69*, 879-892.e5. https://doi.org/10.1016/j.molcel.2018.01.031.

Huertas, P., and Jackson, S.P. (2009). Human CtIP mediates cell cycle control of DNA end resection and double strand break repair. J. Biol. Chem. *284*, 9558–9565. https://doi.org/10.1074/jbc.M808906200.

Huertas, P., Cortés-Ledesma, F., Sartori, A.A., Aguilera, A., and Jackson, S.P. (2008). CDK targets Sae2 to control DNA-end resection and homologous recombination. Nature *455*, 689–692. https://doi.org/10.1038/nature07215.

Huyen, Y., Zgheib, O., DiTullio Jr, R.A., Gorgoulis, V.G., Zacharatos, P., Petty, T.J., Sheston, E.A., Mellert, H.S., Stavridi, E.S., and Halazonetis, T.D. (2004). Methylated lysine 79 of histone H3 targets 53BP1 to DNA double-strand breaks. Nature *432*, 406–411. https://doi.org/10.1038/nature03114.

Iacovoni, J.S., Caron, P., Lassadi, I., Nicolas, E., Massip, L., Trouche, D., and Legube, G. (2010). High-resolution profiling of γH2AX around DNA double strand breaks in the mammalian genome. EMBO J. *29*, 1446–1457. https://doi.org/10.1038/emboj.2010.38.

Jager, M. de, Noort, J. van, Gent, D.C. van, Dekker, C., Kanaar, R., and Wyman, C. (2001). Human Rad50/Mre11 Is a Flexible Complex that Can Tether DNA Ends. Mol. Cell *8*, 1129–1135. https://doi.org/10.1016/S1097-2765(01)00381-1.

Janke, C., Magiera, M.M., Rathfelder, N., Taxis, C., Reber, S., Maekawa, H., Moreno-Borchart, A., Doenges, G., Schwob, E., Schiebel, E., et al. (2004). A versatile toolbox for PCR-based tagging of yeast genes: new fluorescent proteins, more markers and promoter substitution cassettes. Yeast Chichester Engl. *21*, 947–962. https://doi.org/10.1002/yea.1142.

Jankovic, M., Nussenzweig, A., and Nussenzweig, M.C. (2007). Antigen receptor diversification and chromosome translocations. Nat. Immunol. *8*, 801–808. https://doi.org/10.1038/ni1498.

Javaheri, A., Wysocki, R., Jobin-Robitaille, O., Altaf, M., Côté, J., and Kron, S.J. (2006). Yeast G1 DNA damage checkpoint regulation by H2A phosphorylation is independent of chromatin remodeling. Proc. Natl. Acad. Sci. U. S. A. *103*, 13771–13776. https://doi.org/10.1073/pnas.0511192103.

Jin, C., and Felsenfeld, G. (2007). Nucleosome stability mediated by histone variants H3.3 and H2A.Z. Genes Dev. *21*, 1519–1529. https://doi.org/10.1101/gad.1547707.

Johzuka, K., and Ogawa, H. (1995). Interaction of Mre11 and Rad50: two proteins required for DNA repair and meiosis-specific double-strand break formation in Saccharomyces cerevisiae. Genetics *139*, 1521–1532. https://doi.org/10.1093/genetics/139.4.1521.

Kalb, R., Mallery, D.L., Larkin, C., Huang, J.T.J., and Hiom, K. (2014). BRCA1 Is a Histone-H2A-Specific Ubiquitin Ligase. Cell Rep. *8*, 999–1005. https://doi.org/10.1016/j.celrep.2014.07.025.

Kalocsay, M., Hiller, N.J., and Jentsch, S. (2009). Chromosome-wide Rad51 Spreading and SUMO-H2A.Z-Dependent Chromosome Fixation in Response to a Persistent DNA Double-Strand Break. Mol. Cell *33*, 335–343. https://doi.org/10.1016/j.molcel.2009.01.016.

Kari, V., Mansour, W.Y., Raul, S.K., Baumgart, S.J., Mund, A., Grade, M., Sirma, H., Simon, R., Will, H., Dobbelstein, M., et al. (2016). Loss of CHD1 causes DNA repair defects and enhances prostate cancer therapeutic responsiveness. EMBO Rep. *17*, 1609–1623. https://doi.org/10.15252/embr.201642352.

Karl, L.A., Peritore, M., Galanti, L., and Pfander, B. (2022). DNA Double Strand Break Repair and Its Control by Nucleosome Remodeling. Front. Genet. *12*. .

Keeney, S., and Kleckner, N. (1995). Covalent protein-DNA complexes at the 5' strand termini of meiosis-specific double-strand breaks in yeast. Proc. Natl. Acad. Sci. U. S. A. *92*, 11274–11278. https://doi.org/10.1073/pnas.92.24.11274.

Keeney, S., Giroux, C.N., and Kleckner, N. (1997). Meiosis-Specific DNA Double-Strand Breaks Are Catalyzed by Spo11, a Member of a Widely Conserved Protein Family. Cell *88*, 375–384. https://doi.org/10.1016/S0092-8674(00)81876-0.

Kent, N.A., Chambers, A.L., and Downs, J.A. (2007). Dual Chromatin Remodeling Roles for RSC during DNA Double Strand Break Induction and Repair at the Yeast MAT Locus. J. Biol. Chem. *282*, 27693–27701. https://doi.org/10.1074/jbc.m704707200.

Kim, J.-A., and Haber, J.E. (2009). Chromatin assembly factors Asf1 and CAF-1 have overlapping roles in deactivating the DNA damage checkpoint when DNA repair is complete. Proc. Natl. Acad. Sci. *106*, 1151–1156. https://doi.org/10.1073/pnas.0812578106.

Knoll, K.R., Eustermann, S., Niebauer, V., Oberbeckmann, E., Stoehr, G., Schall, K., Tosi, A., Schwarz, M., Buchfellner, A., Korber, P., et al. (2018). The nuclear actin-containing Arp8 module is a linker DNA sensor driving INO80 chromatin remodeling. Nat. Struct. Mol. Biol. *25*, 823–832. https://doi.org/10.1038/s41594-018-0115-8.

Knop, M., Siegers, K., Pereira, G., Zachariae, W., Winsor, B., Nasmyth, K., and Schiebel, E. (1999). Epitope tagging of yeast genes using a PCR-based strategy: more tags and improved practical routines. Yeast Chichester Engl. *15*, 963–972. https://doi.org/10.1002/(SICI)1097-0061(199907)15:10B<963::AID-YEA399>3.0.CO;2-W.

Kostriken, R., Strathern, J.N., Klar, A.J.S., Hicks, J.B., and Heffron, F. (1983). A site-specific endonuclease essential for mating-type switching in Saccharomyces cerevisiae. Cell *35*, 167–174. https://doi.org/10.1016/0092-8674(83)90219-2.

Kouzarides, T. (2002). Histone methylation in transcriptional control. Curr. Opin. Genet. Dev. *12*, 198–209. https://doi.org/10.1016/S0959-437X(02)00287-3.

Kowalczykowski, S.C. (2015). An Overview of the Molecular Mechanisms of Recombinational DNA Repair. Cold Spring Harb. Perspect. Biol. *7*, a016410. https://doi.org/10.1101/cshperspect.a016410.

Krietenstein, N., Wal, M., Watanabe, S., Park, B., Peterson, C.L., Pugh, B.F., and Korber, P. (2016). Genomic Nucleosome Organization Reconstituted with Pure Proteins. Cell *167*, 709-721.e12. https://doi.org/10.1016/j.cell.2016.09.045.

Kubik, S., Bruzzone, M.J., Challal, D., Dreos, R., Mattarocci, S., Bucher, P., Libri, D., and Shore, D. (2019). Opposing chromatin remodelers control transcription initiation frequency and start site selection. Nat. Struct. Mol. Biol. *26*, 744–754. https://doi.org/10.1038/s41594-019-0273-3.

Lademann, C.A., Renkawitz, J., Pfander, B., and Jentsch, S. (2017). The INO80 Complex Removes H2A.Z to Promote Presynaptic Filament Formation during Homologous Recombination. Cell Rep. *19*, 1294–1303. https://doi.org/10.1016/j.celrep.2017.04.051.

Lagueux, J., Shah, G.M., Ménard, L., Thomassin, H., Duchaine, C., Hengartner, C., and Poirier, G.G. (1994). Poly(ADP-ribose) catabolism in mammalian cells. Mol. Cell. Biochem. *138*, 45–52. https://doi.org/10.1007/BF00928442.

Lai, W.K.M., and Pugh, B.F. (2017). Understanding nucleosome dynamics and their links to gene expression and DNA replication. Nat. Rev. Mol. Cell Biol. *18*, 548–562. https://doi.org/10.1038/nrm.2017.47.

Lam, I., and Keeney, S. (2015). Mechanism and Regulation of Meiotic Recombination Initiation. Cold Spring Harb. Perspect. Biol. *7*, a016634. https://doi.org/10.1101/cshperspect.a016634.

Lan, L., Ui, A., Nakajima, S., Hatakeyama, K., Hoshi, M., Watanabe, R., Janicki, S.M., Ogiwara, H., Kohno, T., Kanno, S., et al. (2010). The ACF1 Complex Is Required for DNA Double-Strand Break Repair in Human Cells. Mol. Cell *40*, 976–987. https://doi.org/10.1016/j.molcel.2010.12.003.

Lazzaro, F., Sapountzi, V., Granata, M., Pellicioli, A., Vaze, M., Haber, J.E., Plevani, P., Lydall, D., and Muzi-Falconi, M. (2008). Histone methyltransferase Dot1 and Rad9 inhibit single-stranded DNA accumulation at DSBs and uncapped telomeres. EMBO J. *27*, 1502–1512. https://doi.org/10.1038/emboj.2008.81.

Le Tallec, B., Millot, G.A., Blin, M.E., Brison, O., Dutrillaux, B., and Debatisse, M. (2013). Common fragile site profiling in epithelial and erythroid cells reveals that most recurrent cancer deletions lie in fragile sites hosting large genes. Cell Rep. *4*, 420–428. https://doi.org/10.1016/j.celrep.2013.07.003.

Lee, C.-S., Lee, K., Legube, G., and Haber, J.E. (2014). Dynamics of yeast histone H2A and H2B phosphorylation in response to a double-strand break. Nat. Struct. Mol. Biol. *21*, 103–109. https://doi.org/10.1038/nsmb.2737.

Lee, C.-S., Wang, R.W., Chang, H.-H., Capurso, D., Segal, M.R., and Haber, J.E. (2016). Chromosome position determines the success of double-strand break repair. Proc. Natl. Acad. Sci. *113*, E146–E154. https://doi.org/10.1073/pnas.1523660113.

Lee, S.E., Moore, J.K., Holmes, A., Umezu, K., Kolodner, R.D., and Haber, J.E. (1998). Saccharomyces Ku70, Mre11/Rad50, and RPA Proteins Regulate Adaptation to G2/M Arrest after DNA Damage. Cell *94*, 399–409. https://doi.org/10.1016/S0092-8674(00)81482-8.

Levikova, M., Pinto, C., and Cejka, P. (2017). The motor activity of DNA2 functions as an ssDNA translocase to promote DNA end resection. Genes Dev. *31*, 493–502. https://doi.org/10.1101/gad.295196.116.

Li, G.-M. (2008). Mechanisms and functions of DNA mismatch repair. Cell Res. *18*, 85–98. https://doi.org/10.1038/cr.2007.115.

Li, J., Coïc, E., Lee, K., Lee, C.-S., Kim, J.-A., Wu, Q., and Haber, J.E. (2012). Regulation of Budding Yeast Mating-Type Switching Donor Preference by the FHA Domain of Fkh1. PLOS Genet. *8*, e1002630. https://doi.org/10.1371/journal.pgen.1002630.

Li, K., Bronk, G., Kondev, J., and Haber, J.E. (2020). Yeast ATM and ATR kinases use different mechanisms to spread histone H2A phosphorylation around a DNA double-strand break. Proc. Natl. Acad. Sci. *117*, 21354–21363. https://doi.org/10.1073/pnas.2002126117.

Li, M., Hada, A., Sen, P., Olufemi, L., Hall, M.A., Smith, B.Y., Forth, S., McKnight, J.N., Patel, A., Bowman, G.D., et al. (2015). Dynamic regulation of transcription factors by nucleosome remodeling. ELife *4*, e06249. https://doi.org/10.7554/elife.06249.

Liang, B., Qiu, J., Ratnakumar, K., and Laurent, B.C. (2007). RSC Functions as an Early Double-Strand-Break Sensor in the Cell's Response to DNA Damage. Curr. Biol. *17*, 1432–1437. https://doi.org/10.1016/j.cub.2007.07.035.

Löbrich, M., and Jeggo, P. (2017). A Process of Resection-Dependent Nonhomologous End Joining Involving the Goddess Artemis. Trends Biochem. Sci. *42*, 690–701. https://doi.org/10.1016/j.tibs.2017.06.011.

Lou, Z., Minter-Dykhouse, K., Franco, S., Gostissa, M., Rivera, M.A., Celeste, A., Manis, J.P., van Deursen, J., Nussenzweig, A., Paull, T.T., et al. (2006). MDC1 maintains genomic stability by participating in the amplification of ATM-dependent DNA damage signals. Mol. Cell *21*, 187–200. https://doi.org/10.1016/j.molcel.2005.11.025.

Luger, K., Mäder, A.W., Richmond, R.K., Sargent, D.F., and Richmond, T.J. (1997). Crystal structure of the nucleosome core particle at 2.8 Å resolution. Nature *389*, 251–260. https://doi.org/10.1038/38444.

Ma, Y., Pannicke, U., Schwarz, K., and Lieber, M.R. (2002). Hairpin opening and overhang processing by an Artemis/DNA-dependent protein kinase complex in nonhomologous end joining and V(D)J recombination. Cell *108*, 781–794. https://doi.org/10.1016/s0092-8674(02)00671-2.

Majka, J., and Burgers, P.M.J. (2003). Yeast Rad17/Mec3/Ddc1: A sliding clamp for the DNA damage checkpoint. Proc. Natl. Acad. Sci. *100*, 2249–2254. https://doi.org/10.1073/pnas.0437148100.

Majka, J., Niedziela-Majka, A., and Burgers, P.M.J. (2006a). The Checkpoint Clamp Activates Mec1 Kinase during Initiation of the DNA Damage Checkpoint. Mol. Cell *24*, 891–901. https://doi.org/10.1016/j.molcel.2006.11.027.

Majka, J., Binz, S.K., Wold, M.S., and Burgers, P.M.J. (2006b). Replication Protein A Directs Loading of the DNA Damage Checkpoint Clamp to 5′-DNA Junctions. J. Biol. Chem. *281*, 27855–27861. https://doi.org/10.1074/jbc.M605176200.

Marheineke, K., and Krude, T. (1998). Nucleosome Assembly Activity and Intracellular Localization of Human CAF-1 Changes during the Cell Division Cycle. J. Biol. Chem. *273*, 15279–15286. https://doi.org/10.1074/jbc.273.24.15279.

Markert, J., Zhou, K., and Luger, K. (2021). SMARCAD1 is an ATP-dependent histone octamer exchange factor with de novo nucleosome assembly activity. Sci. Adv. https://doi.org/10.1126/sciadv.abk2380.

Mateos-Gomez, P.A., Kent, T., Deng, S.K., McDevitt, S., Kashkina, E., Hoang, T.M., Pomerantz, R.T., and Sfeir, A. (2017). The helicase domain of Polθ counteracts RPA to promote alt-NHEJ. Nat. Struct. Mol. Biol. *24*, 1116–1123. https://doi.org/10.1038/nsmb.3494.

Matheson, K., Parsons, L., and Gammie, A. (2017). Whole-Genome Sequence and Variant Analysis of W303, a Widely-Used Strain of Saccharomyces cerevisiae. G3 Bethesda Md *7*, 2219–2226. https://doi.org/10.1534/g3.117.040022.

Mehta, A., and Haber, J.E. (2014). Sources of DNA Double-Strand Breaks and Models of Recombinational DNA Repair. Cold Spring Harb. Perspect. Biol. *6*, a016428. https://doi.org/10.1101/cshperspect.a016428.

Mehta, A., Beach, A., and Haber, J.E. (2017). Homology Requirements and Competition between Gene Conversion and Break-Induced Replication during Double-Strand Break Repair. Mol. Cell *65*, 515-526.e3. https://doi.org/10.1016/j.molcel.2016.12.003.

Messner, S., Altmeyer, M., Zhao, H., Pozivil, A., Roschitzki, B., Gehrig, P., Rutishauser, D., Huang, D., Caflisch, A., and Hottiger, M.O. (2010). PARP1 ADP-ribosylates lysine residues of the core histone tails. Nucleic Acids Res. *38*, 6350–6362. https://doi.org/10.1093/nar/gkq463.

Meyer, M., and Kircher, M. (2010). Illumina Sequencing Library Preparation for Highly Multiplexed Target Capture and Sequencing. Cold Spring Harb. Protoc. *2010*, pdb.prot5448. https://doi.org/10.1101/pdb.prot5448.

Mimitou, E.P., and Symington, L.S. (2008). Sae2, Exo1 and Sgs1 collaborate in DNA double-strand break processing. Nature *455*, 770–774. https://doi.org/10.1038/nature07312.

Mimitou, E.P., and Symington, L.S. (2010). Ku prevents Exo1 and Sgs1-dependent resection of DNA ends in the absence of a functional MRX complex or Sae2. EMBO J. *29*, 3358–3369. https://doi.org/10.1038/emboj.2010.193.

Mimitou, E.P., Yamada, S., and Keeney, S. (2017). A global view of meiotic double-strand break end resection. Science *355*, 40–45. https://doi.org/10.1126/science.aak9704.

Miné-Hattab, J., and Rothstein, R. (2013). DNA in motion during double-strand break repair. Trends Cell Biol. *23*, 529–536. https://doi.org/10.1016/j.tcb.2013.05.006.

Mirkin, E.V., and Mirkin, S.M. (2007). Replication Fork Stalling at Natural Impediments. Microbiol. Mol. Biol. Rev. *71*, 13–35. https://doi.org/10.1128/MMBR.00030-06.

Moon, A.F., Pryor, J.M., Ramsden, D.A., Kunkel, T.A., Bebenek, K., and Pedersen, L.C. (2014). Sustained active site rigidity during synthesis by human DNA polymerase μ. Nat. Struct. Mol. Biol. *21*, 253–260. https://doi.org/10.1038/nsmb.2766.

Moore, J.K., and Haber, J.E. (1996). Cell cycle and genetic requirements of two pathways of nonhomologous end-joining repair of double-strand breaks in Saccharomyces cerevisiae. Mol. Cell. Biol. *16*, 2164–2173. https://doi.org/10.1128/MCB.16.5.2164.

Morawska, M., and Ulrich, H.D. (2013). An expanded tool kit for the auxin-inducible degron system in budding yeast. Yeast *30*, 341–351. https://doi.org/10.1002/yea.2967.

Mordes, D.A., Nam, E.A., and Cortez, D. (2008). Dpb11 activates the Mec1–Ddc2 complex. Proc. Natl. Acad. Sci. *105*, 18730–18734. https://doi.org/10.1073/pnas.0806621105.

Morillo-Huesca, M., Clemente-Ruiz, M., Andújar, E., and Prado, F. (2010). The SWR1 histone replacement complex causes genetic instability and genome-wide transcription misregulation in the absence of H2A.Z. PloS One *5*, e12143. https://doi.org/10.1371/journal.pone.0012143.

Morrison, A.J., Highland, J., Krogan, N.J., Arbel-Eden, A., Greenblatt, J.F., Haber, J.E., and Shen, X. (2004). INO80 and γ-H2AX Interaction Links ATP-Dependent Chromatin Remodeling to DNA Damage Repair. Cell *119*, 767–775. https://doi.org/10.1016/j.cell.2004.11.037.

Myler, L.R., Gallardo, I.F., Soniat, M.M., Deshpande, R.A., Gonzalez, X.B., Kim, Y., Paull, T.T., and Finkelstein, I.J. (2017). Single-Molecule Imaging Reveals How Mre11-Rad50-Nbs1 Initiates DNA Break Repair. Mol. Cell *67*, 891-898.e4. https://doi.org/10.1016/j.molcel.2017.08.002.

Nakamura, K., Kato, A., Kobayashi, J., Yanagihara, H., Sakamoto, S., Oliveira, D.V.N.P., Shimada, M., Tauchi, H., Suzuki, H., Tashiro, S., et al. (2011). Regulation of Homologous Recombination by RNF20-Dependent H2B Ubiquitination. Mol. Cell *41*, 515–528. https://doi.org/10.1016/j.molcel.2011.02.002.

Natale, F., Rapp, A., Yu, W., Maiser, A., Harz, H., Scholl, A., Grulich, S., Anton, T., Hörl, D., Chen, W., et al. (2017). Identification of the elementary structural units of the DNA damage response. Nat. Commun. *8*, 15760. https://doi.org/10.1038/ncomms15760.

Navadgi-Patil, V.M., and Burgers, P.M. (2008). Yeast DNA Replication Protein Dpb11 Activates the Mec1/ATR Checkpoint Kinase. J. Biol. Chem. *283*, 35853–35859. https://doi.org/10.1074/jbc.M807435200.

Navadgi-Patil, V.M., and Burgers, P.M. (2009). The Unstructured C-Terminal Tail of the 9-1-1 Clamp Subunit Ddc1 Activates Mec1/ATR via Two Distinct Mechanisms. Mol. Cell *36*, 743–753. https://doi.org/10.1016/j.molcel.2009.10.014.

Neelsen, K.J., and Lopes, M. (2015). Replication fork reversal in eukaryotes: from dead end to dynamic response. Nat. Rev. Mol. Cell Biol. *16*, 207–220. https://doi.org/10.1038/nrm3935.

Nichols, M.D., DeAngelis, K., Keck, J.L., and Berger, J.M. (1999). Structure and function of an archaeal topoisomerase VI subunit with homology to the meiotic recombination factor Spo11. EMBO J. *18*, 6177–6188. https://doi.org/10.1093/emboj/18.21.6177.

Niehrs, C., and Luke, B. (2020). Regulatory R-loops as facilitators of gene expression and genome stability. Nat. Rev. Mol. Cell Biol. *21*, 167–178. https://doi.org/10.1038/s41580-019-0206-3.

Nimonkar, A.V., Sica, R.A., and Kowalczykowski, S.C. (2009). Rad52 promotes second-end DNA capture in double-stranded break repair to form complement-stabilized joint molecules. Proc. Natl. Acad. Sci. U. S. A. *106*, 3077–3082. https://doi.org/10.1073/pnas.0813247106.

Nishibuchi, I., Suzuki, H., Kinomura, A., Sun, J., Liu, N.-A., Horikoshi, Y., Shima, H., Kusakabe, M., Harata, M., Fukagawa, T., et al. (2014). Reorganization of Damaged Chromatin by the Exchange of Histone Variant H2A.Z-2. Int. J. Radiat. Oncol. *89*, 736–744. https://doi.org/10.1016/j.ijrobp.2014.03.031.

Novarina, D., Amara, F., Lazzaro, F., Plevani, P., and Muzi-Falconi, M. (2011). Mind the gap: Keeping UV lesions in check. DNA Repair *10*, 751–759. https://doi.org/10.1016/j.dnarep.2011.04.030.

Oberbeckmann, E., Wolff, M., Krietenstein, N., Heron, M., Ellins, J.L., Schmid, A., Krebs, S., Blum, H., Gerland, U., and Korber, P. (2019). Absolute nucleosome occupancy map for the Saccharomyces cerevisiae genome. Genome Res. *29*, 1996–2009. https://doi.org/10.1101/gr.253419.119.

Oberbeckmann, E., Krietenstein, N., Niebauer, V., Wang, Y., Schall, K., Moldt, M., Straub, T., Rohs, R., Hopfner, K.-P., Korber, P., et al. (2021a). Genome information processing by the INO80 chromatin remodeler positions nucleosomes. Nat. Commun. *12*, 3231. https://doi.org/10.1038/s41467-021-23016-z.

Oberbeckmann, E., Niebauer, V., Watanabe, S., Farnung, L., Moldt, M., Schmid, A., Cramer, P., Peterson, C.L., Eustermann, S., Hopfner, K.-P., et al. (2021b). Ruler elements in chromatin remodelers set nucleosome array spacing and phasing. Nat. Commun. *12*, 3232. https://doi.org/10.1038/s41467-021-23015-0.

Oberdoerffer, P., Michan, S., McVay, M., Mostoslavsky, R., Vann, J., Park, S.-K., Hartlerode, A., Stegmuller, J., Hafner, A., Loerch, P., et al. (2008). SIRT1 Redistribution on Chromatin Promotes Genomic Stability but Alters Gene Expression during Aging. Cell *135*, 907–918. https://doi.org/10.1016/j.cell.2008.10.025.

Ocampo, J., Chereji, R.V., Eriksson, P.R., and Clark, D.J. (2016). The ISW1 and CHD1 ATP-dependent chromatin remodelers compete to set nucleosome spacing in vivo. Nucleic Acids Res. *44*, 4625–4635. https://doi.org/10.1093/nar/gkw068.

Ochs, F., Karemore, G., Miron, E., Brown, J., Sedlackova, H., Rask, M.-B., Lampe, M., Buckle, V., Schermelleh, L., Lukas, J., et al. (2019). Stabilization of chromatin topology safeguards genome integrity. Nature *574*, 571–574. https://doi.org/10.1038/s41586-019-1659-4.

Ogiwara, H., Ui, A., Otsuka, A., Satoh, H., Yokomi, I., Nakajima, S., Yasui, A., Yokota, J., and Kohno, T. (2011). Histone acetylation by CBP and p300 at double-strand break sites facilitates SWI/SNF chromatin remodeling and the recruitment of non-homologous end joining factors. Oncogene *30*, 2135–2146. https://doi.org/10.1038/onc.2010.592.

Ohle, C., Tesorero, R., Schermann, G., Dobrev, N., Sinning, I., and Fischer, T. (2016). Transient RNA-DNA Hybrids Are Required for Efficient Double-Strand Break Repair. Cell *167*, 1001-1013.e7. https://doi.org/10.1016/j.cell.2016.10.001.

Orthwein, A., Noordermeer, S.M., Wilson, M.D., Landry, S., Enchev, R.I., Sherker, A., Munro, M., Pinder, J., Salsman, J., Dellaire, G., et al. (2015). A mechanism for the suppression of homologous recombination in G1 cells. Nature *528*, 422–426. https://doi.org/10.1038/nature16142.

Palmbos, P.L., Wu, D., Daley, J.M., and Wilson, T.E. (2008). Recruitment of Saccharomyces cerevisiae Dnl4-Lif1 complex to a double-strand break requires interactions with Yku80 and

the Xrs2 FHA domain. Genetics *180*, 1809–1819. https://doi.org/10.1534/genetics.108.095539.

Palter, K.B., Foe, V.E., and Alberts, B.M. (1979). Evidence for the formation of nucleosome-like histone complexes on single-stranded dna. Cell *18*, 451–467. https://doi.org/10.1016/0092-8674(79)90064-3.

Pannunzio, N.R., Watanabe, G., and Lieber, M.R. (2018). Nonhomologous DNA end-joining for repair of DNA double-strand breaks. J. Biol. Chem. *293*, 10512–10523. https://doi.org/10.1074/jbc.TM117.000374.

Papamichos-Chronakis, M., and Peterson, C.L. (2013). Chromatin and the genome integrity network. Nat. Rev. Genet. *14*, 62–75. https://doi.org/10.1038/nrg3345.

Papamichos-Chronakis, M., Krebs, J.E., and Peterson, C.L. (2006). Interplay between Ino80 and Swr1 chromatin remodeling enzymes regulates cell cycle checkpoint adaptationin response to DNA damage. Genes Dev. *20*, 2437–2449. https://doi.org/10.1101/gad.1440206.

Papamichos-Chronakis, M., Watanabe, S., Rando, O.J., and Peterson, C.L. (2011). Global Regulation of H2A.Z Localization by the INO80 Chromatin-Remodeling Enzyme Is Essential for Genome Integrity. Cell *144*, 200–213. https://doi.org/10.1016/j.cell.2010.12.021.

Park, J., Park, E., Lee, H., Kim, S.J., Hur, S., Imbalzano, A.N., and Kwon, J. (2006). Mammalian SWI/SNF complexes facilitate DNA double-strand break repair by promoting γ-H2AX induction. EMBO J. *25*, 3986–3997. https://doi.org/10.1038/sj.emboj.7601291.

Paull, T.T., and Gellert, M. (1998). The 3' to 5' exonuclease activity of Mre 11 facilitates repair of DNA double-strand breaks. Mol. Cell *1*, 969–979. https://doi.org/10.1016/s1097-2765(00)80097-0.

Pepe, A., and West, S.C. (2014). Substrate specificity of the MUS81-EME2 structure selective endonuclease. Nucleic Acids Res. *42*, 3833–3845. https://doi.org/10.1093/nar/gkt1333.

Peritore, M., Reusswig, K.-U., Bantele, S.C.S., Straub, T., and Pfander, B. (2021). Strand-specific ChIP-seq at DNA breaks distinguishes ssDNA versus dsDNA binding and refutes single-stranded nucleosomes. Mol. Cell *81*, 1841-1853.e4. https://doi.org/10.1016/j.molcel.2021.02.005.

Pfander, B., and Diffley, J.F.X. (2011). Dpb11 coordinates Mec1 kinase activation with cell cycle-regulated Rad9 recruitment. EMBO J. *30*, 4897–4907. https://doi.org/10.1038/emboj.2011.345.

Piazza, A., Bordelet, H., Dumont, A., Thierry, A., Savocco, J., Girard, F., and Koszul, R. (2021). Cohesin regulates homology search during recombinational DNA repair. Nat. Cell Biol. *23*, 1176–1186. https://doi.org/10.1038/s41556-021-00783-x.

Pinto, C., Kasaciunaite, K., Seidel, R., and Cejka, P. (2016). Human DNA2 possesses a cryptic DNA unwinding activity that functionally integrates with BLM or WRN helicases. ELife *5*, e18574. https://doi.org/10.7554/eLife.18574.

Piya, G., Mueller, E.N., Haas, H.K., Ghospurkar, P.L., Wilson, T.M., Jensen, J.L., Colbert, C.L., and Haring, S.J. (2015). Characterization of the Interaction between Rfa1 and Rad24 in Saccharomyces cerevisiae. PLOS ONE *10*, e0116512. https://doi.org/10.1371/journal.pone.0116512.

Poirier, G.G., de Murcia, G., Jongstra-Bilen, J., Niedergang, C., and Mandel, P. (1982). Poly(ADP-ribosyl)ation of polynucleosomes causes relaxation of chromatin structure. Proc. Natl. Acad. Sci. *79*, 3423–3427. https://doi.org/10.1073/pnas.79.11.3423.

Polo, S.E., and Almouzni, G. (2015). Chromatin dynamics after DNA damage: The legacy of the access–repair–restore model. DNA Repair *36*, 114–121. https://doi.org/10.1016/j.dnarep.2015.09.014.

Polo, S.E., Theocharis, S.E., Klijanienko, J., Savignoni, A., Asselain, B., Vielh, P., and Almouzni, G. (2004). Chromatin Assembly Factor-1, a Marker of Clinical Value to Distinguish Quiescent from Proliferating Cells. Cancer Res. *64*, 2371–2381. https://doi.org/10.1158/0008-5472.CAN-03-2893.

Pombo, A., and Dillon, N. (2015). Three-dimensional genome architecture: players and mechanisms. Nat. Rev. Mol. Cell Biol. *16*, 245–257. https://doi.org/10.1038/nrm3965.

Puddu, F., Granata, M., Di Nola, L., Balestrini, A., Piergiovanni, G., Lazzaro, F., Giannattasio, M., Plevani, P., and Muzi-Falconi, M. (2008). Phosphorylation of the budding yeast 9-1-1 complex is required for Dpb11 function in the full activation of the UV-induced DNA damage checkpoint. Mol. Cell. Biol. *28*, 4782–4793. https://doi.org/10.1128/MCB.00330-08.

Qiu, H., Biernat, E., Govind, C.K., Rawal, Y., Chereji, R.V., Clark, D.J., and Hinnebusch, A.G. (2020). Chromatin remodeler Ino80C acts independently of H2A.Z to evict promoter nucleosomes and stimulate transcription of highly expressed genes in yeast. Nucleic Acids Res. *48*, gkaa571-. https://doi.org/10.1093/nar/gkaa571.

Ramsden, D.A., and Gellert, M. (1998). Ku protein stimulates DNA end joining by mammalian DNA ligases: a direct role for Ku in repair of DNA double-strand breaks. EMBO J. *17*, 609–614. https://doi.org/10.1093/emboj/17.2.609.

Ranjha, L., Howard, S.M., and Cejka, P. (2018). Main steps in DNA double-strand break repair: an introduction to homologous recombination and related processes. Chromosoma *127*, 187–214. https://doi.org/10.1007/s00412-017-0658-1.

Rao, S.S.P., Huntley, M.H., Durand, N.C., Stamenova, E.K., Bochkov, I.D., Robinson, J.T., Sanborn, A.L., Machol, I., Omer, A.D., Lander, E.S., et al. (2014). A 3D Map of the Human Genome at Kilobase Resolution Reveals Principles of Chromatin Looping. Cell *159*, 1665–1680. https://doi.org/10.1016/j.cell.2014.11.021.

Rass, U. (2013). Resolving branched DNA intermediates with structure-specific nucleases during replication in eukaryotes. Chromosoma *122*, 499–515. https://doi.org/10.1007/s00412-013-0431-z.

Rass, E., Grabarz, A., Plo, I., Gautier, J., Bertrand, P., and Lopez, B.S. (2009). Role of Mre11 in chromosomal nonhomologous end joining in mammalian cells. Nat. Struct. Mol. Biol. *16*, 819–824. https://doi.org/10.1038/nsmb.1641.

Rass, U., Compton, S.A., Matos, J., Singleton, M.R., Ip, S.C.Y., Blanco, M.G., Griffith, J.D., and West, S.C. (2010). Mechanism of Holliday junction resolution by the human GEN1 protein. Genes Dev. *24*, 1559–1569. https://doi.org/10.1101/gad.585310.

Redon, C., Pilch, D., Rogakou, E., Sedelnikova, O., Newrock, K., and Bonner, W. (2002). Histone H2A variants H2AX and H2AZ. Curr. Opin. Genet. Dev. *12*, 162–169. https://doi.org/10.1016/S0959-437X(02)00282-4.

Reindl, J., Girst, S., Walsh, D.W.M., Greubel, C., Schwarz, B., Siebenwirth, C., Drexler, G.A., Friedl, A.A., and Dollinger, G. (2017). Chromatin organization revealed by nanostructure of irradiation

induced γH2AX, 53BP1 and Rad51 foci. Sci. Rep. *7*, 40616. https://doi.org/10.1038/srep40616.

Renkawitz, J., Lademann, C.A., Kalocsay, M., and Jentsch, S. (2013a). Monitoring Homology Search during DNA Double-Strand Break Repair In Vivo. Mol. Cell *50*, 261–272. https://doi.org/10.1016/j.molcel.2013.02.020.

Renkawitz, J., Lademann, C.A., and Jentsch, S. (2013b). γH2AX spreading linked to homology search. Cell Cycle Georget. Tex *12*, 2526–2527. https://doi.org/10.4161/cc.25836.

Renkawitz, J., Lademann, C.A., and Jentsch, S. (2014). Mechanisms and principles of homology search during recombination. Nat. Rev. Mol. Cell Biol. *15*, 369–383. https://doi.org/10.1038/nrm3805.

Reusswig, K.-U., Bittmann, J., Peritore, M., Wierer, M., Mann, M., and Pfander, B. (2021). BioRxiv. Unscheduled DNA replication in G1 causes genome instability through head-to-tail replication fork collisions. 2021.09.06.459115. https://doi.org/10.1101/2021.09.06.459115.

Rinaldi, C., Pizzul, P., Longhese, M.P., and Bonetti, D. (2021). Sensing R-Loop-Associated DNA Damage to Safeguard Genome Stability. Front. Cell Dev. Biol. *8*. .

Rogakou, E.P., Boon, C., Redon, C., and Bonner, W.M. (1999). Megabase Chromatin Domains Involved in DNA Double-Strand Breaks in Vivo. J. Cell Biol. *146*, 905–916. https://doi.org/10.1083/jcb.146.5.905.

Rossi, M.J., Lai, W.K.M., and Pugh, B.F. (2018). Genome-wide determinants of sequence-specific DNA binding of general regulatory factors. Genome Res. *28*, 497–508. https://doi.org/10.1101/gr.229518.117.

Rother, M.B., Pellegrino, S., Smith, R., Gatti, M., Meisenberg, C., Wiegant, W.W., Luijsterburg, M.S., Imhof, R., Downs, J.A., Vertegaal, A.C.O., et al. (2020). CHD7 and 53BP1 regulate distinct pathways for the re-ligation of DNA double-strand breaks. Nat. Commun. *11*, 5775. https://doi.org/10.1038/s41467-020-19502-5.

Rothstein, R.J. (1983). One-step gene disruption in yeast. Methods Enzymol. *101*, 202–211. https://doi.org/10.1016/0076-6879(83)01015-0.

Rouse, J., and Jackson, S.P. (2002). Interfaces Between the Detection, Signaling, and Repair of DNA Damage. Science https://doi.org/10.1126/science.1074740.

Sakofsky, C.J., and Malkova, A. (2017). Break induced replication in eukaryotes: mechanisms, functions, and consequences. Crit. Rev. Biochem. Mol. Biol. *52*, 395–413. https://doi.org/10.1080/10409238.2017.1314444.

San Filippo, J., Sung, P., and Klein, H. (2008). Mechanism of Eukaryotic Homologous Recombination. Annu. Rev. Biochem. *77*, 229–257. https://doi.org/10.1146/annurev.biochem.77.061306.125255.

Sartori, A.A., Lukas, C., Coates, J., Mistrik, M., Fu, S., Bartek, J., Baer, R., Lukas, J., and Jackson, S.P. (2007). Human CtIP promotes DNA end resection. Nature *450*, 509–514. https://doi.org/10.1038/nature06337.

Schärer, O.D. (2005). DNA Interstrand Crosslinks: Natural and Drug-Induced DNA Adducts that Induce Unique Cellular Responses. ChemBioChem *6*, 27–32. https://doi.org/10.1002/cbic.200400287.

Schumacher, B., Pothof, J., Vijg, J., and Hoeijmakers, J.H.J. (2021). The central role of DNA damage in the ageing process. Nature *592*, 695–703. https://doi.org/10.1038/s41586-021-03307-7.

Seeber, A., Hauer, M., and Gasser, S.M. (2013). Nucleosome remodelers in double-strand break repair. Curr. Opin. Genet. Dev. *23*, 174–184. https://doi.org/10.1016/j.gde.2012.12.008.

Seeber, A., Hauer, M.H., and Gasser, S.M. (2018). Chromosome Dynamics in Response to DNA Damage. Annu. Rev. Genet. *52*, 295–319. https://doi.org/10.1146/annurev-genet-120417-031334.

Seigneur, M., Bidnenko, V., Ehrlich, S.D., and Michel, B. (1998). RuvAB acts at arrested replication forks. Cell *95*, 419–430. https://doi.org/10.1016/s0092-8674(00)81772-9.

Seol, J.-H., Shim, E.Y., and Lee, S.E. (2018). Microhomology-mediated end joining: Good, bad and ugly. Mutat. Res. Mol. Mech. Mutagen. *809*, 81–87. https://doi.org/10.1016/j.mrfmmm.2017.07.002.

Sfeir, A., and Symington, L.S. (2015). Microhomology-Mediated End Joining: A Back-up Survival Mechanism or Dedicated Pathway? Trends Biochem. Sci. *40*, 701–714. https://doi.org/10.1016/j.tibs.2015.08.006.

Shim, E.Y., Ma, J.-L., Oum, J.-H., Yanez, Y., and Lee, S.E. (2005). The Yeast Chromatin Remodeler RSC Complex Facilitates End Joining Repair of DNA Double-Strand Breaks†. Mol. Cell. Biol. *25*, 3934–3944. https://doi.org/10.1128/mcb.25.10.3934-3944.2005.

Shim, E.Y., Hong, S.J., Oum, J.-H., Yanez, Y., Zhang, Y., and Lee, S.E. (2007). RSC Mobilizes Nucleosomes To Improve Accessibility of Repair Machinery to the Damaged Chromatin ▿ †. Mol. Cell. Biol. *27*, 1602–1613. https://doi.org/10.1128/mcb.01956-06.

Shroff, R., Arbel-Eden, A., Pilch, D., Ira, G., Bonner, W.M., Petrini, J.H., Haber, J.E., and Lichten, M. (2004). Distribution and Dynamics of Chromatin Modification Induced by a Defined DNA Double-Strand Break. Curr. Biol. *14*, 1703–1711. https://doi.org/10.1016/j.cub.2004.09.047.

Sibanda, B.L., Critchlow, S.E., Begun, J., Pei, X.Y., Jackson, S.P., Blundell, T.L., and Pellegrini, L. (2001). Crystal structure of an Xrcc4–DNA ligase IV complex. Nat. Struct. Biol. *8*, 1015–1019. https://doi.org/10.1038/nsb725.

Sinha, M., and Peterson, C.L. (2009). Chromatin dynamics during repair of chromosomal DNA double-strand breaks. Epigenomics *1*, 371–385. https://doi.org/10.2217/epi.09.22.

Sjögren, C., and Nasmyth, K. (2001). Sister chromatid cohesion is required for postreplicative double-strand break repair in Saccharomyces cerevisiae. Curr. Biol. CB *11*, 991–995. https://doi.org/10.1016/s0960-9822(01)00271-8.

Smeenk, G., and van Attikum, H. (2013). The Chromatin Response to DNA Breaks: Leaving a Mark on Genome Integrity. Annu. Rev. Biochem. *82*, 55–80. https://doi.org/10.1146/annurev-biochem-061809-174504.

Smeenk, G., Wiegant, W.W., Marteijn, J.A., Luijsterburg, M.S., Sroczynski, N., Costelloe, T., Romeijn, R.J., Pastink, A., Mailand, N., Vermeulen, W., et al. (2012). Poly(ADP-ribosyl)ation links the chromatin remodeler SMARCA5/SNF2H to RNF168-dependent DNA damage signaling. J. Cell Sci. *126*, 889–903. https://doi.org/10.1242/jcs.109413.

Sogo, J.M., Lopes, M., and Foiani, M. (2002). Fork reversal and ssDNA accumulation at stalled replication forks owing to checkpoint defects. Science *297*, 599–602. https://doi.org/10.1126/science.1074023.

Solinger, J.A., and Heyer, W.-D. (2001). Rad54 protein stimulates the postsynaptic phase of Rad51 protein-mediated DNA strand exchange. Proc. Natl. Acad. Sci. U. S. A. *98*, 8447–8453. https://doi.org/10.1073/pnas.121009898.

Soshnev, A.A., Josefowicz, S.Z., and Allis, C.D. (2016). Greater Than the Sum of Parts: Complexity of the Dynamic Epigenome. Mol. Cell *62*, 681–694. https://doi.org/10.1016/j.molcel.2016.05.004.

Soulas-Sprauel, P., Rivera-Munoz, P., Malivert, L., Le Guyader, G., Abramowski, V., Revy, P., and de Villartay, J.-P. (2007). V(D)J and immunoglobulin class switch recombinations: a paradigm to study the regulation of DNA end-joining. Oncogene *26*, 7780–7791. https://doi.org/10.1038/sj.onc.1210875.

Strathern, J.N., Klar, A.J., Hicks, J.B., Abraham, J.A., Ivy, J.M., Nasmyth, K.A., and McGill, C. (1982). Homothallic switching of yeast mating type cassettes is initiated by a double-stranded cut in the MAT locus. Cell *31*, 183–192. https://doi.org/10.1016/0092-8674(82)90418-4.

Strom, A.R., and Brangwynne, C.P. (2019). The liquid nucleome – phase transitions in the nucleus at a glance. J. Cell Sci. *132*. https://doi.org/10.1242/jcs.235093.

Ström, L., Lindroos, H.B., Shirahige, K., and Sjögren, C. (2004). Postreplicative recruitment of cohesin to double-strand breaks is required for DNA repair. Mol. Cell *16*, 1003–1015. https://doi.org/10.1016/j.molcel.2004.11.026.

Sturzenegger, A., Burdova, K., Kanagaraj, R., Levikova, M., Pinto, C., Cejka, P., and Janscak, P. (2014). DNA2 cooperates with the WRN and BLM RecQ helicases to mediate long-range DNA end resection in human cells. J. Biol. Chem. *289*, 27314–27326. https://doi.org/10.1074/jbc.M114.578823.

Sugawara, N., Ira, G., and Haber, J.E. (2000). DNA length dependence of the single-strand annealing pathway and the role of Saccharomyces cerevisiae RAD59 in double-strand break repair. Mol. Cell. Biol. *20*, 5300–5309. https://doi.org/10.1128/MCB.20.14.5300-5309.2000.

Sung, P., and Robberson, D.L. (1995). DNA strand exchange mediated by a RAD51-ssDNA nucleoprotein filament with polarity opposite to that of RecA. Cell *82*, 453–461. https://doi.org/10.1016/0092-8674(95)90434-4.

Symington, L.S., and Gautier, J. (2011). Double-Strand Break End Resection and Repair Pathway Choice. Annu. Rev. Genet. *45*, 247–271. https://doi.org/10.1146/annurev-genet-110410-132435.

Talbert, P.B., and Henikoff, S. (2010). Histone variants - ancient wrap artists of the epigenome. Nat. Rev. Mol. Cell Biol. *11*, 264–275. https://doi.org/10.1038/nrm2861.

Talbert, P.B., and Henikoff, S. (2017). Histone variants on the move: substrates for chromatin dynamics. Nat. Rev. Mol. Cell Biol. *18*, 115–126. https://doi.org/10.1038/nrm.2016.148.

Tamburini, B.A., and Tyler, J.K. (2005). Localized Histone Acetylation and Deacetylation Triggered by the Homologous Recombination Pathway of Double-Strand DNA Repair. Mol. Cell. Biol. *25*, 4903–4913. https://doi.org/10.1128/MCB.25.12.4903-4913.2005.

Técher, H., and Pasero, P. (2021). The Replication Stress Response on a Narrow Path Between Genomic Instability and Inflammation. Front. Cell Dev. Biol. *9*. .

Técher, H., Koundrioukoff, S., Nicolas, A., and Debatisse, M. (2017). The impact of replication stress on replication dynamics and DNA damage in vertebrate cells. Nat. Rev. Genet. *18*, 535–550. https://doi.org/10.1038/nrg.2017.46.

Teo, S.-H., and Jackson, S.P. (2000). Lif1p targets the DNA ligase Lig4p to sites of DNA double-strand breaks. Curr. Biol. *10*, 165–168. https://doi.org/10.1016/S0960-9822(00)00317-1.

Toh, G.W.-L., O'Shaughnessy, A.M., Jimeno, S., Dobbie, I.M., Grenon, M., Maffini, S., O'Rorke, A., and Lowndes, N.F. (2006). Histone H2A phosphorylation and H3 methylation are required for a novel Rad9 DSB repair function following checkpoint activation. DNA Repair *5*, 693–703. https://doi.org/10.1016/j.dnarep.2006.03.005.

Toiber, D., Erdel, F., Bouazoune, K., Silberman, D.M., Zhong, L., Mulligan, P., Sebastian, C., Cosentino, C., Martinez-Pastor, B., Giacosa, S., et al. (2013). SIRT6 Recruits SNF2H to DNA Break Sites, Preventing Genomic Instability through Chromatin Remodeling. Mol. Cell *51*, 454–468. https://doi.org/10.1016/j.molcel.2013.06.018.

Tosi, A., Haas, C., Herzog, F., Gilmozzi, A., Berninghausen, O., Ungewickell, C., Gerhold, C.B., Lakomek, K., Aebersold, R., Beckmann, R., et al. (2013). Structure and Subunit Topology of the INO80 Chromatin Remodeler and Its Nucleosome Complex. Cell *154*, 1207–1219. https://doi.org/10.1016/j.cell.2013.08.016.

Tran, P.T., Erdeniz, N., Dudley, S., and Liskay, R.M. (2002). Characterization of nuclease-dependent functions of Exo1p in Saccharomyces cerevisiae. DNA Repair *1*, 895–912. https://doi.org/10.1016/S1568-7864(02)00114-3.

Tripuraneni, V., Memisoglu, G., MacAlpine, H.K., Tran, T.Q., Zhu, W., Hartemink, A.J., Haber, J.E., and MacAlpine, D.M. (2021). Local nucleosome dynamics and eviction following a double-strand break are reversible by NHEJ-mediated repair in the absence of DNA replication. Genome Res. *31*, 775–788. https://doi.org/10.1101/gr.271155.120.

Tsabar, M., Hicks, W.M., Tsaponina, O., and Haber, J.E. (2016). Re-establishment of nucleosome occupancy during double-strand break repair in budding yeast. DNA Repair *47*, 21–29. https://doi.org/10.1016/j.dnarep.2016.09.005.

Tseng, H.-M., and Tomkinson, A.E. (2002). A physical and functional interaction between yeast Pol4 and Dnl4-Lif1 links DNA synthesis and ligation in nonhomologous end joining. J. Biol. Chem. *277*, 45630–45637. https://doi.org/10.1074/jbc.M206861200.

Tseng, H.-M., and Tomkinson, A.E. (2004). Processing and joining of DNA ends coordinated by interactions among Dnl4/Lif1, Pol4, and FEN-1. J. Biol. Chem. *279*, 47580–47588. https://doi.org/10.1074/jbc.M404492200.

Tsukamoto, Y., Mitsuoka, C., Terasawa, M., Ogawa, H., and Ogawa, T. (2005). Xrs2p Regulates Mre11p Translocation to the Nucleus and Plays a Role in Telomere Elongation and Meiotic Recombination. Mol. Biol. Cell *16*, 597–608. https://doi.org/10.1091/mbc.e04-09-0782.

Tsukuda, T., Fleming, A.B., Nickoloff, J.A., and Osley, M.A. (2005). Chromatin remodelling at a DNA double-strand break site in Saccharomyces cerevisiae. Nature *438*, 379–383. https://doi.org/10.1038/nature04148.

Tsukuda, T., Lo, Y.-C., Krishna, S., Sterk, R., Osley, M.A., and Nickoloff, J.A. (2009). INO80-dependent chromatin remodeling regulates early and late stages of mitotic homologous recombination. DNA Repair *8*, 360–369. https://doi.org/10.1016/j.dnarep.2008.11.014.

Tubbs, A., and Nussenzweig, A. (2017). Endogenous DNA Damage as a Source of Genomic Instability in Cancer. Cell *168*, 644–656. https://doi.org/10.1016/j.cell.2017.01.002.

Unal, E., Heidinger-Pauli, J.M., and Koshland, D. (2007). DNA double-strand breaks trigger genome-wide sister-chromatid cohesion through Eco1 (Ctf7). Science *317*, 245–248. https://doi.org/10.1126/science.1140637.

Van, H.T., and Santos, M.A. (2018). Histone modifications and the DNA double-strand break response. Cell Cycle *17*, 2399–2410. https://doi.org/10.1080/15384101.2018.1542899.

Wang, J.C. (2002). Cellular roles of DNA topoisomerases: a molecular perspective. Nat. Rev. Mol. Cell Biol. *3*, 430–440. https://doi.org/10.1038/nrm831.

Wang, X., and Haber, J.E. (2004). Role of Saccharomyces single-stranded DNA-binding protein RPA in the strand invasion step of double-strand break repair. PLoS Biol. *2*, E21. https://doi.org/10.1371/journal.pbio.0020021.

Wang, W., Daley, J.M., Kwon, Y., Krasner, D.S., and Sung, P. (2017). Plasticity of the Mre11-Rad50-Xrs2-Sae2 nuclease ensemble in the processing of DNA-bound obstacles. Genes Dev. *31*, 2331–2336. https://doi.org/10.1101/gad.307900.117.

Ward, J.F. (1988). DNA damage produced by ionizing radiation in mammalian cells: identities, mechanisms of formation, and reparability. Prog. Nucleic Acid Res. Mol. Biol. *35*, 95–125. https://doi.org/10.1016/s0079-6603(08)60611-x.

Ward, J.F. (1994). The Complexity of DNA Damage: Relevance to Biological Consequences. Int. J. Radiat. Biol. *66*, 427–432. https://doi.org/10.1080/09553009414551401.

Wechsler, T., Newman, S., and West, S.C. (2011). Aberrant chromosome morphology in human cells defective for Holliday junction resolution. Nature *471*, 642–646. https://doi.org/10.1038/nature09790.

Weiner, A., Hughes, A., Yassour, M., Rando, O.J., and Friedman, N. (2010). High-resolution nucleosome mapping reveals transcription-dependent promoter packaging. Genome Res. *20*, 90–100. https://doi.org/10.1101/gr.098509.109.

Whelan, D.R., and Rothenberg, E. (2021). Super-resolution mapping of cellular double-strand break resection complexes during homologous recombination. Proc. Natl. Acad. Sci. *118*. https://doi.org/10.1073/pnas.2021963118.

Wiechens, N., Singh, V., Gkikopoulos, T., Schofield, P., Rocha, S., and Owen-Hughes, T. (2016). The Chromatin Remodelling Enzymes SNF2H and SNF2L Position Nucleosomes adjacent to CTCF and Other Transcription Factors. PLOS Genet. *12*, e1005940. https://doi.org/10.1371/journal.pgen.1005940.

Wiest, N.E., Houghtaling, S., Sanchez, J.C., Tomkinson, A.E., and Osley, M.A. (2017). The SWI/SNF ATP-dependent nucleosome remodeler promotes resection initiation at a DNA double-strand break in yeast. Nucleic Acids Res. *45*, 5887–5900. https://doi.org/10.1093/nar/gkx221.

Wilson, T.E., and Lieber, M.R. (1999). Efficient processing of DNA ends during yeast nonhomologous end joining. Evidence for a DNA polymerase beta (Pol4)-dependent pathway. J. Biol. Chem. *274*, 23599–23609. https://doi.org/10.1074/jbc.274.33.23599.

Wilson, M.D., Benlekbir, S., Fradet-Turcotte, A., Sherker, A., Julien, J.-P., McEwan, A., Noordermeer, S.M., Sicheri, F., Rubinstein, J.L., and Durocher, D. (2016). The structural basis of modified nucleosome recognition by 53BP1. Nature *536*, 100–103. https://doi.org/10.1038/nature18951.

Wilson, T.E., Grawunder, U., and Lieber, M.R. (1997). Yeast DNA ligase IV mediates non-homologous DNA end joining. Nature *388*, 495–498. https://doi.org/10.1038/41365.

Wilson, T.E., Arlt, M.F., Park, S.H., Rajendran, S., Paulsen, M., Ljungman, M., and Glover, T.W. (2015). Large transcription units unify copy number variants and common fragile sites arising under replication stress. Genome Res. *25*, 189–200. https://doi.org/10.1101/gr.177121.114.

Wiltzius, J.J.W., Hohl, M., Fleming, J.C., and Petrini, J.H.J. (2005). The Rad50 hook domain is a critical determinant of Mre11 complex functions. Nat. Struct. Mol. Biol. *12*, 403–407. https://doi.org/10.1038/nsmb928.

Witus, S.R., Burrell, A.L., Farrell, D.P., Kang, J., Wang, M., Hansen, J.M., Pravat, A., Tuttle, L.M., Stewart, M.D., Brzovic, P.S., et al. (2021). BRCA1/BARD1 site-specific ubiquitylation of nucleosomal H2A is directed by BARD1. Nat. Struct. Mol. Biol. *28*, 268–277. https://doi.org/10.1038/s41594-020-00556-4.

Wold, M.S. (1997). Replication protein A: a heterotrimeric, single-stranded DNA-binding protein required for eukaryotic DNA metabolism. Annu. Rev. Biochem. *66*, 61–92. https://doi.org/10.1146/annurev.biochem.66.1.61.

Wright, W.D., and Heyer, W.-D. (2014). Rad54 functions as a heteroduplex DNA pump modulated by its DNA substrates and Rad51 during D loop formation. Mol. Cell *53*, 420–432. https://doi.org/10.1016/j.molcel.2013.12.027.

Wright, W.D., Shah, S.S., and Heyer, W.-D. (2018). Homologous recombination and the repair of DNA double-strand breaks. J. Biol. Chem. *293*, 10524–10535. https://doi.org/10.1074/jbc.TM118.000372.

Wu, D., Topper, L.M., and Wilson, T.E. (2008). Recruitment and dissociation of nonhomologous end joining proteins at a DNA double-strand break in Saccharomyces cerevisiae. Genetics *178*, 1237–1249. https://doi.org/10.1534/genetics.107.083535.

Wu, X., Wilson, T.E., and Lieber, M.R. (1999). A role for FEN-1 in nonhomologous DNA end joining: the order of strand annealing and nucleolytic processing events. Proc. Natl. Acad. Sci. U. S. A. *96*, 1303–1308. https://doi.org/10.1073/pnas.96.4.1303.

Wyatt, H.D.M., Sarbajna, S., Matos, J., and West, S.C. (2013). Coordinated actions of SLX1-SLX4 and MUS81-EME1 for Holliday junction resolution in human cells. Mol. Cell *52*, 234–247. https://doi.org/10.1016/j.molcel.2013.08.035.

Wysocki, R., Javaheri, A., Allard, S., Sha, F., Côté, J., and Kron, S.J. (2005). Role of Dot1-Dependent Histone H3 Methylation in G1 and S Phase DNA Damage Checkpoint Functions of Rad9. Mol. Cell. Biol.

Xie, A., Kwok, A., and Scully, R. (2009). Role of mammalian Mre11 in classical and alternative nonhomologous end joining. Nat. Struct. Mol. Biol. *16*, 814–818. https://doi.org/10.1038/nsmb.1640.

Xu, Y., Ayrapetov, M.K., Xu, C., Gursoy-Yuzugullu, O., Hu, Y., and Price, B.D. (2012). Histone H2A.Z Controls a Critical Chromatin Remodeling Step Required for DNA Double-Strand Break Repair. Mol. Cell *48*, 723–733. https://doi.org/10.1016/j.molcel.2012.09.026.

Yamada, K., Frouws, T.D., Angst, B., Fitzgerald, D.J., DeLuca, C., Schimmele, K., Sargent, D.F., and Richmond, T.J. (2011). Structure and mechanism of the chromatin remodelling factor ISW1a. Nature *472*, 448–453. https://doi.org/10.1038/nature09947.

Yamane, A., Robbiani, D.F., Resch, W., Bothmer, A., Nakahashi, H., Oliveira, T., Rommel, P.C., Brown, E.J., Nussenzweig, A., Nussenzweig, M.C., et al. (2013). RPA Accumulation during Class Switch Recombination Represents 5′–3′ DNA-End Resection during the S–G2/M Phase of the Cell Cycle. Cell Rep. *3*, 138–147. https://doi.org/10.1016/j.celrep.2012.12.006.

Yang, H., Matsumoto, Y., Trujillo, K.M., Lees-Miller, S.P., Osley, M.A., and Tomkinson, A.E. (2015). Role of the yeast DNA repair protein Nej1 in end processing during the repair of DNA double

strand breaks by non-homologous end joining. DNA Repair *31*, 1–10. https://doi.org/10.1016/j.dnarep.2015.04.003.

Yu, C., Gan, H., Han, J., Zhou, Z.-X., Jia, S., Chabes, A., Farrugia, G., Ordog, T., and Zhang, Z. (2014). Strand-Specific Analysis Shows Protein Binding at Replication Forks and PCNA Unloading from Lagging Strands when Forks Stall. Mol. Cell *56*, 551–563. https://doi.org/10.1016/j.molcel.2014.09.017.

Yu, R., Sun, L., Sun, Y., Han, X., Qin, L., and Dang, W. (2019). Cellular response to moderate chromatin architectural defects promotes longevity. Sci. Adv. *5*. https://doi.org/10.1126/sciadv.aav1165.

Yuan, G.-C., Liu, Y.-J., Dion, M.F., Slack, M.D., Wu, L.F., Altschuler, S.J., and Rando, O.J. (2005). Genome-Scale Identification of Nucleosome Positions in S. cerevisiae. Science *309*, 626–630. https://doi.org/10.1126/science.1112178.

Zeman, M.K., and Cimprich, K.A. (2014). Causes and consequences of replication stress. Nat. Cell Biol. *16*, 2–9. https://doi.org/10.1038/ncb2897.

Zhang, H., Roberts, D.N., and Cairns, B.R. (2005). Genome-Wide Dynamics of Htz1, a Histone H2A Variant that Poises Repressed/Basal Promoters for Activation through Histone Loss. Cell *123*, 219–231. https://doi.org/10.1016/j.cell.2005.08.036.

Zhang, Y., Hefferin, M.L., Chen, L., Shim, E.Y., Tseng, H.-M., Kwon, Y., Sung, P., Lee, S.E., and Tomkinson, A.E. (2007). Role of Dnl4-Lif1 in nonhomologous end-joining repair complex assembly and suppression of homologous recombination. Nat. Struct. Mol. Biol. *14*, 639–646. https://doi.org/10.1038/nsmb1261.

Zhang, Y., McCord, R.P., Ho, Y.-J., Lajoie, B.R., Hildebrand, D.G., Simon, A.C., Becker, M.S., Alt, F.W., and Dekker, J. (2012). Spatial Organization of the Mouse Genome and Its Role in Recurrent Chromosomal Translocations. Cell *148*, 908–921. https://doi.org/10.1016/j.cell.2012.02.002.

Zheng, F., Georgescu, R.E., Yao, N.Y., O'Donnell, M.E., and Li, H. (2021). Rad24-RFC loads the 9-1-1 clamp by inserting DNA from the top of a wide-open ring, opposite the mechanism of RFC/PCNA. 2021.10.01.462756. https://doi.org/10.1101/2021.10.01.462756.

Zhou, J., Li, J., Serafim, R.B., Ketchum, S., Ferreira, C.G., Liu, J.C., Coe, K.A., Price, B.D., and Yusufzai, T. (2018). Human CHD1 is required for early DNA-damage signaling and is uniquely regulated by its N terminus. Nucleic Acids Res. *46*, gky128-. https://doi.org/10.1093/nar/gky128.

Zhu, Y., Biernacka, A., Pardo, B., Dojer, N., Forey, R., Skrzypczak, M., Fongang, B., Nde, J., Yousefi, R., Pasero, P., et al. (2019). qDSB-Seq is a general method for genome-wide quantification of DNA double-strand breaks using sequencing. Nat. Commun. *10*, 2313. https://doi.org/10.1038/s41467-019-10332-8.

Zhu, Z., Chung, W.-H., Shim, E.Y., Lee, S.E., and Ira, G. (2008). Sgs1 Helicase and Two Nucleases Dna2 and Exo1 Resect DNA Double-Strand Break Ends. Cell *134*, 981–994. https://doi.org/10.1016/j.cell.2008.08.037.

Zierhut, C., and Diffley, J.F.X. (2008). Break dosage, cell cycle stage and DNA replication influence DNA double strand break response. EMBO J. *27*, 1875–1885. https://doi.org/10.1038/emboj.2008.111.

Zou, L., and Elledge, S.J. (2003). Sensing DNA damage through ATRIP recognition of RPA-ssDNA complexes. Science *300*, 1542–1548. https://doi.org/10.1126/science.1083430.

Zou, L., Liu, D., and Elledge, S.J. (2003). Replication protein A-mediated recruitment and activation of Rad17 complexes. Proc. Natl. Acad. Sci. U. S. A. *100*, 13827–13832. https://doi.org/10.1073/pnas.2336100100.

Acknowledgements

First and foremost, I would like to express my deepest gratitude to my supervisor and mentor Prof. Boris Pfander. Thank you for guiding me through this journey and for supporting my scientific development, your advice has always been invaluable. I feel extremely lucky to have had the chance to be part of your team, I truly felt welcomed and appreciated. Thank you for believing in my potential, for being open to my ideas and being always available for discussions. It has been an incredible experience.

I would also like to express my sincere gratitude to the members of my TAC, Prof. Elena Conti, Prof. Philipp Korber, Prof. Julian Stingele and Dr. Gaëlle Legube. Thank you for your constant support and for all the insightful discussions we had.

Furthermore, I am thankful to our collaborator Dr. Tobias Straub, not only for his contribution to this project, but also for helping me navigate through the bioinformatic analysis of my data. I also want to thank Dr. Stefan Krebs as well as the other members of LAFUGA and the members of the MPI NGS core facility Dr. Marja Driessen, Dr. Rin Ho Kim and Renate Gautsch for the technical support and the sequencing of our samples.

Thank you to the IMPRS coordination office, Hans-Jörg Schäffer, Ingrid Wolf and Maxi Reif, for always having an open ear and for organizing such a rich program.

A big thank you goes to Dr. Elizabeth Schroeder-Reiter for the great job she is doing in coordinating the IRTG and for being always available for discussions and new ideas.

I also would like to thank all the people I had the pleasure to meet during my time at the BMC. Thank you for introducing me to the wonderful world of chromatin and thank you for lighting up my days (and sometimes nights) at the BMC.

Thank you to all the members of the junior group wing, to Massimo and Beate for the constant supplies of media, buffers and plates and a big thank you to Bianca for helping with any administrative task and more.

A really big thank you goes to all the past and present members of the Pfander lab, with whom I had the privilege to share this adventure. It was a lot of fun to work side by side with you all! Thank you to our technicians Uschi and Sandra for their invaluable support. Thanks to Jonah, who helped me with my project. Julia, thank you for always being available for discussion, scientific or not, especially during our countless coffee breaks

and rounds! Thank you for being supportive, it meant a lot to me. Susi, thank you for sharing your enthusiasm (for science and literally any other thing) and funny stories with us. Thank you also for teaching me all about ChIP. Kalle, thank you for being the voice of wisdom and for sharing your knowledge, I really appreciated your company during the late lab hours. Lorenzo, I certainly have to thank you for having had this opportunity. Thank you for sharing all of your yeast tips-and-tricks, for being available whenever I needed and generally for all the funny moments we lived together. Leo, thank you for your positivity and for always being up to spend time together in and outside of the lab. And thank you also for being our plant caretaker!

I am grateful to all the people that made my time at the MPI and in Munich not only rich scientifically but also personally. It was a life-changing experience that I will treasure forever. I especially want to acknowledge the MPI volleyball group for the countless afternoons and evenings we spent having fun together.

Last, but not least, I want to thank my friends and family that supported me throughout this journey. A big thank you to my friends in Italy: Ste, Bery, Darione, Enry, Andre, Mella, Davide & Mary. Thank you for all the unforgettable trips we went on. It is incredible to think that, despite our different lives, we stuck around for basically fifteen (!!!) years.
Magdalini, I cannot imagine how all of this would have been without you. You have been a sister more than a friend. Thank you for your constant support, for believing in me even before myself, for all your kind words and for just being there through the bad and the good times. Your friendship means the world to me.
Christos, thank you for being by my side through this last and probably more difficult part of the journey. Your love and support are invaluable to me. I am grateful for having you in my life and I am looking forward to starting the next chapter together.
Mamma, Papà, thank you for all the sacrifices you have made to make me pursue my dreams. Rosetta, thank you for your kindness, you are like family to me. I am grateful for my grandparents as well, Spiro and Giovanna, you were the rocks of our family. I will cherish every moment I spent with you. I miss you dearly.

Mamma, Papà, grazie per tutti i sacrifici che avete fatto per farmi inseguire i miei sogni. Rosetta, grazie per la tua gentilezza, siete come una seconda famiglia per me. Sono grata di aver avuto al mio fianco i miei nonni, Spiro e Giovanna. Siete stati i pilastri della nostra famiglia. Custodirò ogni momento passato con voi. Mi mancate tanto.